2007-12-19

# Pyridinium Bisretinoids: Synthesis and Photoactivated Cytotoxicity

Junping Gao
*Brigham Young University - Provo*

# Pyridinium Bisretinoids:

# Synthesis and Photoactivated Cytotoxicity

by

Junping Gao

A thesis submitted to the faculty of

Brigham Young University

in partial fulfillment of the requirements for the degree of

Master of Science

Department of Chemistry and Biochemistry

Brigham Young University

April 2008

BRIGHAM YOUNG UNIVERSITY

GRADUATE COMMITTEE APPROVAL

of a thesis submitted by

Junping Gao

This thesis has been read by each member of the following graduate committee and by majority vote has been found to be satisfactory.

| | |
|---|---|
| Date | Heidi R. Vollmer-Snarr, Chair |
| Date | Merritt B. Andrus |
| Date | Steven A. Fleming |
| Date | Steven W. Graves |

BRIGHAM YOUNG UNIVERSITY

As chair of the candidate's graduate committee, I have read the thesis of Junping Gao in its final form and have found that (1) its format, citations, and bibliographical style are consistent and acceptable fulfill university and department; (2) its illustrative materials including figures, tables, and charts are in place; and (3) the final manuscript is satisfactory to be graduate committee is ready for submission to the university library.

| | |
|---|---|
| Date | Heidi R. Vollmer-Snarr<br>Chair, Graduate Committee |

Accepted for the Department

| | |
|---|---|
| Date | David V. Dearden<br>Graduate Coordinator |

Accepted for the College

| | |
|---|---|
| Date | Thomas W. Sederberg<br>Associate Dean, College of Physical and Mathematical Sciences |

# Abstract

This thesis discusses pyridinium bisretinoid compounds (PBRs), which were prepared for two purposes: 1) to use them as standards for detection of novel fluorophores in human RPE cells, which may be involved in age-related macular degeneration (AMD), and 2) to use them in the development of a targeted and triggered drug delivery system for cancer therapy. We prepared a selection of PBRs using a one-pot biomimetic method; synthesis, mechanisms for formation, and characterization of these compounds is described. We also explored the photoreactivity of three novel PBR compounds and found that these PBRs form oxidation products under blue-light irradiation. The photoinduced cytotoxity of A2P and A2EE was examined in HL-60 cells. Results from this work suggest that the PBRs presented have the potential to be involved in AMD and to be developed into a targeted and triggered drug delivery system for cancer therapy.

## Acknowledgements

I would like to express my gratitude to many people. Without the support of these people, the completion of this thesis and my research work would not have been possible.

I will always be indebted to my adviser, Dr. Vollmer-Snarr, for her guidance, trust, encouragement, and support throughout my graduate studies. I can sincerely say that what I have learned from her is invaluable for my future career and life. I am very grateful to her for giving me this chance to work and study in her group.

I would like to extend thanks to all my committee members, Dr. Steven A. Fleming, Dr. Merritt B. Andrus and Dr. Steven W. Graves for their guidance, discussions and suggestions, and support of my research.

I would like to thank Dr. Greg. F. Burton to allow me to use the reader in his lab freely and thank Dr. Kim O'Neill to provide HL-60 cancer cells for our lab. Thanks for your help!

I would also like to thank my lab-mates, McKenzie Pew, Eddie Law, Joseph Ostler, Bryce Harbertson, Jonathan Nielson, David Glabe, and others. Thank you for helping me with my English, revising my thesis, and making my stay at Brigham Young University a pleasant one. Keep up the good work!

I am also grateful to my friends, Mike Christiansen and Shanshan Luo for their help and advice on my thesis. Thanks a lot!

Most of all I would like to extend my appreciation to my husband, Yanshu, for his

extensive help with this thesis. Without his love, encouragement, and support in me this thesis would not have been finished.

I am grateful to the National Kidney Foundation and the American Health Assistance Foundation for funding.

Finally, I sincerely acknowledge the Department of Chemistry and Biochemistry at Brigham Young University for offering me this opportunity and financial support to complete my Masters Degree. I have amazing memories from living and studying here that I will keep with me for the rest of my life.

# Table of Contents

# List of Figures

# List of Schemes

# List of Tables

Chapter 2 – Introduction

# Chapter 1. Introduction

## 1.1. Photoreceptor and Retinal Pigment Epithelial Cells

The human eye is made up of three main layers (Figure 1.1). The external layer contains the sclera and cornea**.** The middle layer includes an anterior portion consisting of the iris and ciliary body and a posterior portion containing the choroid. The internal layer is the retina; the central portion of which is called the macula, which is responsible for central, high-acuity vision.

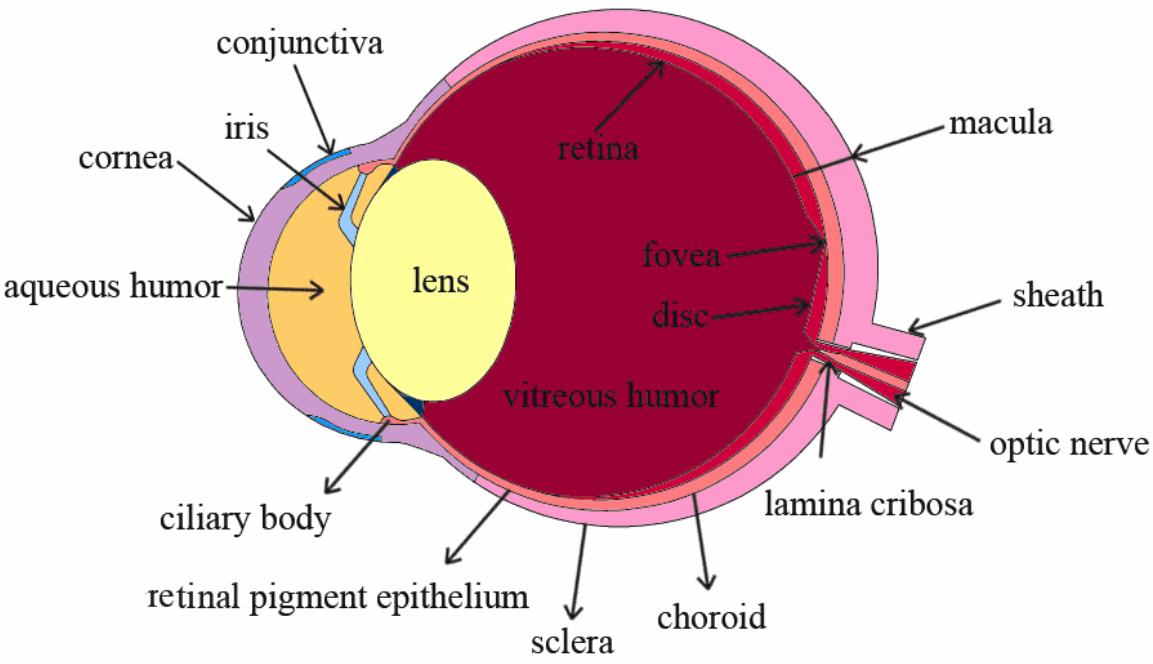


**Figure 1.1. Adult Human Eye**

Photons of light enter the eye through the cornea. This light is focused and travels through the lens, where it is fine-tuned to focus on the retina. Light travels through the

layers of cells in the retina as shown in Figure 1.2. The photoreceptors, made up of rods and cones, receive signals and transfer information from these signals to the optic nerve, which relays the information to be processed in the brain.

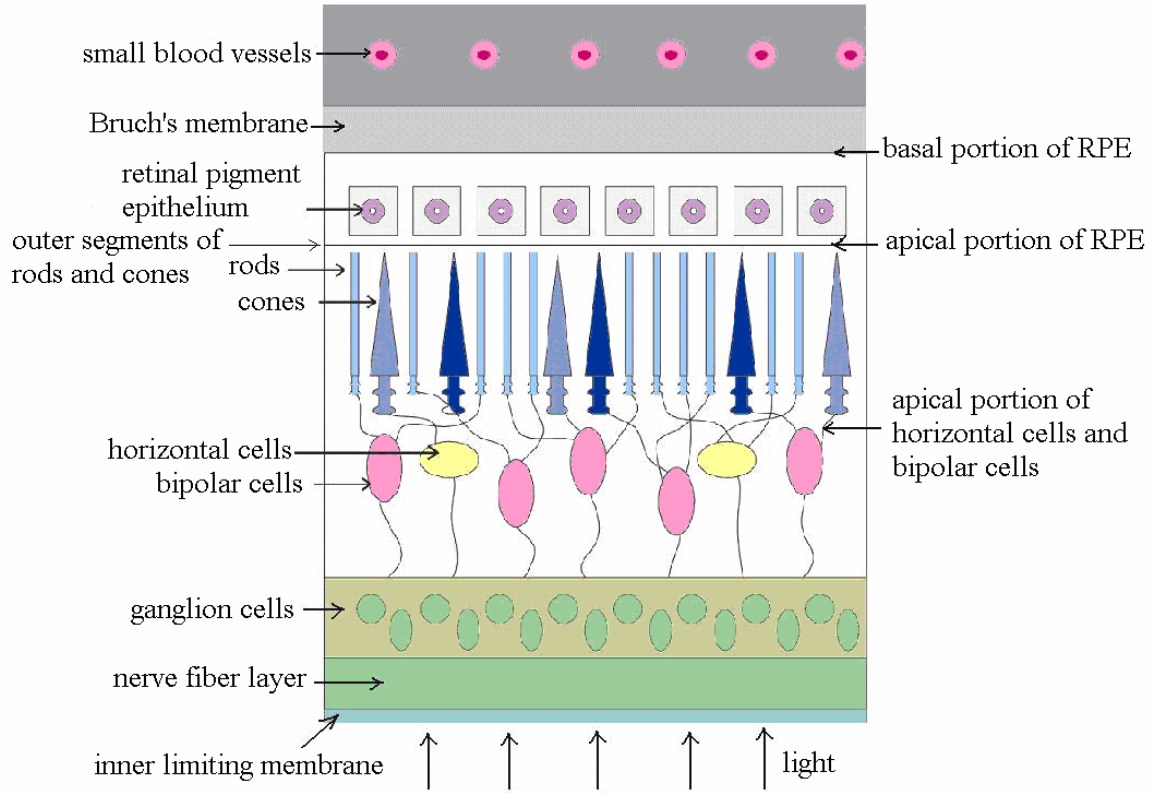


**Figure 1.2. Cells in the Retina and RPE**

Photoreceptor cells are differentiated neurons containing stacks of photosensitive disks in their outer segments (OS). The disks include rhodopsin and other bound proteins named opsins, where photons are captured and visual transduction is processed.[1] The photoreceptors need constant rebuilding through the shedding of their OS and

phagocytosis in retinal pigment epithelial (RPE) cells. This process consists of several metabolic and transport reactions and is called "the visual cycle" (Figure 1.3).[2]

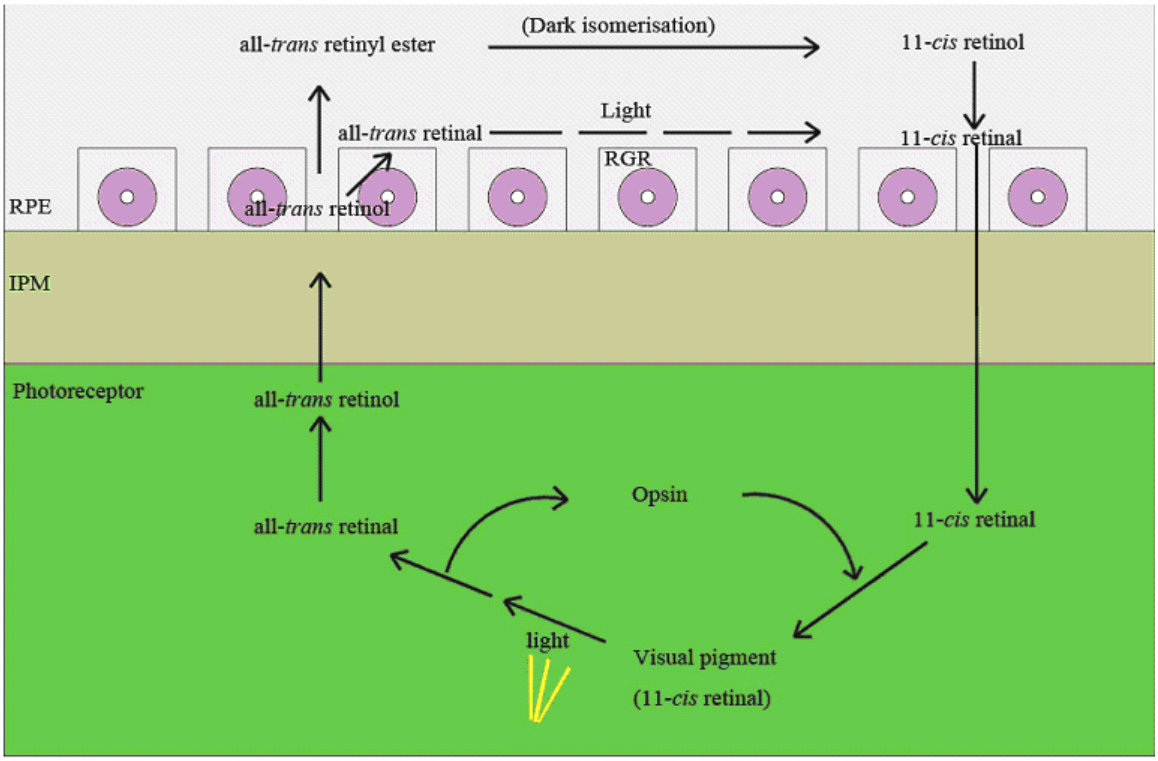


**Figure 1.3. The Visual Cycle**

The initial step of the visual cycle is the light-activated isomerization of 11-*cis* retinal to all-*trans*-retinal.[3] When exposed to light, 11-*cis*-retinal dissociates from opsin and changes to the all-*trans* form. Free opsin is converted into a photosensitive visual pigment with an empty chromophore pocket and regenerates by binding another molecule of 11-*cis*-retinal. All-*trans*-retinal is reduced to all-*trans* retinol by all-*trans*-retinol dehydrogenase after it is transferred from the interior membrane disk to the photoreceptor outer segment.[4] The all-*trans*-retinol is moved through an extracellular compartment, the interphotoreceptor matrix (IPM), to the RPE. In the RPE, all-*trans*-retinol is metabolized

to the 11-*cis* conformation by esterification, isomerization, and oxidation—all steps that occur in darkness. The newly produced 11-*cis* retinal moves from the RPE back to the photoreceptors, where it binds to opsin again and starts a new visual pigment cycle.

One side of the photoreceptor cells connects to the apical portion of horizontal cells and bipolar cells, and the other side connects to the apical portion of the RPE. The RPE is a monolayer of cells that lies between the OS of photoreceptors and Bruch's membrane (Figure 1.2). The RPE has no photoreceptive or neural functions, but it supports the viability of the photoreceptors and plays an important role in photoreceptor growth and maturation.[4, 5] The RPE acts as a barrier, called the blood-retinal barrier, by selectively pumping metabolites and because of its tight intercellular junctions. This barrier prevents the passage of larger or harmful chemicals to the retina, thereby providing a stable and clean retinal environment.[6-8]

The apical layer of the RPE contains microfilaments, microtubules, and highly concentrated melanin granules. Melanin is a heterogeneous polymer consisting of various monomers that come from oxidation products of dihydroxyphenylalinine derived from tyrosine.[9] The melanin in the RPE acts as a photoprotective species by absorbing radiation and consuming free radicals and reactive oxygen species (ROS).[10] The rods and cones are very sensitive to light, and any reflected or scattered light could cause light damage on the photosensitive retina leading to a loss of image signals. The RPE is thus viewed as a protector of photosensitized rods and cones.

## 1.2. Age-related Macular Degeneration

Age-related macular degeneration (AMD) is a condition of advanced degeneration of central vision. AMD occurs as a result of the cellular (photoreceptor and RPE) degeneration in the central part of the retina called the macula, when photoprotective melanin pigments have degraded, because of age. AMD affects nearly 20% of people between the ages of 65 and 75 and greater than 35% of people over the age of 75.[11] It is the leading cause of blindness in developed countries. The disease severely compromises visual tasks such as reading, facial recognition (Figure 1.4), and depth perception.

**Figure 1.4. Normal Vision (right) and Advanced AMD (left)**

There are two main types of AMD, the exudative or wet form, and the atrophic or dry form. Both types of AMD may be caused by oxidative stress. Although there are many mechanisms in the retina to prevent and reduce oxidative stress, many of these mechanisms become less effective over time, which is why the risk of contracting AMD increases with age.[12] Despite the rising prevalence of AMD as a result of increasing life

expectancy, its underlying pathogenesis is poorly understood, and limited treatment options are available.

Exudative AMD affects only 10% of the people with this disease and is caused by abnormal growth of blood vessels in the back of retina. This abnormal blood vessel growth leads to hemorrhage, exudation, or serious retinal detachment.[13] Exudative AMD is also linked to the accumulation of ROS, which may damage the blood-retinal barrier formed by the RPE; this damage results in sudden blindness when the vessels leak or rupture.[14] Laser therapies, including photodynamic therapy, have been used to treat exudative AMD.

Atrophic AMD is the most common form of AMD, which affects 90% of the people with this disease and occurs when the light-sensitive photoreceptor and RPE cells in the macula are deteriorated by ROS stress.[15] Because both photoreceptor and RPE cells are non-replicating (post-mitotic), and they will not reproduce after they have matured, they are often greatly depleted after years of oxidative insult.[16] Currently no treatments exist for atrophic AMD.

Two factors have been implicated in the cause of atrophic AMD: 1) the formation of drusen, and 2) the accumulation of fluorescent lipofuscin in RPE cells.[17-20] Some of the synthetic compounds described in this thesis (Chapter 2) may be present in RPE lipofuscin.

Drusen consists of small yellowish, extracellular materials such as lipid, protein, and cellular debris, existing beneath the RPE.[21] Soft drusen, characterized by deposits in

the macula without visual loss, are considered to be a precursor to advanced AMD.[22, 23] Soft drusen accumulates over time between the RPE and Bruch's membrane, making Bruch's membrane thicker, and impacting the transportation and diffusion of nutrients and oxygen between the RPE and the choroid.[24] Gradually drusen significantly affects the blood-retinal barrier, the RPE's operation, and leads to atrophy of the RPE and adjacent support membrane, resulting in advanced AMD.[25]

Lipofuscin (LF) or "aging pigment," is thought to be another possible biomarker in the development of AMD.[26, 27] LF is a deposit of indigestible waste of oxidative debris from postmitotic cells in the aging process. LF is a heterogeneous complex of fluorescent, lipid-protein aggregates, the exact composition of which is poorly understood. In vitro experiments show that some pigments in LF gradually interrupt the phagocytosis of the RPE by engendering phototoxic ROS such as singlet oxygen, superoxide radical anion, and hydrogen peroxide.[28] For this reason, identification of the fluorescent pigments in LF might help in clarifying the mechanism of atrophic AMD and preventing its occurrence. Analysis of these pigments has shown that they contain the retinoid, all-*trans*-retinol, coming from the chemical visual cycle (Figure 1.3), as well as the bisretinoid compounds, A2E (**1**) and *iso*-A2E (**2**) (Figure 1.5).[29] Recently Fishkin et al. [30] reported that they found the presence of another fluorophore, the all-*trans*-retinal dimer conjugate (**3**) (Figure 1.6), in LF extracts.

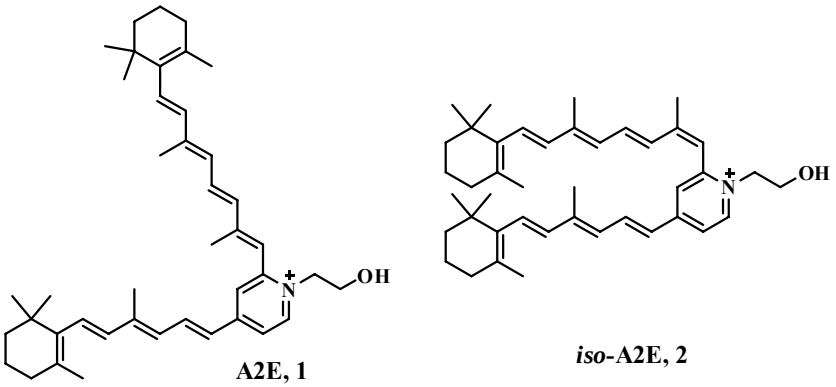


A2E, 1 *iso*-A2E, 2

**Figure 1.5. Structures of A2E and *iso*-A2E**

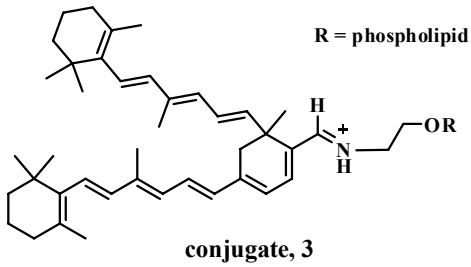


conjugate, 3

**Figure 1.6. all-*trans*-retinal dimer conjugate**

## 1.3. Identification and Synthesis of A2E

In 1988, Eldred and Katz [31] first reported that several blue-absorbing chromophores were separated from RPE cellular extracts. Five years later, Wolf [32] found by performing thin layer chromatography (TLC) analysis on the extracts that the chromophores they studied were a mixture of several fluorescent components. These fluorescent chromophores or fluorophores were hypothesized to be the source of phototoxicity in RPE LF. One of these fluorophores was purified and studied by mass spectrometry (MS) and found to have a mass of 592.4520 and a molecular formula $C_{42}H_{58}NO$.[29] Eldred proposed the structure of the isolated fluorophore to be a bisretinoid

compound, but did not get the structure exactly right.[33, 34] In 1996, Sakai et al.[35] correctly identified the structure as a pyridinium *bis*retinoid using MS and NMR techniques. The IUPAC name of this structure is 2-[2,6-dimethyl-8-(2,6,6-trimethyl-1-cyclohexen-1-yl) -1*E*,3*E*,5*E*,7*E*-octatetraenyl]1-(2-hydroxyethyl)-4-[4-methyl-6-(2,6,6-trimethyl-1-cyclohe xen-1-yl)-1*E*,3*E*,5*E*-hexatrienyl]-pyridinium (Figure 1.5). Because the molecule is a combination of two vitamin A aldehyde (all-*trans*-retinal) molecules and one molecule of ethanolamine, it was called A2E.[35, 36] Two years later Reinboth et al.[37] detected the presence of A2E in albino rat eyes using high-performance liquid chromatography (HPLC). Parish and coworkers[38] used HPLC and NMR to identify the presence of all-*trans*-A2E and the 13'-*cis* isomer of A2E (*iso*-A2E) the following year. Ben-Shabat et al.[39] found that all-*trans*-A2E and *iso*-A2E reach equilibrium in a 4:1 ratio if pure all-*trans*-A2E is exposed to room light. The appearance of up to seven isomers was observed in an improved HPLC assay, after all-*trans*-A2E was exposed to room light for 35 minutes. All the isomers have similar UV spectra and the same MS data as all-*trans*-A2E. Because all-*trans*-A2E is unstable and easily isomerizes, the term "A2E" in this thesis means a collection of all these isomers, in which most of them are all-*trans*-A2E and 13'-*cis*-A2E.

Sakai et al. [35] first reported a biomimetic synthesis of A2E with only a 0.5 % yield after extensive chromatography. Later, Parish et al.[38] reported a one-step biomimetic preparation of A2E achieving 49% yield after purification via silica gel column chromatography. They prepared A2E in only one pot with a 2:1:1 mixture of

all-*trans*-retinal, ethanolamine, and acetic acid. Parish attributed the reasons for the increase in yield of A2E to the addition of one equivalent of acetic acid and to the use of ethanol as a solvent. This optimized methodology of the one-pot biomimetic synthesis has made it possible to make large quantities of A2E for use in biological studies.

Ren et al.[40] completed A2E's first total synthesis and produced a mixture of A2E isomers in the ratio of 4:3:3:2, which can be 90% converted to the all-*trans* isomer by heating and refluxing overnight in nitromethane in the absence of light. Following Ren's preparation of A2E, Tanaka et al.[41] improved the total synthesis of A2E by decreasing the number of steps. Recently Sicre et al.[42] reported a convergent total synthesis of A2E. Although Sicre's method represents a stereoselective preparation of A2E, it still required 10 steps with an overall yield of only 14%.

Of the syntheses reported, the one-step method proposed by Parish [38] is the best choice, because of the efficiency and yield. The proposed mechanism for formation of A2E using this one pot biomimetic preparation is illustrated in Scheme 1.1.[35] First, one all-*trans*-retinal molecule **4** reacts with ethanolamine to form a Schiff base intermediate **6**. This molecule **6** undergoes a 1,5-H shift to afford an intermediate enamine **7**. The enamine **7** reacts with a second all-*trans*-retinal molecule to give an iminium ion **8**. This iminium **8** proceeds through an aza-6π-electrocyclization to afford A2E's precursor **9**. Compound **9** undergoes an auto-oxidation to yield the final product A2E **1**.

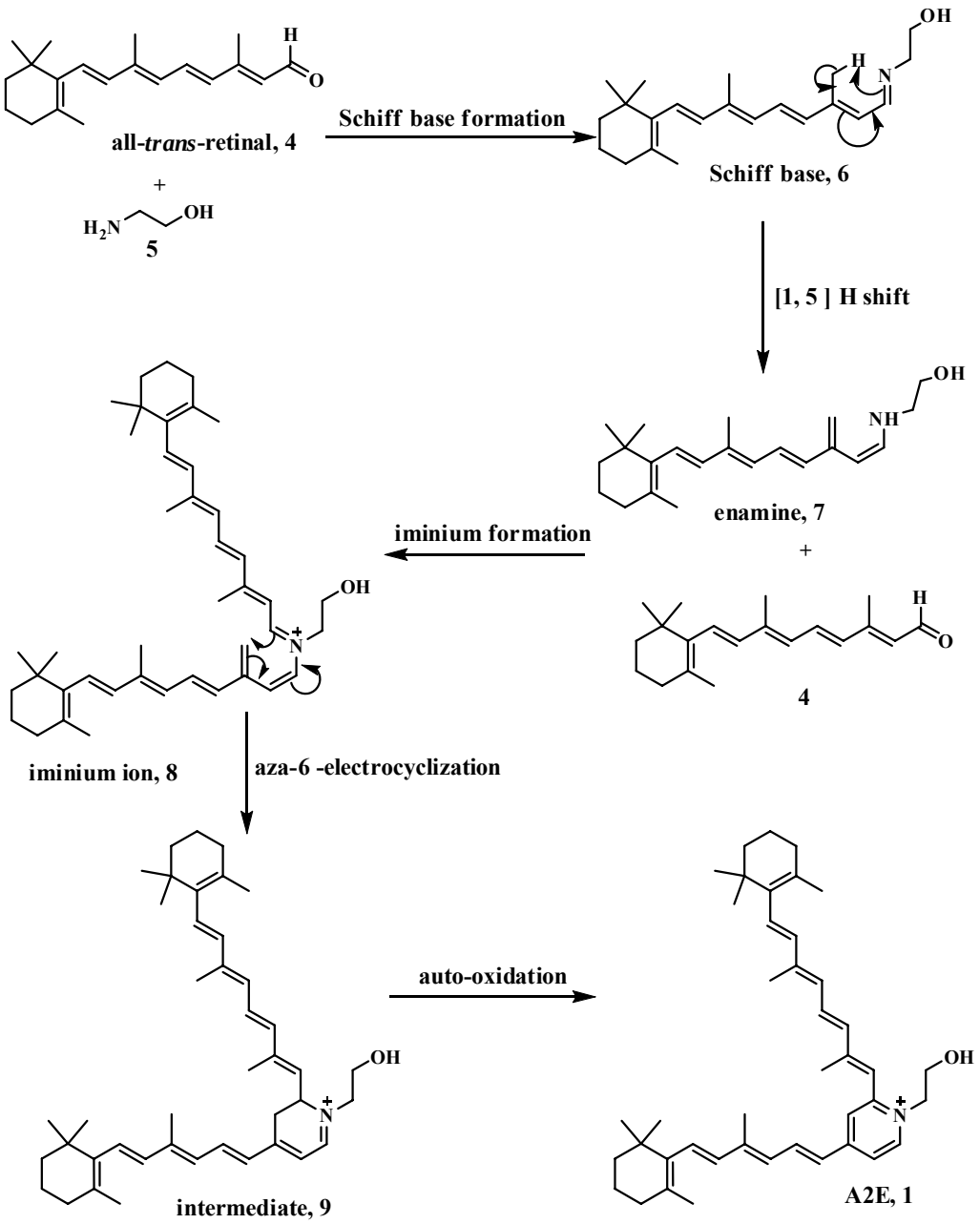


**Scheme 1.1 Biomimetic Synthesis of A2E**

Disputes about where A2E **1** is biosynthesized have been ongoing. Eldred [36] reported that the formation of A2E **1** starts in the acidic RPE lysosomes, and if A2E **1** can not be digested it accumulates in the lysosomes. Parish proposed that the formation of

A2E takes place in the photoreceptor OS, which are eventually phagocytosed to the RPE. To determine the actual mechanism of A2E's formation, Liu et al.[43] explored the biosynthesis of A2E using in vitro experiments. The results suggest that all-*trans* retinal **4** first reacts with phosphatidylethanolamine (PE) to form A2PE (**10**) (Figure 1.7), which was then hydrolyzed to A2E **1.** A2PE (**10),** which was consequently considered a precursor of A2E **1**, was only detected in the OS and not in RPE. This finding suggests that the biosynthesis of A2E **1** begins in the photoreceptor OS.

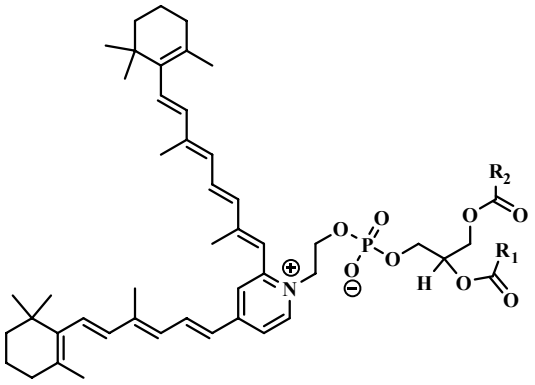


**A2PE, 10**

**Figure 1.7. Structure of A2PE**
$R_1$ and $R_2$ represent biological lipids

To elucidate more of the biosynthetic details of A2E **1,** Ben-Shabat et al.[39] incubated bovine retinas with exogenous all-*trans*-retinal. After this incubation, A2PE **10** was isolated from the retinas. The authors went on to investigate the details of the hydrolysis of A2PE **10**.

A2PE **10** was incubated in an environment similar to the lysosome for 24 hours, however no A2E **1** was found. In addition, only a tiny amount of A2PE **10** was converted to A2E **1** after a one week incubation. When A2PE **10** was incubated in bovine OS with OS specific enzymes, A2PE **10** was converted to A2E **1**. According to the results of the experiments, A2PE **10** appears to be less able to convert to A2E **1** in the RPE, but does convert to A2E **1** in the OS. Thus, these experiments suggest that the biosynthesis of A2E occurs entirely in the OS. A2E must enter the RPE when the OS are phagocytosed. Because A2E is not enzymatically degraded during this process, it is deposited in the RPE as LF and builds up over time.

### 1.4. Toxicity of A2E

A2E's effects on lysosomal function, mitochondrial proteins, and cellular membranes have been studied extensively. A summary of the findings is reported below. Overall, the non-photoirradiative effects of A2E described below are minimal compared to the phototoxicity that will be described in the next section (1.5).

There have been several studies of A2E's effect on lysosomal function. The first study was reported by Eldred.[36] He proposed that A2E is able to inhibit lysosomal function and suggested that A2E behaves similarly to quaternary amines, which form complexes with enzymes. Schutt et al. [44] made a similar observation, and they found that the accumulation of A2E in the lysosome raises the pH of the lysosome. Holz et al. [45] incubated RPE cells with A2E and found that A2E is a dose-dependent and selective

inhibitor of lysosomal function. The in vivo experiment performed by Bermann et al.[46] revealed that A2E does not inhibit the lysosomal hydrolases directly but affects other lysosomal pathways. Finnemann et al.[47] incubated RPE cells with A2E for 6 hours and found that the rate at which RPE cells degrade the OS lipids was decreased, especially the phosphatidylcholine, the most abundant lipid in the OS. It was proposed that this decrease in phosphatidylcholine degradation results from A2E's selective inhibition of phagolysosomal degradation, which results in accumulation of undigested lipids over time in RPE cells.

A2E's effect on mitochondrial function has also been studied. Suter et al.[48] incubated A2E with murine cerebellar granule cells, which have a high concentration of mitochondria. Two proapoptotic proteins, cytochrome *c* and apoptosis-inducing factor, were released, and the mitochondrial function was disrupted when the concentration of A2E was more than 10 μM. It was proposed that A2E facilitates the detachment of cytochrome *c* from the mitochondria, leading to apoptosis. Additional experiments on mitochondria isolated from rat livers demonstrated different effects between A2E isomers.[49] All-*trans*-A2E decreases the oxygen consumption of the mitochondria, whereas the 13'-*cis* isomer had no effect. Additionally, A2E was found to bind tightly with cytochrome *c* oxidase and produce more ROS, loading extra oxidative stress on RPE cells.

The disruption of cell membranes by A2E has also been studied. The positive charge on the pyridinium ring combined with the two hydrophobic retinoid side chains in

A2E make it function like a detergent. This property enables A2E to bind the lipids in cell membranes and disrupt the integrity of the membranes. Sparrow et al.[50] incubated RPE cells with A2E to examine the effect of the amphiphilic property of A2E in RPE cells. It was concluded that disruption of RPE cell membranes by A2E is dependent on its concentration. Schutt et al.[51] examined the effect of A2E on the integrity of cellular organelle membranes. The results revealed that the membrane integrity was destroyed by very low concentrations of A2E, 1 μM A2E in the mitochondria, 2 μM A2E in the lysosomes, and 5 μM A2E in the microsomes. Other retinoids and detergents have similar effects on membrane integrity and induce apoptosis by lysosomal leakage. It was proposed that A2E might arouse the degeneration of organelle membranes and induced apoptosis. De and Sakmar [52] explored the effect of A2E on model membranes by checking the aggregation concentration of A2E in water through fluorescence anisotropy. The results demonstrated that the concentration of A2E required for the instigation of membrane solubilization depended on the lipid composition of the vesicle.

### 1.5. Photoinduced Toxicity of A2E

The phototoxicity of A2E has been extensively studied. Sparrow et al.[53] incubated human RPE (ARPE-19) cells with A2E. These cells were exposed to blue and green light. Cell death increased with increased blue light exposure and increased concentrations of A2E. Green light exposure did not cause cell death. Neither blue light exposure without A2E or A2E in RPE cells without light exposure caused cell death. In the same paper,

DNA damage was also observed after blue light exposure in A2E-loaded cells. This damage was also dose and exposure-time dependent.

Sparrow et al. [54] also explored the effect of singlet oxygen in the photoinduced toxicity of A2E. It was hypothesized that singlet oxygen plays a role in the photoinduced toxicity of A2E. To test this hypothesis, RPE cells loaded with A2E were exposed to blue light in the presence and absence of molecular oxygen. Cell death decreased significantly in cell cultures incubated with oxygen depleters (histidine, sodium azide, 1,4-diazabicyclooctane, and 1,3-dimethyl-2-thiourea), which remove the oxygen dissolved in the solution. Moreover, A2E-loaded cells that remained in the dark and were incubated with oxygen depleters incurred no cell death. To further investigate the hypothesis that singlet oxygen plays a role in cell death, RPE cells loaded with A2E were incubated in a salt buffer of $D_2O$, which is well known to enhance the lifetime of singlet oxygen. Cell death in $D_2O$ treated cells was increased by 66 % after irradiation with blue light.

In the same paper, the authors explored the possible products of A2E oxidation. They observed that the UV-vis absorbance of light–exposed A2E decreased, which suggested a loss of conjugation in the light–exposed compound. The photo–irradiation products of A2E were analyzed by fast atom bombardment-mass spectrometry (FAB-MS); a series of peaks were observed in increments of +16 atomic mass units, suggesting that oxygen was adding to A2E. The same +16 peaks were observed after

A2E-loaded RPE cells were irradiated with blue light; these photo-oxidation products were not found in A2E-loaded RPE cells without irradiation.

Ben-Shabat et al.[55] examined the structures of these oxidation products and concluded that that the double bonds of A2E reacted with singlet oxygen to form A2E-epoxides (Figure 1.8). FAB-MS showed 9 peaks after the 592 peak (*m/z* of A2E), each at increments of +16, starting with 608 and ending at 736. The *m/z* 736 was postulated to be nonaoxirane (**11**). NMR characterization of the reaction product of A2E and *meta*-chloroperbenzoic acid (MCPBA) revealed that the 7, 8, 7', 8'-bisoxirane (**12**) might also form during the irradiation. Additional experiments were performed to investigate whether the irradiation of A2E produced singlet oxygen. The rate of photo-oxidation increased three times when A2E was irradiated in $D_2O$ compared to irradiation in $H_2O$. When A2E was irradiated in $CHCl_3$, a 1270 nm absorbance was observed, which typically suggests the presence of singlet oxygen. It was concluded that A2E is a photosensitizer and produces singlet oxygen from triplet oxygen dissolved in solution; this singlet oxygen reacts with A2E to form A2E-epoxides.

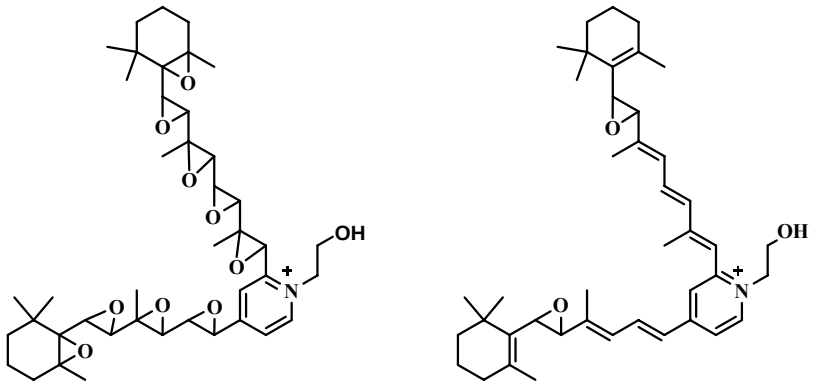


**Nonaoxirane, m/z=736, 11** **Bisoxirane, m/z=736, 12**

**Figure 1.8. Products of A2E Photo-oxidation**

After the A2E-epoxide structures were proposed, Sparrow et al.[56] explored the cellular toxicity of these purported A2E oxidation products. RPE cells were incubated with photoirradiated A2E as opposed to previous experiments in which the RPE cells loaded with A2E were irradiated. Alkaline comet assays were used to examine the effect of the A2E photoproducts on RPE cells. The assay results showed that the DNA of the cells incubated with the A2E oxidation products was severely damaged compared with the cells exposed to unirradiated A2E. Sparrow & co-workers suggested that A2E may be quenching singlet oxygen, and in turn the A2E oxidation products are causing the cellular damage. They proposed that the epoxides were acting as electrophiles and reacting with the DNA directly leading to cell death.

Dillon et al. [57] reported that two of the photooxidation products of A2E might be a monofuran-A2E (Figure 1.9, **13**) and a 5, 8, 5', 8'-bisfuran–A2E (**14**) based on NMR analysis and the fragmentation patterns in tandem mass spectrometry. They suggested that these may be the oxidation products that are present in RPE cells and that epoxides

are simply fleeting intermediates. Jang et al.[58] investigated the photo-oxidation products of A2E by reacting A2E with 1,4-dimethylnaphthalene endoperoxide, a singlet oxygen producer. They found that peroxides **15** and **16** were formed and proposed that they may also be forming in the RPE.

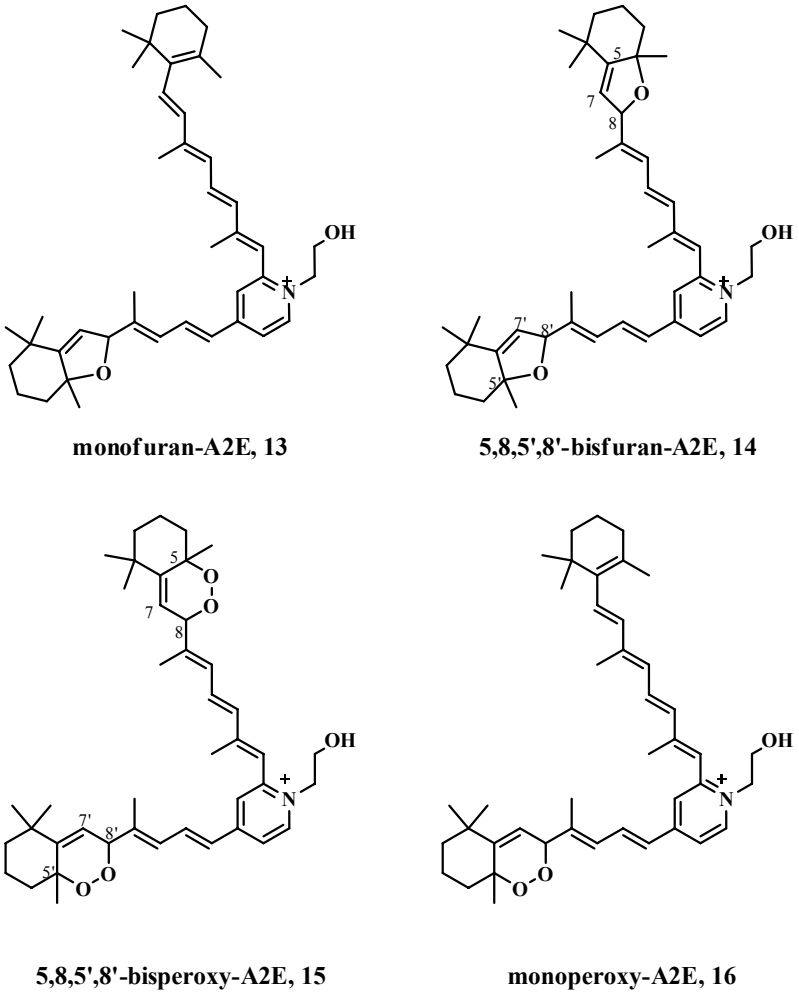


**monofuran-A2E, 13**

**5,8,5',8'-bisfuran-A2E, 14**

**5,8,5',8'-bisperoxy-A2E, 15**

**monoperoxy-A2E, 16**

**Figure 1.9. Putative Products of A2E Photo-oxidation**

The oxidation of A2E is a debated and complicated area of study. Although the structures and the amount of singlet oxygen that A2E produces is under debate, it is clear that whatever happens when A2E is photo-oxidized, the photo-oxidation prodcucts of A2E cause significant damage to RPE cells. This damage may contribute to the cellular atrophy associated with AMD.

## 1.6. Development of a Targeted and Triggered Drug Delivery System for Cancer Therapy

The phototoxicity of A2E in RPE cells was detailed in the preceding section. Because photoirradiated A2E effectively kills RPE cells, we proposed that it might have similar reactivity in cancer cells. We decided to harness this reactivity and use PBRs to develop a triggered drug delivery system for cancer. Although not described in this thesis, in our laboratory, we are also attaching the PBRs to folic acid (**17**), because of the ability of folate bioconjugates to target cancer cells.[59-66]

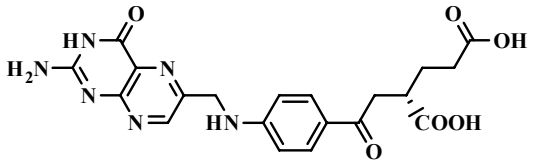


**Figure 1.10. folic acid (17)**

## 1.7. Novel Pyridium Bisretinoid Compounds

In this thesis we describe the preparation of a library of pyridium bisretinoids (PBRs), which are analogs of A2E. Because the majority of the composition of LF, which is implicated in the cause of AMD, remains unknown, these compounds can be used to identify novel fluorophores in human RPE LF. Evidence suggests that A2E plays a role in the cause of AMD; therefore, other PBRs, which may also form in the photoreceptor OS may also be involved in the pathology of AMD. For this purpose biogenic amines which are likely present in the human retina including, tyramine (**18**), L-serine (**19**), guanine (**20**), cytosine (**21**), histidine (**22**), arginine (**23**), propanolamine (**24**), cysteamine (**25**), *N*-(3-aminopropyl)-1,3- propanoldiamine (**26**), 2-(2-aminoethoxy) ethanol (**27**), 2-(2-aminoethylamino) ethanol (**28**), octanamine (**29**), and 1-amino-2-propanol (**30**) were reacted with all-*trans*-retinal in an attempt to form additional PBRs (Figure 1.11). The PBRs resulting from this synthesis will be used as standards for their detection in RPE cells.

Because unoxidized A2E is not significantly toxic in RPE cells at low concentrations and becomes cytotoxic after photo-oxidation with blue light, we decided to assess the potential of PBRs, in addition to A2E, for triggered cytotoxicity on cancer cells. Two amines, aminoacetaldehyde dimethyl acetate (Figure 1.11, **31**) and aminoacetaldehyde diethyl acetate (Figure 1.11, **32**), in addition to those described above were reacted with all-*trans*-retinal to build a PBR library. A small selection of these compounds were tested for cancer cell cytotoxicity.

The synthetic details of PBRs and mechanisms for their formation are discussed in Chapter 2. The blue-light photoreactivity of the synthesized compounds is described in Chapter 3. Cytotoxicity studies of photoirradiated PBRs in HL-60 cells are detailed in Chapter 4.

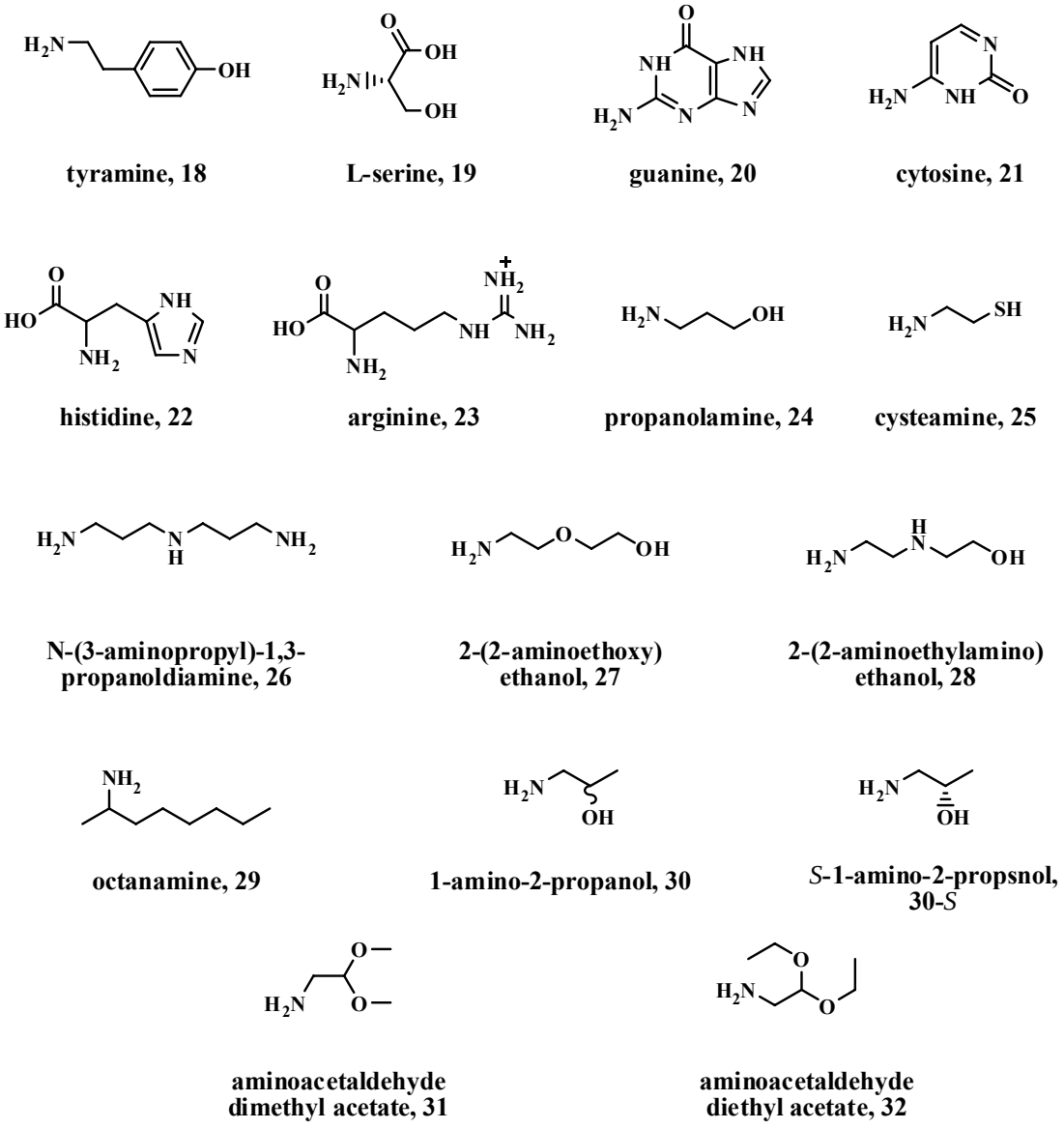


**Figure 1.11. Structures of Amines**

## 1.8. References


1. Travis, H. G.; Golczak, M.; Moise, R. A.; Palczewski, K. *Annu. Rev. Pharmacol. Toxicol.* **2007**, *47*, 469–512.

2. McBee, J. K.; Palczewski, K.; Baehr, W.; Pepperberg, R. D. *Prog. Retin. Eye Res.* **2001**, *20*, 46–529.

3. Wald, G. *Science* **1968**, *162*, 230–239.

4. Marmor, M. Structure, function, and disease of the retinal pigment epithelium. *The Retinal Pigment Epithelium*; Marmor, M., Wolffensberger, T., Eds.; Oxford University Press: New York, 1998; Introduction, pp 3-12; Vol 4, pp 66-87; Vol 9, 175–185.

5. Lin, N.; Sheedlo, H. J.; Aschenbrenner, J. E.; Turner, J. E. *Curr. Eye Res.* **1996**, *15*, 1069–1077.

6. Steinberg, R. H. *Exp. Eye Res.* **1986,** *43*, 696–706.

7. Törnquist, P.; Alm, A. Bill, A. *Eye* **1990,** *4,* 303–309.

8. Grierson, I.; Hiscott, P.; Hogg, P.; Robey, H.; Mazure, A.; Larkin, G. *Eye* **1994,** *8*, 255–262.

9. Sealy, R. C.; Hyde, J. S.; Felix, C. C.; Menon, I. A.; Prota, G.; Swartz, H. M.; Pearsad, S.; Haberman, H. F. *Proc. Natl. Acad. Sci. USA* **1982**, *79*, 2885–2889.

10. Rozanowska, M.; Sarna, T.; Land, E.; Truscott, T. *Free Radical Biol. Med.* **1999**，*26*, 518–525.

11. Stone, E. M.; Sheffield, V. C.; Hageman, G. S. *Hum. Mol. Genet.* **2001**, *10*, 2285–2292.

12. Godley, B. F.; Jin, G. F.; Guo, Y. S.; Hurst, J. S. *Exp. Eye Res.* **2002**, *74*, 663–669.

13. Crabb, J. W.; Miyagi, M.; Gu, X.; Shadrach, K.; West, K. A.; Sakaguchi , H.;Kamei, M.; Hasan , A.; Yan , L.; Rayborn , M. E.; Salomon , R. G.; Hollyfield, J. G. *Proc. Natl. Acad. Sci.USA* **2002**, *99*, 14682–14687.

14. Bora P. S.; Hu, Z.; Tezel, H.; Sohn, J.; Kang, S. G.; Cruz, J. M.; Bora, N. S.; Garen, A.; Kaplan, H. J. *Proc. Natl. Acad. Sci. USA* **2003**, *100*, 2679–2684.

15. Chen, L.; Dentchev, T.; Wong, R.; Hahn, P.; Wen, R; Bennett, J.; Dunaief, J. L. *Mol. Vis*. **2003**, *9*, 151–158.

16. Hong, L.; Garquilo, J.; Azaldi, L.; Edwards, G. S. *Photochem. and Photobiol.* **2006,** *82*, 1475–1481.

17 Campochiaro, P. A. *Expert. Opin. Biol. Ther.* **2004**, *4*, 1395–1402.

18. Kijlstra, A.; La Heij, E. C.; Hendrikse F. *Ocul. Immunol. Inflam.* **2005**, *13*, 3–11.

19. Sparrow, J. R.; Boulton, M. *Exp. Eye Res.* **2005**, *80*, 595–606.

20. Wiktorowska-Owczarek, A.; Nowak, J. Z. *Pol. J. Environ. Stud.* **2006**, *15*, 69–72.

21. Fine, S. L.; Berger, J. W.; Maguire, M. G. *New Engl. J. Med*. **2000**, *342*, 483–492.

22. Algvere, P. V.; Seregard, S. *Acta. Ophthalmol. Scand.* **2003**, *81*, 427–429.

23. Bressler, N. M.; Silva, J. C.; Bressler, S. B.; Fine, S. L.; Green,W. R. *Retina* **1994**, *14*, 130–142.

24. Anderson, D. H.; Mullins, R. E.; Hageman, G. S.; Johnson, L. V. *Am. J. Ophthalmol.* **2002**, *134*, 411–431.

25. Johnson, P. T.; Lewis, G. P.; Talaga, K. C.; Brown, M. N.; Kappel, P. J.; Fisher, S. K.; Anderson, D. H.; Johnson, L. V. *Invest. Ophthalmol. Vis. Sci*. **2003**, *44*, 4481–4488.

26. Dorey, C. K.; Wu, G.; Ebenstein, D.; Garsd, A.; Weiter, J. J. *Invest. Ophthalmol. Vis. Sci.* **1989**, *30*, 1691–1699.

27. Feeney-Burns, L.; Hilderbrand, E. S.; Eldridge, S. *Invest. Ophthalmol. Vis. Sci.* **1984**, *25*, 195–200.

28. Haralampus-Grynaviski, N. M.; Lamb, L. E.; Clancy, C. M.; Skumatz, C.; Burke, J. M; Sarna, T.; Simon. J. D. *Proc. Natl. Acad. Sci. USA* **2003**, *100*, 3179–3184.

29. Eldred, G. E.; Lasky, M. R. *Nature* **1993**, *361*, 724–726.

30. Fishkin, N. E.; Sparrow, J. R.; Allikmets, R.; Nakanishi, K. *Proc. Natl. Acad. Sci. USA* **2005**, *102*, 7091–7096.

31. Eldred, G. E.; Katz, M. L. *Exp. Eye Res*. **1988**, *47*, 71–86.

32. Wolf, G. *Nutr. Rev.* **1993**, *51*, 205–206.

33. Eldred, G. E. *Nature* **1993**, *364*, 396.

34. Wolf, G. *Nutr. Rev.* **1993**, *51*, 348.

35. Sakai, N.; Decatur, K.; Nakanishi, K.; Eldred, G. E. *J. Am. Chem. Soc*. **1996**, *118*, 1559–1560.

36. Eldred, G. E. *Gerontology* **1995**, *41*, 15–26.

37. Reinboth, J. J.; Gautschi, K.; Munz, K.; Eldred, G. E.; Reme, C. E. *Exp. Eye Res.* **1997**, *65*, 639–643.

38. Parish, C. A.; Hashimoto, M.; Nakanishi, K.; Dillon, J.; Sparrow, J. R. *Proc. Natl. Acad. Sci. USA* **1998**, *95*, 14609–14613.

39. Ben-Shabat, S.; Parish, C. A.; Vollmer-Snarr, H. R.; Itagaki, Y.; Fishkin, N.; Nakanishi, K.; Sparrow, J. R. *J. Biol. Chem*. **2002**, *277*, 7183–7190.

40. Ren, R. X. F.; Sakai, N.; Nakanishi, K. *J. Am. Chem. Soc.* **1997**, *119*, 3619–3620.

41. (a) Tanaka, K.; Katsumura, S. *Org. Lett*. **2000**, *2*, 373–375. (b) Tanaka, K.; Mori, H.; Yamamoto, M.; Katsumura, S. *J.Org. Chem.* **2001**, *66*, 3099–3110.

42. Sicre, C.; Cid, M. M. *Org. Lett.* **2005**, *7*, 5737–5739.

43. Liu, J.; Itagaki, Y.; Ben-Shabat, S.; Nakanishi, K.; Sparrow, J. R. *J. Biol. Chem.* **2000**, *275*, 29354–29360.

44. Schutt, F.; Davies, S.; kopitz, J.; Boulton, M.; Holz, F. G. *Ophthalmologe* **2000**, *97*, 682–687.

45. Holz, F. G.; Schutt, F.; Kopitz, J.; Eldred, G. E.; Kruse, F. E.; Volcker, H. E.; Cantz, M. *Investig. Ophthalmol. Vis. Sci.* **1999**, *40*, 737–743.

46. (a) Schutt, F.; Bergmann, M.; Kopita, J.; Holz, F. G. *Ophthalmologe* **2001**, *98*, 721–724. (b) Bergmann, M.; Schutt, F.; Holz, F. G.; Kopita, J. *Exp. Eye Res*. **2001**, *72*, 191–195.

47. Finnemann, S. C.; Leung, L. W.; Rodriguez-Boulan, E. *Proc. Natl. Acad. Sci. USA* **2002**, *99*, 3842–3847.

48. Suter, M.; Reme, C.; Grimm, C.; Wenzel, A.; Jäättela, M. Esser, P.; Kociok, N. Leist, M.; Richter, C. *J. Biol. Chem.* **2000**, *275*, 39625–39630.

49. Shaban, H.; Gazzotti, P.; Richter, C. *Arch. Biochem. Biophys.* **2001**, *394*, 111-116.

50. Sparrow, J. R.; Parish, C. A.; Hashimoto, M.; Nakanishi, K. *Invets. Ophthalmol. Vis. Sci.* **1999**, *40*, 2988–2995.

51. (a) Schutt, F.; Bergmann, M.; Holz, F. G.; Kopitz, J. *Graefe's Arch. Clin. Exp. Opthalmol.* **2002**, *240*, 983–988. (b) Schutt, F.; Bergmann, M.; Kopitz, J.; Holz, F. G. *Ophthalmologe* **2002**, *99*, 861–865.

52. De, S.; Sakmar, T. P. *J. Gen. Physiol.* **2002**, *120*, 147–157.

53. Sparrow, J. R.; Nakanishi, K.; Parish, C. A. *Invest. Ophthalmol. Vis. Sci.* **2000**, *41*, 1981–1989.

54. Sparrow, J. R.; Zhou, J.; Ben-Shabat, S.; Vollmer-Snarr, H. R.; Itagaki, Y.; Nakanishi, K. *Invest. Ophthalmol. Vis. Sci.* **2002**, *43*, 1222–1227.

55. Ben-Shabat, S.; Itagaki, Y.; Jockusch, S.; Sparrow, J. R.; Turro, N. J.; Nakanishi, K. *Angew. Chem. Int. Ed.* **2002**, *41*, 814–817.

56. Sparrow, J. R.; Vollmer-Snarr, H. R.; Zhou, J.; Jang, Y. P.; Jockusch, S.; Itagaki, Y.; Nakanishi, K. *J. Biol. Chem.* **2003**, *278*, 18207–18213.

57. Dillon, J.; Wang, Z.; Avalle, L. B.; Gaillard, E. R. *Exp. Eye Res.* **2004**, *79*, 537-542.

58. Jang, Y. P.; Matsuda, H.; Itagaki, Y.; Nakanishi, K.; Sparrow, J. R. *J. Biol. Chem.* **2005**, *280*, 39732–39739.

59. Sudimack, J.; Lee, R. J. *Adv. Drug. Rev*. **2000**, *41*, 147–162.

60. Weitman, S. D.; Frazier, K. M.; Kamen, B. A. *J. Neurooncol.* **1994**, *21*, 107–112.

61. Ross, J. F.; Chaudhuri, P. K.; Ratnam, M. *Cancer* **1994**, *73*, 2432–2443.

62. Pillai, M. R.; Chacko, P.; Kesari, L. A.; Jayaprakash, P. G.; Jayaram, H. N. *J. Clin. Pathol.* **2003**, *56*, 569–574.

63. Gabizon, A.; Horowitz, T.; Goren, D.; Tzemach, D.; Mandelbaum-Shavit, F.; Qazen, M. M.; Zalipsky, S. *Bioconjug. Chem*. **1999**, *10*, 289–298.

64. Poss, J. F.; Wang, H.; Behm, F. G.; Mathew, P.; Wu, M.; Booth, R.; Ratnam, M. *Cancer* **1999**, *85*, 348–357.

65. Xu, L.; Pirollo, K. F.; Chang, E. H. *J. Control. Release* **2001**, *74*, 115–128.

66. Lu, Y.; Low, P. S. *Adv. Drug. Deliv. Rev.* **2002**, *54*, 675–693.

## Chapter 2. Synthesis of Pyridinium Bisretinoids & the All-*Trans*-Retinal Dimer

### 2.1. Introduction

The goal of the work in this chapter was to synthesize a library of pyridinium bisretinoid (PBR) compounds to be used as standards for detection in lipofuscin (LF) and to be studied for their therapeutic potential against cancer. We compared two one-pot biomimetic methods for their synthesis, one used by Parish et al.[1] in the synthesis of A2-ethanolamine (A2E) and the other used by Pezzella and Prota[2] in the synthesis of A1-dopamine (A1D). Because ion-exchange occurs during chromatography, the acetate anion is the counter ion for all the PBRs reported. Each PBR is named as A2X, where *A* represents vitamin A, and *X* represents the amine.

Although the yields resulting from the one-pot syntheses are low, they are similiar to the overall yields in the 7-9 step total synthetic routes reported in the literature[3-4] and attempted in our laboratory. It is therefore more economical and timely to pursue one-pot syntheses, instead of total synthetic routes. Despite the low yields obtained in these reactions, the syntheses of PBRs described in this chapter represent straightforward, biomimetic methods for obtaining a wide variety of compounds, which may have significant biological importance.

## 2.2. Synthesis of A2-Tyramine

We compared the efficacy of the two one-pot biomimetic methods described above in reactions between ATR and tyramine (**18**) (Table 2.1). Parish's A2E methodology was used in reactions 1, 3, and 4, and Pezzela's A1D methodology was used in reaction 2.

To optimize the reaction conditions, parallel reactions were set up and monitored by thin layer chromatography (TLC). In reactions 1 and 4, most of the starting material had been consumed in 24 hours, and the reactions went to completion in 48 hours. In reactions 2 and 3, the reaction rates were much slower than those of reactions 1 and 4; some of the ATR starting material still remained after 48 hours. Table 2.1 summarizes the conditions used in each reaction and the resulting yields of A2-tyramine (A2T, **33**) obtained.

As shown in Table 2.1, reaction 1 produced the highest yield. The mechanism for formation of A2T using reaction conditions described in reaction 1 should be comparable to that for A2E illustrated in Chapter 1 (Scheme 1.1). The acidic conditions promote the reaction to move forward to products because the aldehyde is protonated and therefore becomes more electrophilic. Consequently, the amine attacks the carbonyl more easily, thereby facilitating conversion to the product. Additionally, the solvent in reaction 2 is aqueous phosphate buffered saline (PBS) with sodium dodecyl sulfate (SDS). The presence of water inhibits the formation of key Schiff base intermediate **6** (Scheme 1.1).

We therefore chose to continue to synthesize A2T and the other PBRs described in this thesis according to the procedure used in reaction 1.

**Table 2.1 Synthesis of A2 -Tyramine**

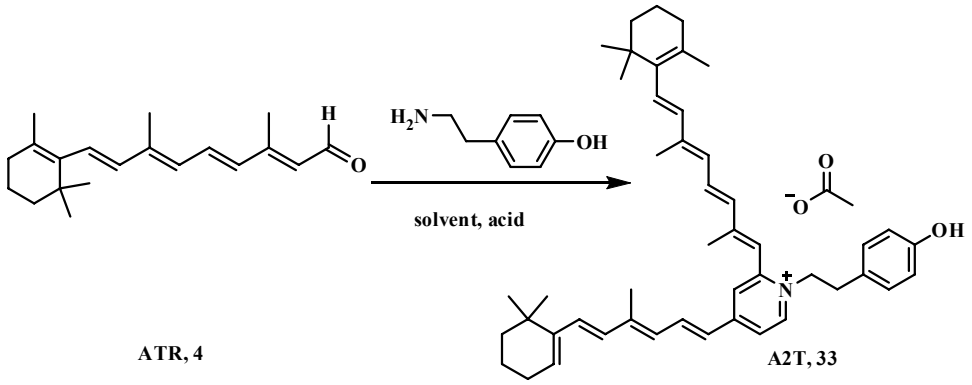


| Reaction | Solvent | Acid | | Time (h) | % yield |
|---|---|---|---|---|---|
| 1 | ethanol | acetic acid |  | 48 | 15 |
| 2 | aqueous PBS | | | 48 | 5 |
| 3 | ethanol | p-toluenesulfonic acid | 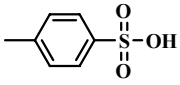 | 56 | 12 |
| 4 | ethanol | trifluoroacetic acid | 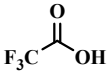 | 48 | 14 |

## 2.3. Reactions of All-*Trans*-Retinal with Selected Amino Acids

L-serine (**19**), guanine (**20**), cytosine (**21**), histidine (**22**) and arginine (**23**) (Figure 1.11) were reacted with ATR using the same conditions described for reaction 1 (Table 2.1). Progress in the reactions were monitored by MS, but no target compounds were

observed. Each of the amino acids reacted has a 2° amine and either a carboxylic acid or amide in their structure. Because the 2° amine is more sterically hindered than the 1° amine in tyramine (**18**), this steric hindrance may have prevented the reaction with the ATR aldehyde (**4**). Protection of the carboxylic acid or amide groups may have also aided the synthesis, but because we desired the synthesis to be one-pot, we did not attempt these protections. Instead we focused on the reaction of several 1° amines (both biogenic and unnatural) that possessed longer hydrocarbon chains lacked carboxylic acids and amides in their structures.

### 2.4. Reactions of All-*Trans*-Retinal with Ethanolamine, Propanolamine, & Cysteamine

Ethanolamine (2-aminoethanol, **5**), propanolamine (3-aminopropan-1-ol, **24**), and cysteamine (2-aminoethanethiol, 2**5**) were reacted with ATR using the same conditions described for reaction 1 (Table 2.1). The yields of these reactions are summarized in Table 2.2. Reactions with ethanolamine and propanolamine resulted in the formation of the corresponding PBRs, whereas no PBR was observed in the reaction with cysteamine.

**Table 2.2 Reactions of All-*Trans*-Retinal with Aminoalcohols and Aminothiol**

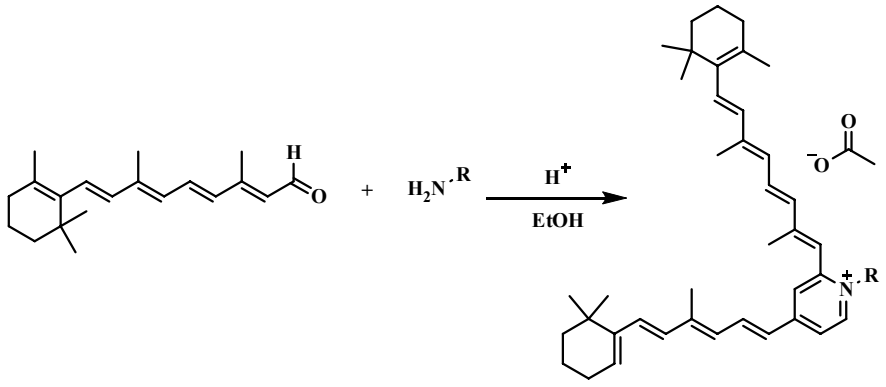


ATR, 4 PBRs

| Entry | Amine's Name | R= | %YIELD |
|---|---|---|---|
| 1 | Ethanolamine, 5 | 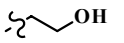 | 18† |
| 2 | Propanolamine, 24 | 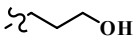 | 13 |
| 3 | Cysteamine, 25 | 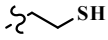 | 0 |

† 18% is obtained by our lab and 49% was the litrature value.

Reaction of ethanolamine and ATR produced A2-ethanolamine (A2E, **1**) in 18 % yield. This yield differs from the value reported in the literature (49 %),[1] because the literature value may represent a crude yield. The reaction with ethanolamine was attempted several times in our laboratory, and we were unable to get the yield of pure material to exceed 18 %. In order to obtain pure material, 2 – 3 chromatographic columns were necessary, which resulted in lower yields.

The optimized reaction between propanolamine and ATR produced A2-propanolamine (A2P, **34**) in 13 % yield. This reaction was also attempted several times and required extensive chromatography for product purification.

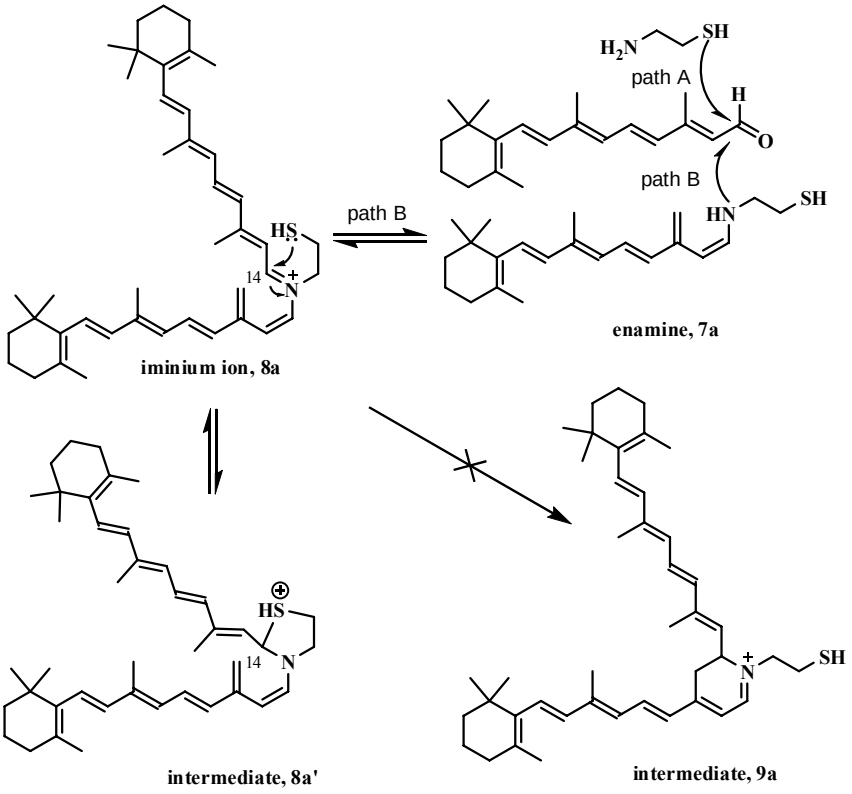


**Scheme 2.1 Reaction of All-*Trans*-Retinal and Cysteamine**

No PBR product was observed in the reaction between cysteamine and ATR. Several obstacles to the A2-cysteamine (A2Cys, **35**) exist. Sulfur is more nucleophilic than the nitrogen, so sulfur would likely attack the ATR aldehyde more readily than nitrogen. If nitrogen did attack the ATR aldehyde to form the Schiff base, then the sulfur would still have a higher probability than nitrogen to attack the second ATR aldehyde (path A in Scheme 2.1). However, if iminium ion **8a** did form, the sulfur might attack carbon 14 adjacent to the iminium ion to give the 5 member ring intermediate **8a'** (path B

in Scheme 2.1). Cysteamine's sulfur is a better nucleophile than the oxygen in ethanolamine and propanolamine, so sulfur is more likely to form the proposed 5 member ring intermediate than oxygen. As demonstrated, there are at least 3 major barriers to the formation of A2Cys.

### 2.5. Reactions of All-*Trans*-Retinal with Polyamines and Hydroxylamines

*N*-(3-Aminopropyl)propane-1,3-diamine (NPD, **26**), 2-(2-aminoethoxy)ethanol (EE, **27**), and 2-(2-aminoethylamino)ethanol (EAE, **28**) were reacted with ATR using the same conditions described for reaction 1 (Table 2.1). The yields of these reactions are summarized in Table 2.3. Reactions with **27** resulted in the formation of the corresponding PBR, whereas no PBRs were observed in the reactions with **26** and **28**.

After attempting to synthesize A2NPD (3**6**) using reaction 1 methodology, no PBR products were observed. As a result, we tried using the methodology described in reaction 2 (Table 2.1). Disappointingly, the desired PBR products were not observed after the reaction was checked at 48 h, 72 h, 96 h and 7 days (Table 2.3).

**Table 3. Reactions of All-*Trans*-Retinal with Polyamines and Hydroxylamines**

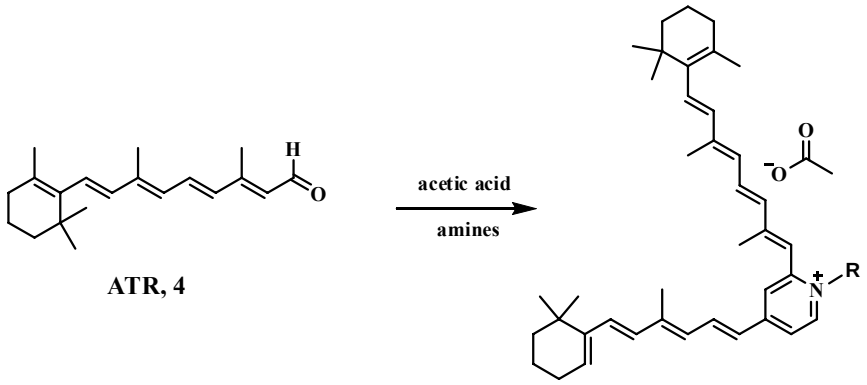


ATR, 4

PBRs

| Entry | Amine | PBRs' name | Time | % Yield |
|---|---|---|---|---|
| 1 | 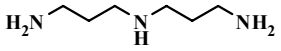 *N*-(3-aminopropyl)propane-1,3-diamine, 26 | A2NPD, 36 | one week | 0 |
| 2 | 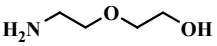 2-(2-aminoethoxy)ethanol, 27 | A2EE, 37 | 48 h | 16 |
| 3 | 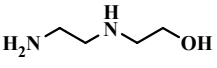 2-(2-aminoethylamino)ethanol, 28 | A2EAE, 38 | 96 h | 0 |

In an attempt to obtain a PBR product, we decided to replace the 2° and one of the 1° nitrogens in NPD with oxygen atoms. In addition, the carbon chains are each 1 carbon shorter. EE was reacted with all-*trans*-retinal to give A2EE (**37**) in 16 % yield. After forming A2EE in an acceptable yield for PBR synthesis, we reasoned that a 6-membered ring intermediate may be forming, similar to the proposed 5-membered ring in the attempted A2Cy synthesis (Scheme 2.2).

In order to further probe the proposed 5- and 6-membered ring formation, we attempted the reaction with the 2° nitrogen in EE exchanged with an oxygen atom. When

EAE was reacted with all-*trans*-retinal no A2EAE (**38**) was observed (Table 2.3). In this reaction a 5-membered ring intermediate likely forms, suppressing the formation of A2EAE (Scheme 2.2).

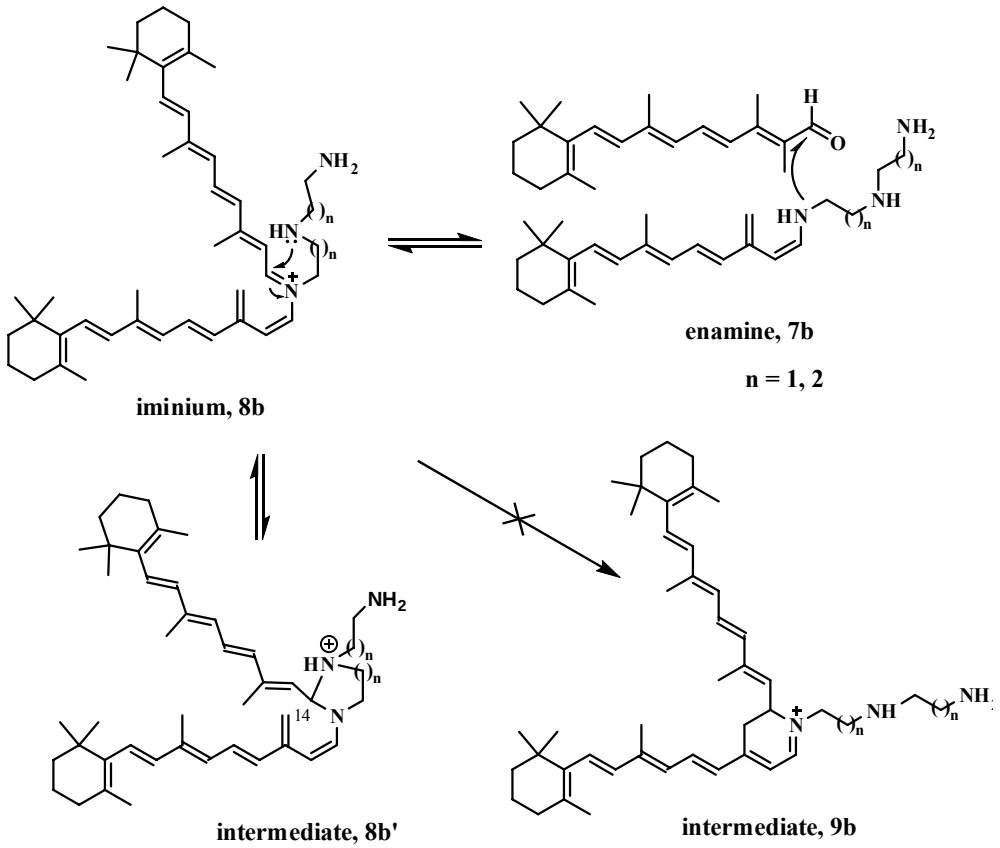


**Scheme 2.2 Attempted Synthesis of A2NPD and A2EAE**

As pictured in Scheme 2.2 iminium **8b** can't proceed to the PBR **9b** because the amino groups in NPD and EAE may attack the carbon adjacent to the iminium ion and return to **7b** through the 5 or 6 member ring **8b**'. The A2EE preparation succeeded because the ether oxygen is not a strong enough nucleophile to break the carbon nitrogen bond of the iminium ion.

## 2.6. Reactions of All-*Trans*-Retinal with Additional Amines

Aminoacetaldehyde dimethyl acetate (DM, **31**), aminoacetaldehyde diethyl acetate (DE, **32**), 2-octanamine (OA, **29**), 1-amino-1-propanol (AP, **30**), and *S*-1-amino-2-propanol (*S*-AP, **30-*S***) were reacted with ATR using the same conditions described for reaction 1 (Table 2.1).

**Table 2.4 Reactions of All-*Trans*-Retinal with Additional Amines**

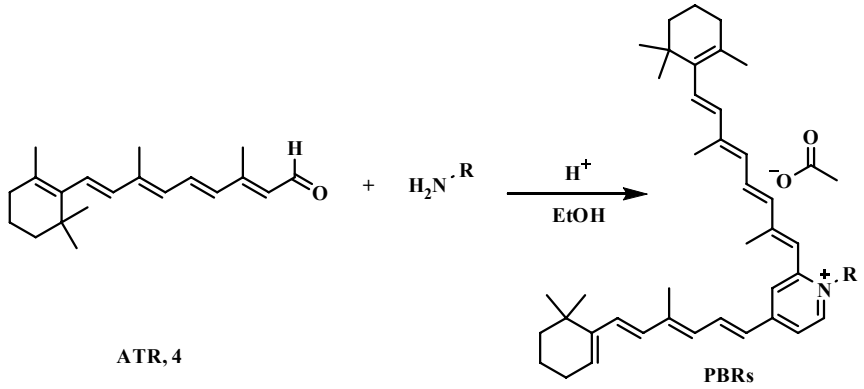


ATR, 4 PBRs

| Entry | Amine | PBR's name | R= | yield % |
|---|---|---|---|---|
| 1 | aminoacetaldehyde dimethyl acetate, 31 | A2DM, 39 | 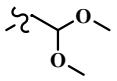 | 8 |
| 2 | aminoacetaldehyde diethyl acetate, 32 | A2DE, 40 | 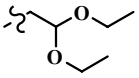 | 10 |
| 3 | 2-octanamine, 29 | A2OA, 41 | 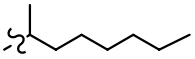 | 10 |
| 4 | 1-amino-2-propanol, 30 | A2AP, 42 |  | 8 |
| 5 | *S*-1-amino-2-propanol, 30S | *S*-A2AP, 42-S |  | 8 |

A2-Aminoacetaldehyde dimethyl acetate (A2DM, **39**), A2-aminoacetaldehyde diethyl acetate (A2DE, **40**), A2-aminooctane (A2AO, **41**), A2-1-amino-2-propanol (A2AP, **42**), and A2-*S*-1-amino-2-propanol (*S*-A2AP, **42-*S***) were synthesized in low yield (Table 2.4). The yields of PBRs with these amines are substantially lower than with the amines reported above which successfully produced PBRs. This is likely due to the steric hindrance caused by the acetal or the closer proximity of the hydroxyl groups in reactions reported in Table 2.4; in addition, 2-octanamine is a 2° amine and all of the higher yielding amines reacted are 1°.

## 2.7. Biomimetic Synthesis of the All-*Trans*-Retinal Dimer (43)

A new retinoid derivative, the all-*trans*-retinal (ATR) dimer (**43**), was found in retinal pigment epithelial (RPE) cell fluorophores by Fishkin *et al*.[5] The authors also synthetically prepared the ATR dimer (**43**) by treating ATR (**4**) with 1 equivalent of sodium hydride (NaH) in dry tetrahydrofuran (THF) using a method developed by Verdegem.[6]

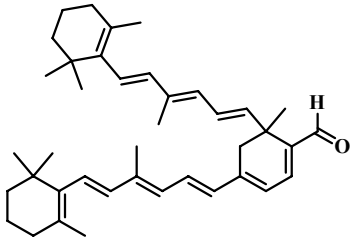


**All-*trans*-retinal (ATR) dimer, 43**
Chemical Formula: $C_{40}H_{54}O$
Exact Mass: 550.4
Molecular Weight: 550.9

**Figure 2.1 Structure of ATR dimer**

When we synthesized A2-ethanolamine (A2E, **1**) *via* the biomimetic method proposed by Parish et al,[1] we found the ATR dimer (**43**) generated as a byproduct (Table 2.5). This marks the first time that the ATR dimer was observed as a result of a biomimetic synthesis. Previously the only synthesis was observed as a result of using harshly basic conditions. We show that the ATR dimer is also formed under mildly acidic conditions.

We decided to analyze some of the other reactions listed in previous sections for the ATR dimer side product (Table 2.5) and found that in 4 out of 5 reactions analyzed, that the ATR dimer was indeed forming in low yield. The ATR dimer formed when ATR was reacted with the alkyl amines, ethanolamine, propanolamine, NPD and EAE, but did not form in the reaction with the aromatic tyramine (4-(2-aminoethyl)phenol).

The low yields of the ATR dimer in the biomimetic syntheses are likely due to several factors; many of these are similar to those for PBRs. First, PBRs and ATR dimer have many double bonds that easily isomerize. Second, they are highly sensitive to light; ambient light exposure may have caused undesired photooxidation and decomposition, even though all reactions and purifications were done in the dark. Photo-oxidation products were continually observed by MS. Third, ATR and PBRs are unstable at room temperature due to the reactivity of their polyene structures and the ATR aldehyde. Fourth, some PBR and ATR dimer products may be lost in the process of chromatography—2 to 3 columns per reaction has been necessary to isolate them without impurities. Additionally, most of the ATR reacts with the amine in the biomimetic reactions to

produce PBRs, decreasing the possibility to afford dimer. Finally, the dimer is an unstable aldehyde with adjacent bulky quaternary carbons, so they may not be stable.

**Table 2.5 Biomimetic Synthesis of the All-*Trans*-Retinal Dimer**

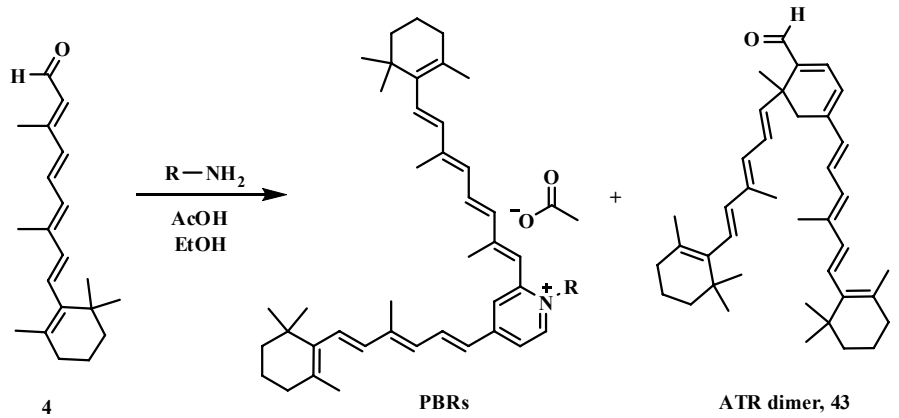


4 PBRs ATR dimer, 43

| Entry | Amines | R= | yield %, PBRs | yield %, 43 |
|---|---|---|---|---|
| 1 | Ethanolamine, 5 | 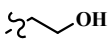 | 18 | 3[7] |
| 2 | Propanolamine, 24 | 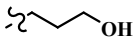 | 13 | 3 |
| 3 | Tyramine, 18 | 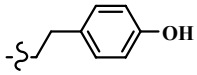 | 15 | 0 |
| 4 | NPD, 26 | 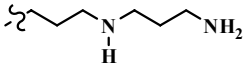 | 0 | 4 |
| 5 | EAE, 28 | 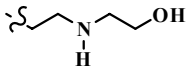 | 0 | 4 |

Initially when we found the ATR dimer as a side–product in the synthesis of A2E, we examined the MS of products formed during the preparation of PBRs, A2P and A2T. A large peak at 551.4249 (Figure 2.2 A), belonging to the ATR dimer, was observed in the

synthesis of A2P. When A2T was synthesized the MS did not show any peak related to the ATR dimer (Figure 2.2 B).

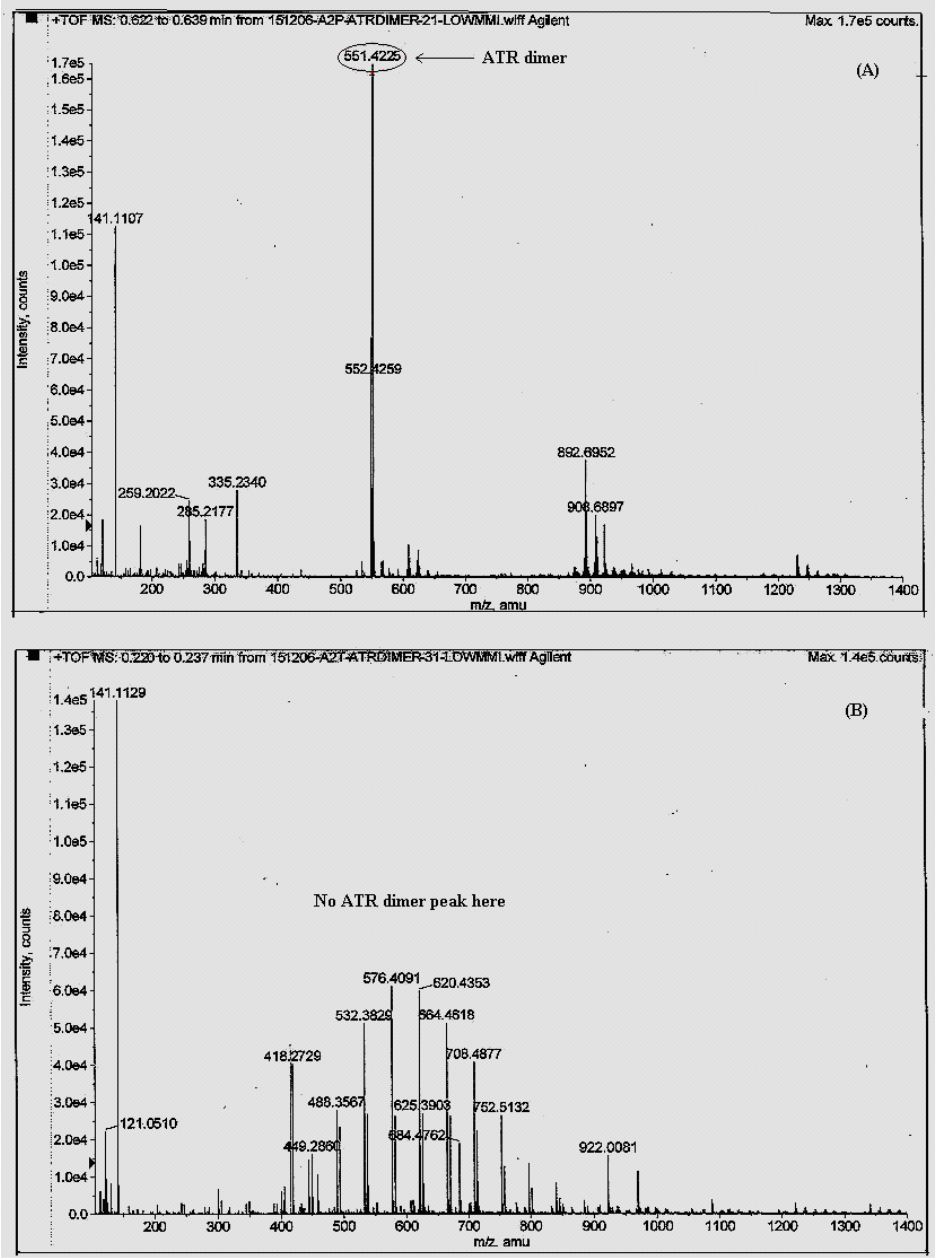


**Figure 2.2. MS of ATR dimer: (A) In preparation of A2P;**

**(B) In preparation of A2T.**

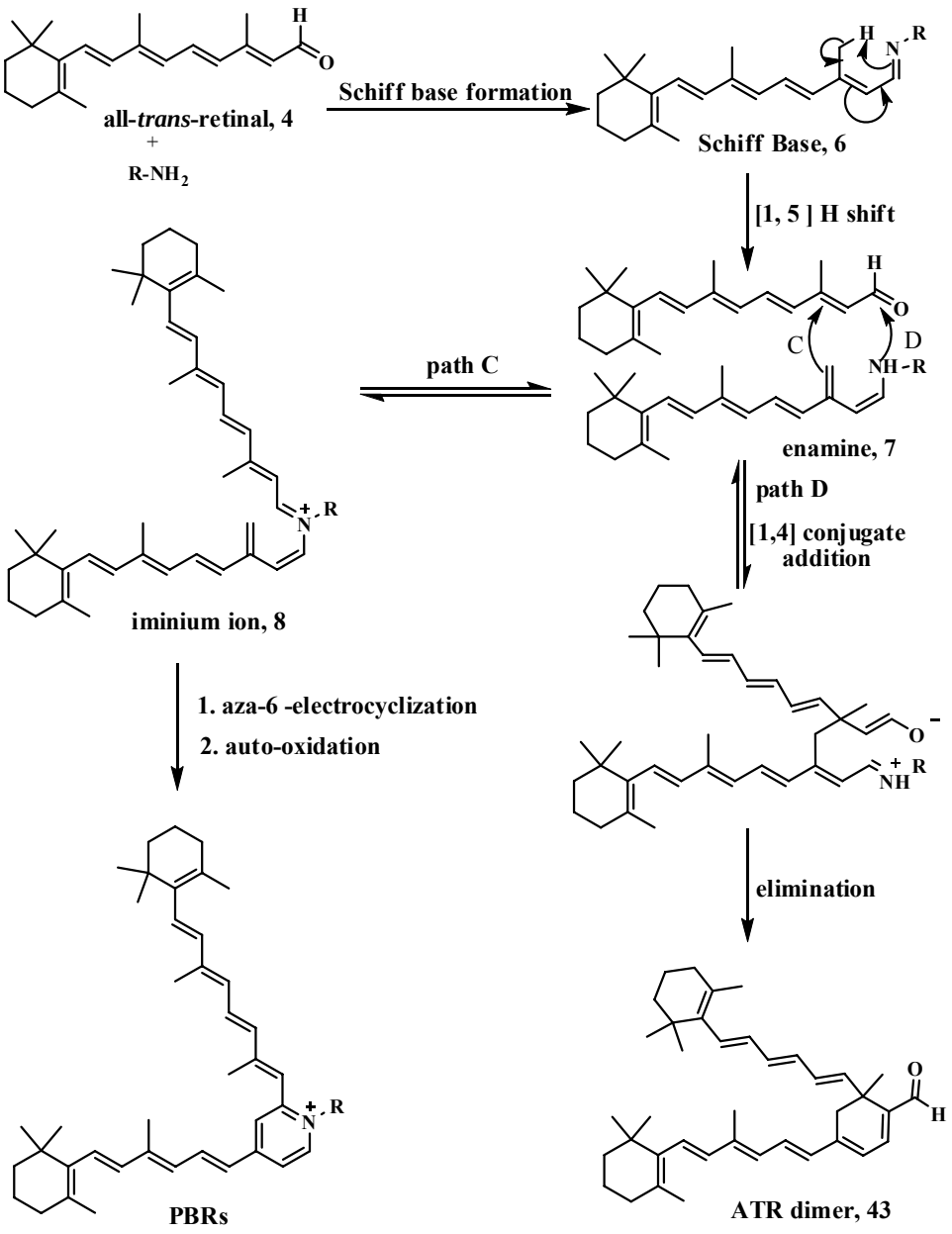


**Scheme 2.3 Synthesis of ATR dimer and PBRs**

To explain why the ATR dimer was formed in preparation of A2E and A2P but not in A2T, we analyzed the biosynthetic pathway of the ATR dimer and A2E proposed by Fishkin (Scheme 2.3).[5] In Scheme 2.3 the general path is illustrated towards all PBRs

(path C). Path C and path D are competitive and path C is favorable in the case of preparation of A2E, A2P, and A2T.

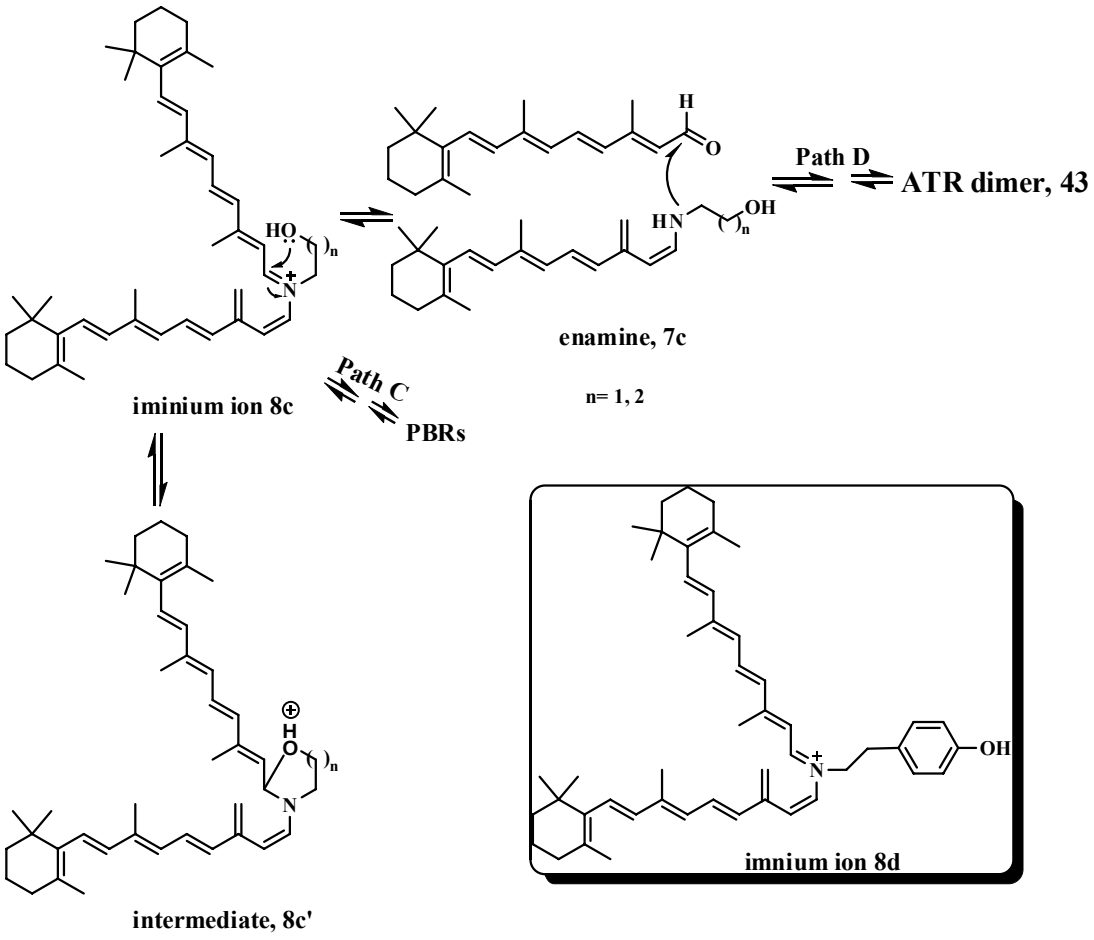


**Scheme 2.4 ATR Dimer *vs* PBR Formation**

When ethanolamine and propanolamine were used in the reaction, the hydroxyl group of iminium ion **8c** (Scheme 2.4) can attack the carbon of the iminium ion to form the 5 or 6-member-ring **8c'**. Cyclic **8c'** competes the progression of path C and equilibrates back to the enamine 7c. This process makes the enamine more available to proceed on path D which leads to the formation of the ATR dimer. The hydroxyl group in

tyramine is much less likely to form a 9-membered cyclic intermediate, because the rigid aromatic ring (iminium ion **8d**) won't allow the hydroxyl group to attack the carbon of the iminium ion. Therefore, the iminium ion continues on path C unimpeded, resulting in the formation solely of A2T without the ATR dimer side–product.

To test our proposed theory, we examined two other reactions for the existence of the ATR dimer—the ATR reactions with NPD and EAE (Table 2.5). As indicated in Scheme 2.3, the 5 or 6-member-ring intermediate likely forms in these reactions. The β and γ nitrogens in NPD and EAE amines are more nucleophilic than that of the oxygens in ethanolamine and propanolamine, and therefore form more stable 5 or 6 member ring intermediates **8b**. These intermediates impede intermediate **8b** in Scheme 2.2 from proceeding through an aza-6π-electrocyclization to continue on path C. Instead they equilibrate back to intermediate **7b**, which may then follow path D and generate ATR dimer **43**. This is why PBR products, A2NPD and A2EAE, were not observed in these reactions and the ATR dimer was formed.

## 2.8 Summary and Conclusions

It has been demonstrated that the biomimetic synthetic method proposed by Parish et al. [1] can be applied efficiently to the syntheses of PBRs other than A2E. This approach can be further used to access ATR dimer, when ATR is reacted with alkyl amines that have a nucleophilic atom which enables the formation of 5- or 6-membered ring intermediates.

The experimentation summarized in this thesis shows that the most important aspect in synthesizing the reported PBRs is the amine's structure. The β or γ nucleophilic heteroatoms in the amines may direct the reaction mechanism along a pathway that does not lead to PBRs or greatly decreases their yields, while increases the possibility of forming the ATR dimer. The more nucleophilic the β or γ heteroatom, the more likely the ATR dimer will be produced.

Finally, the syntheses of eight novel PBRs have been reported. Each of these can now be investigated for their involvement in age-related macular degeneration or as potential anticancer agents, by evaluating their reactivity, photochemistry, and cytotoxicity.

**2.9 References**


1. Parish, C. A.; Hashimoto, M.; Nakanishi, K.; Dillon, J.; Sparrow, J. R. *Proc. Natl. Acad. Sci. USA* **1998**, *95*, 14609–14613.
2. Pezzella A.; Prota G. *Tetrahedron Lett.* **2002**, *43*, 6719–6721.
3. Ren, R. X. F.; Sakai, N.; Nakanishi, K. *J. Am. Chem. Soc.* **1997**, *119*, 3619–3620.
4. Tanaka, K.; Mori, H.; Yamamoto, M.; Katsumura, S. *J.Org. Chem.* **2001**, *66*, 3099–3110.
5. Fishkin, N. E.; Sparrow, J. R.; Allikmets, R.; Nakanishi, K. *Proc. Natl. Acad. Sci. USA*, **2005**, *102*, 7091–7096.

6. Verdegem, P. J. E.; Monnee, M. C. F.; Mulder, P. P. J.; Lugtenburg, J. *Tetrahedron Lett*. **1997**, *38*, 5355–5358.

7. Alvarez, M. A. L. Pyridinium *Bis*-Retinoids: Extraction, Synthesis, and Folate Coupling. M.S. Thesis, Brigham Young University, April 2007.

## Chapter 3. Blue-Light Irradiation of Pyridinium Bisretinoids

### 3.1. Introduction

As described in Chapter 1, the fluorophore A2E (**1**, Figure 3.1), has been observed to form a series of oxidation products when exposed to blue light (Figures 1.8 and 1.9).[1-3] Jang et al.[3] used UV-vis spectroscopy to follow the photo-oxidation and to identify which retinoid chain on A2E was being chemically altered. The UV-vis absorption wavelength of 337.4 nm corresponds to the shorter retinoid chain in A2E (**1**, $\lambda_{max}$ S, Figures 3.1 and 3.2) and of 440.4 nm corresponds to the longer chain ($\lambda_{max}$ L). Oxidation on either chain of A2E leads to a hypochromic shift in the corresponding wavelength. In the UV-vis spectrum of monofuran-A2E (**13,** Figure 1.9) and monoperoxy-A2E (**16**), only $\lambda_{max}$ S is blue-shifted, while both $\lambda_{max}$ S and L are blue-shifted by about 40 nm in bisfuran-A2E (**14**) and bisperoxy-A2E (**15**).

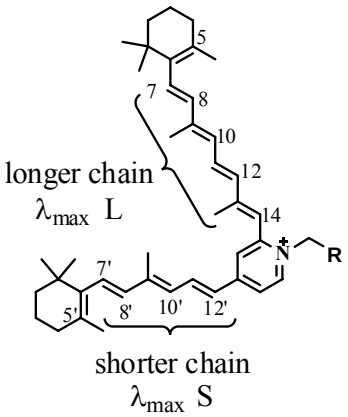


R = $CH_2OH$, A2E, **1**

R= $CH_2CH_2OH$, A2P, **34**

R = $CH_2OCH_2CH_2OH$, A2EE, **37**

R = $CH(OCH_3)_2$, A2DM, **39**

**Figure 3.1. Generic Pyridinium Bisretinoid Compounds**

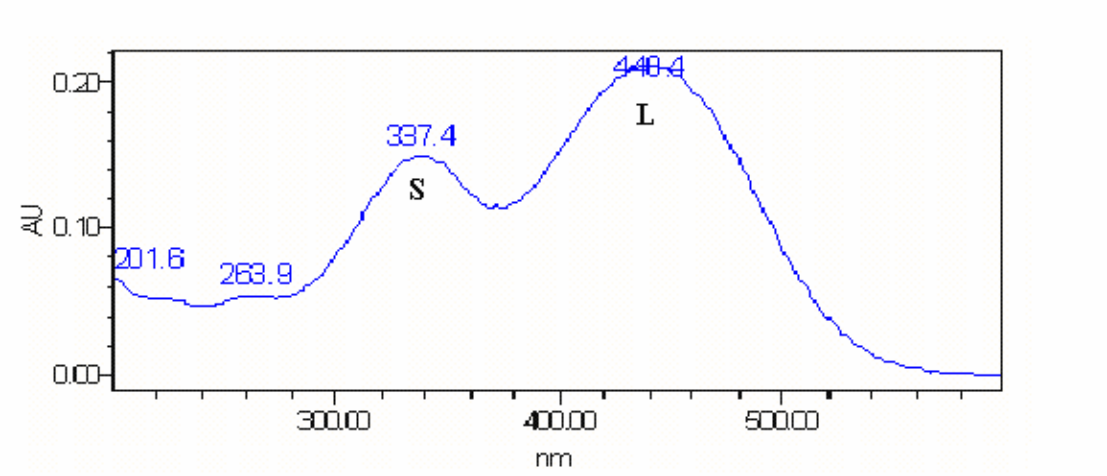


**Figure 3.2. UV-vis Spectrum of A2E**

Because of the facile photo-oxidation of A2E, we proposed that other homologous PBRs should exhibit similar photoreactivity. We irradiated a selection of PBRs with blue light (Figure 3.3) and analyzed their photoproducts using electrospray ionization-mass spectrometry (ESI-MS) and HPLC.

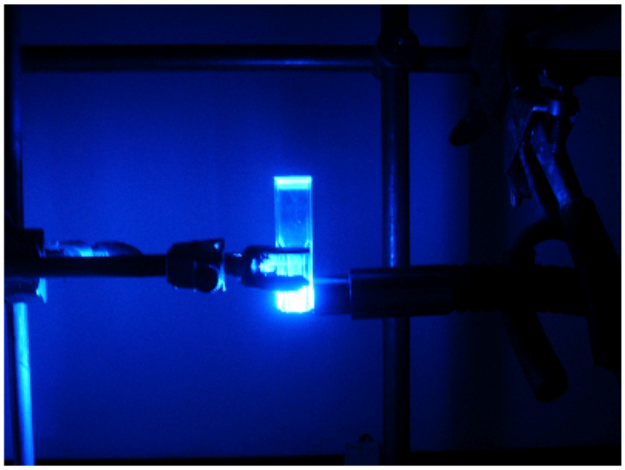

**Figure 3.3. Photo-oxidation Experiment Setup**

### 3.2. Blue-Light Irradiation of A2-Propanolamine

A2-Propanolamine (A2P, **34**, Figure 3.1) was exposed to blue light (442 ±10 nm) for five hours. Samples were taken every hour starting immediately prior to irradiation (0 hours) and analyzed by ESI-MS and HPLC. The MS results for A2P irradiation at zero, one, four, and five hours are shown in Figure 3.4.

Prior to irradiation (0 hours), the MS shows a single peak with a mass-to-charge ratio (*m/z*) of 606, corresponding to the unoxidized pyridinium bisretinoid, A2P (**34**). After one hour of irradiation, seven oxidation products appeared, each in increments of +16 from the last, starting at the peak with an *m/z* of 622. This peak is consistent with the addition of one oxygen atom to A2P. Peaks with *m/z* 638, 654, 670, 686, 702, and 718 likely represent the addition of two, three, four, five, six, and seven oxygen atoms on either or both of the two retinoid arms of A2P. The highest intensity peak after one hour of irradiation has an *m/z* of 638 (bisoxygenated A2P), the next highest has an *m/z* of 654 (trioxygenated A2P), and the next has an *m/z* of 622 (mono-oxygenated A2P). The MS results of A2P blue-light irradiation at two and three hours are similar to those observed after one hour of irradiation.

The longer that A2P is exposed to blue light the more A2P deceases in concentration and its oxidation products increase. After four hours of irradiation the MS shows almost complete consumption of A2P, while the purported mono-, bis-, and tri-oxygenated A2P compounds (*m/z* 622, 638, and 654) have all increased in concentration.

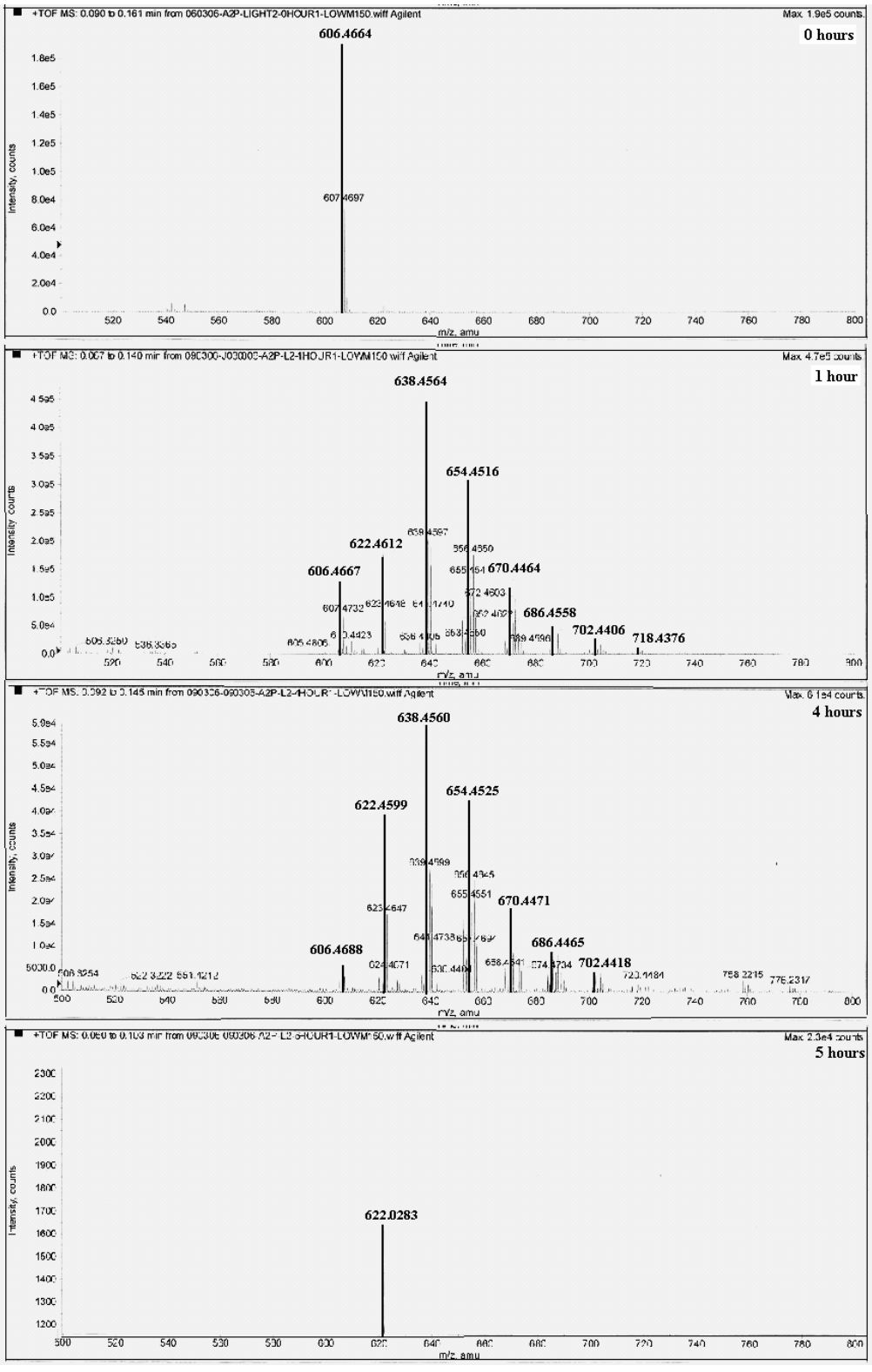


**Figure 3.4. ESI-MS Spectra of A2P Blue-Light Irradiation**

After five hours of irradiation, no A2P (*m/z* 606) was observed and only a trace amount of bisoxygenated A2P (*m/z* 638) showed up on the MS. In summary, the ESI-MS results show that A2P formed seven oxidation products during irradiation (*m/z* 622, 638, 654, 679, 686, 702 and 718), which fluctuate in concentration depending on the length of irradiation.

Like A2E, A2P has one shorter and one longer retinoid chain attached to its pyridinium ring (R = $CH_2CH_2OH$, A2P, **34**, Figure 3.1). Jang et al.[3] found that A2E's short retinoid chain is more readily oxidized than its longer chain. We examined which A2P chain was more reactive using HPLC analysis.

The irradiation process of A2P was analyzed by comparing its HPLC data before irradiation (0 hours, Figure 3.5) and after one hour of irradiation (1 hour). The HPLC data after 2-5 hours of irradiation did not show any significant A2P or oxidation peaks, which suggests that the A2P was converted into a complex mixture of products after 2 hours; only the MS was sensitive enough to pick up signals from these products.

Prior to irradiation, HPLC reveals a single peak with a retention time of 9.60 minutes. After one hour of exposure to blue light, additional peaks appeared. The UV-vis profile of the peaks labeled B reveals an absorbance at 227.4 nm. These peaks could be solvent front, although they are not present before irradiation (0 hours). The peaks are likely some type of A2P degradation products, but from UV-vis analysis they do not appear to be oxidized A2P.

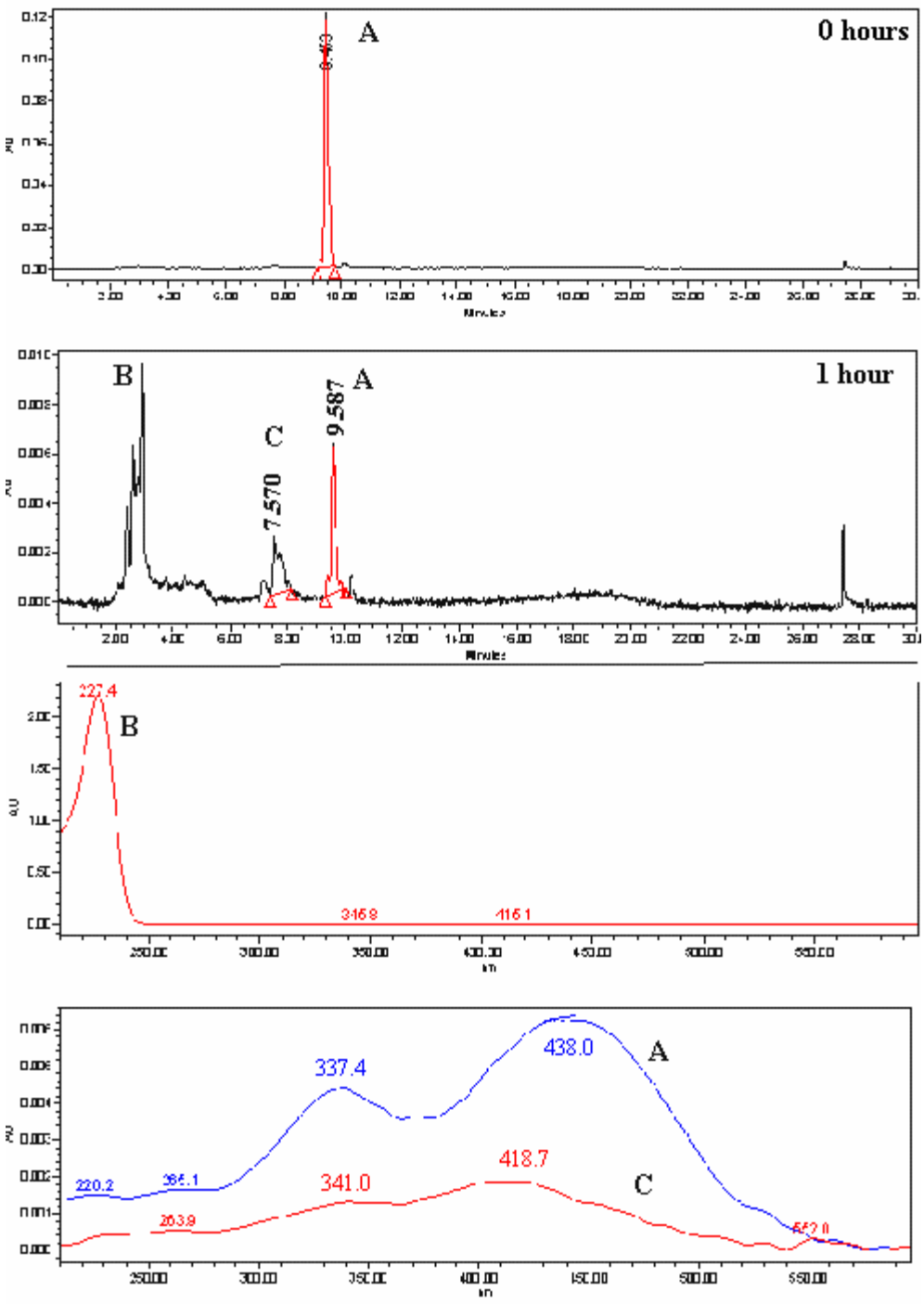


**Figure 3.5. HPLC Results of A2P Blue-Light Irradiation**

The UV-vis spectrum of peak C was also examined and appears to be a mono-oxidation product of A2P (**44**, **45**, or **46**, R = $CH_2CH_2OH$, Figure 3.6). Comparing

the UV-vis of peak C to that of peak A, the initial oxidation of A2P appears to occur on the longer retinoid chain. A blue shift of 20 nm from 438 to 418 nm occurs after irradiation, which suggests a loss of conjugation on the longer retinoid chain. No significant change is observed in $\lambda_{max}$ S, which moved from 341 to 337 nm. These results suggest that A2P's longer retinoid chain is more photoreactive than its shorter chain.

The oxidation product mixtures of A2E and A2P are complicated. On A2E, the short retinoid chain is oxidized first (**13** and **16**, Figure 1.9), and on A2P, which simply has one additional methylene, the long retinoid chain is oxidized first (**44–46**, R = $CH_2CH_2OH$, Figure 3.6). Additionally, the maximum number of oxygen atoms added to A2E is nine when it is photo-oxidized, while we only observed the addition of seven oxygen atoms to A2P.

In the oxidation of A2P, the HPLC results appear to conflict with the ESI-MS results, because HPLC reveals more mono-oxidation and MS reveals more bisoxidation. Because MS is not a good tool for quantification, it is possible that the bisoxidation product simply flies better in the MS than the mono-oxidation product.

The ESI-MS and HPLC data collected in A2E's photo-oxidation studies,[1-3] as well as for A2P's photo-oxidation, were all taken into account when assigning structures for A2P's possible oxidation products. Some of the possible A2P oxidation products are shown in Figure 3.6.

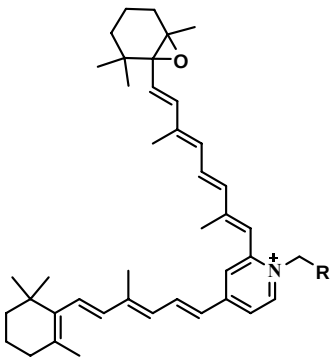

**5,6-epoxide-PBR**, **44**

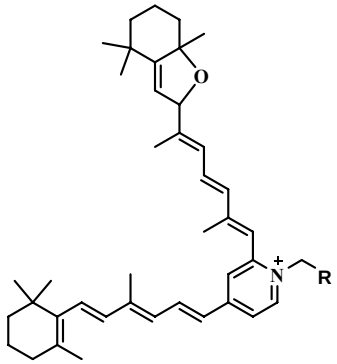

**monofuran-PBR**, **45**

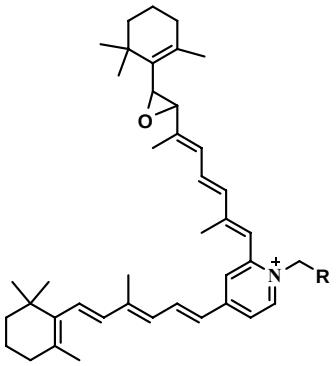

**7,8-epoxide-PBR**, **46**

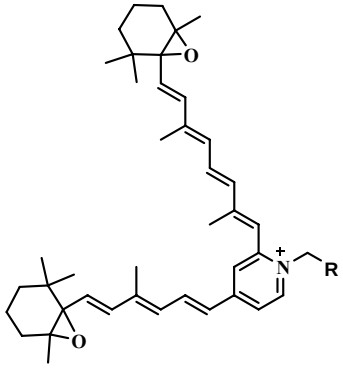

**bisoxirane-PBR**, **47**

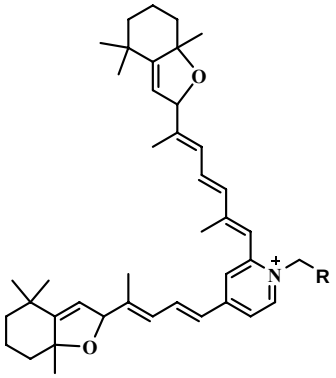

**bisfuran-PBR**, **48**

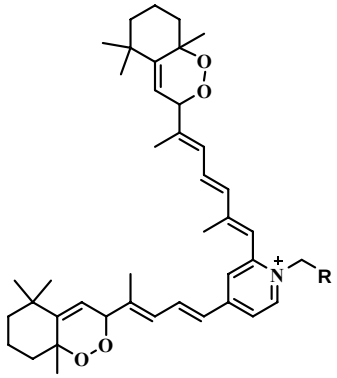

**bisperoxy-PBR, 49**

**Figure 3.6. Possible Photo-oxidation Products of PBRs**

R= $CH_2CH_2OH$, PBR=A2P, **34**
R = $CH_2OCH_2CH_2OH$, PBR=A2EE, **37**
R = $CH(OCH_3)_2$, PBR=A2DM, **39**

A2P's oxidation likely starts with the formation of the epoxides (**44**, **46**, and **47**) and then rearranges to the furanoxides (**45** and **48**). The MS peak with an *m/z* of 670 is

associated with the addition four oxygen atoms to A2P. Because tetraoxygenated A2E is reported to be the bisperoxy A2E (**15**, Figure 1.9),[3] the proposed structure for tetraoxygenated A2P is likewise the bisperoxy compound (**49**, R = $CH_2CH_2OH$, Figure 3.6). The oxidation products of these PBRs are difficult to deconvolute, and we are only beginning to gain small insights into their structures.

### 3.3. Blue-Light Irradiation of A2-2-(2-Aminoethoxy)ethanol

Because A2-2-(2-aminoethoxy)ethanol (A2EE, **37**, Figure 3.1) is similar in structure to A2E (**1**), but with an additional hydroxyethyl group, we proposed that A2EE might produce similar photo-oxidation products to A2E (**1**) and A2P (**34**). Photo-oxidation of A2EE (**37**) was performed using the same methods described for A2P (**34**, Section 3.2). Aliquots were taken every hour for five hours, and the reaction was monitored by ESI-MS and HPLC.

The ESI-MS results prior to irradiation of A2EE (0 hours) reveal a single peak with an *m/z* of 636, corresponding to pure A2EE. At one hour, three new peaks with *m/z* 652, 668 and 684 appear, suggestive of A2EE oxidation products containing one to three new oxygen atoms (Figure 3.7). The ratio of A2EE to the three new MS oxidation peaks after one, two, and three hours is similar to that shown in Figure 3.7 after one hour of irradiation; A2EE is still clearly the predominant MS peak.

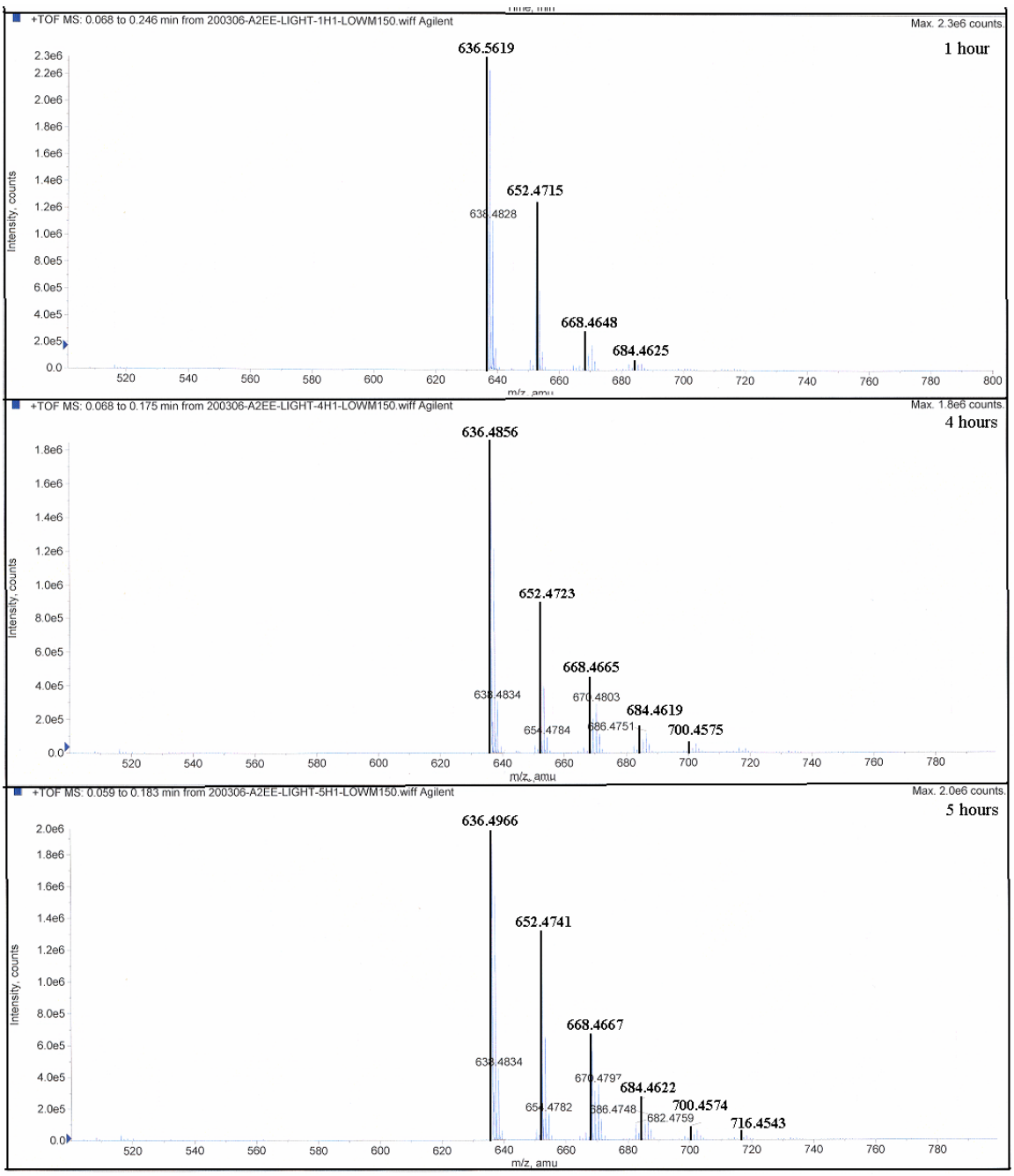


**Figure 3.7. ESI-MS of A2EE Blue-Light Irradiation**

After four hours of blue-light irradiation, a fourth, smaller oxidation peak with an *m/z* of 700 is observed, suggestive of tetraoxygenated A2EE. The ratio of bis- to mono-oxygenated A2EE also increases. Finally, at five hours, the ratios of oxidation

peaks to the parent A2EE peak changes even more significantly. At this point the mono-oxidation peak with an *m/z* of 652 is closer in intensity to the A2EE peak with an *m/z* of 636 compared to previous hours. Additionally, a new oxidation peak (*m/z* 716) appeared, corresponding to the addition of five oxygen atoms to A2EE.

Throughout the five hours of blue-light irradiation, the peak with an *m/z* of 636, corresponding to A2EE, was the most abundant. The next largest peak corresponded to bisoxygenated A2EE (*m/z* 652). The peaks corresponding to higher oxygenated products (tri-, tetra-, and penta-) decreased in intensity respectively as the number of oxygen atoms increased. The longer A2EE was exposed to blue light, however, the more its associated peak decreased in intensity as the oxidation product peaks increased. Overall, the turnover from the parent A2EE to its oxidation products did not occur as readily as it did for A2E (with nine oxidation products) and A2P (with seven oxidation products).

HPLC was also used to monitor the oxidation of A2EE. Figure 3.8 shows a chromatogram before blue-light irradiation, as well as after four hours of irradiation. The data after one, two, and three hours is not shown, because no significant oxidation products were observed until four hours. Likewise, the data after five hours of irradiation is not shown, because it is similar to that observed after four hours.

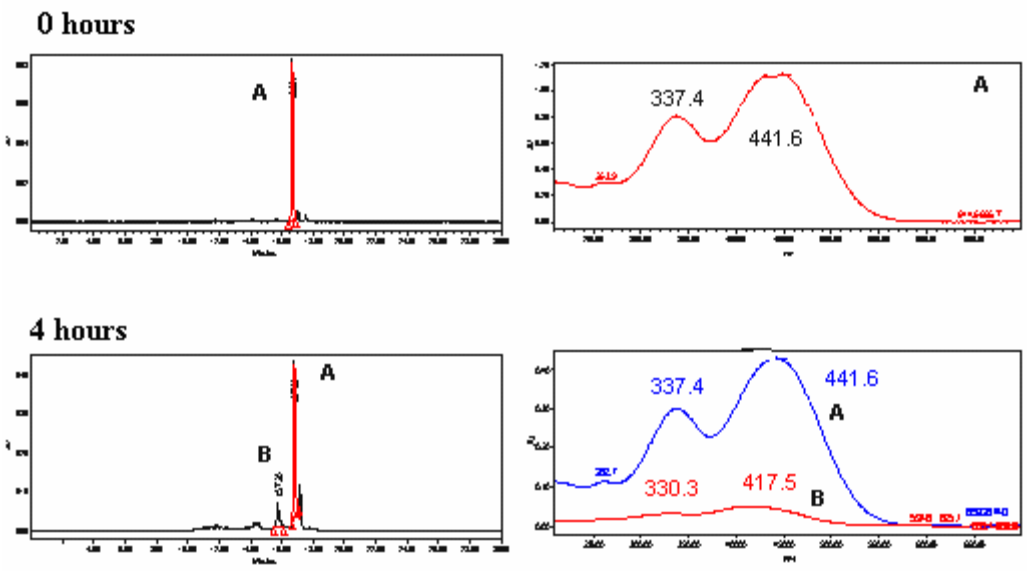


**Figure 3.8. HPLC Results of A2EE Blue-Light Irradiation**

Before irradiation, a single peak (**A**, 0 hours), corresponding to A2EE, has a UV-vis spectrum with two wavelength maxima at 337 and 441 nm. In Figure 3.1, $\lambda_{max}$ S corresponds to 337 nm and $\lambda_{max}$ L corresponds to 441 nm for A2EE (**37**), R = $CH_2OCH_2CH_2OH$.

After four hours of irradiation, approximately 75 % of the A2EE still remained and new peaks appeared (Figure 3.8, 4 hours). The UV-vis spectrum of peak B, the largest of the new peaks, was compared to that of A2EE. We observe that only $\lambda_{max}$ L of peak B is significantly blue shifted (from 441 nm to 417 nm). This suggests that peak B might be mono-oxygenated A2EE (*m/z* of 652), which is also the second most intense peak observed on MS at 4 hours (Figure 3.7). Based on the UV-vis data, A2EE appears to be oxidized first on its longer retinoid chain (**44**, **45**, or **46**, R = $CH_2OCH_2CH_2OH$, Figure 3.6).

In summary, A2EE does not appear to be as labile to photo-oxidation as A2E and A2P. A2EE forms a total of 5 oxidation products after five hours. Its longer retinoid chain appears to more readily photo-oxidize than the shorter one.

### 3.4. Blue Light Irradiation of A2-Aminoacetaldehydedimethylacetate

Photo-oxidation of A2-aminoacetaldehydedimethylacetate (A2DM, **39**, Figure 3.1) was performed using the same methods described for A2P (**34**, Section 3.2). Figure 3.10 shows the ESI-MS results of photoirradiation of A2DM (**39**) at one and three hours. Before irradiation a single peak is observed with an *m/z* of 636, corresponding to A2DM. After one hour, six new peaks were formed starting from *m/z* 652 and increasing in increments of +16. The most abundant peak at 1 hour corresponds to mono-oxygenated A2DM. Peaks at *m/z* 668, 684, 700, 716, and 732 correspond to the addition of two, three, four five and six oxygen atoms to A2DM. The MS results at two hours are similar to that at one hour except that the peak with an *m/z* of 668 (bisoxygenated-A2DM) is the largest one.

At 3 hours A2DM's peak (*m/z* 636) was small compared to its oxidation product peaks, and the bisoxygenated-A2EE peak (*m/z* 668) was still at the highest intensity. After 4 hours, all of the A2DM was consumed and only its oxidation products were observed.

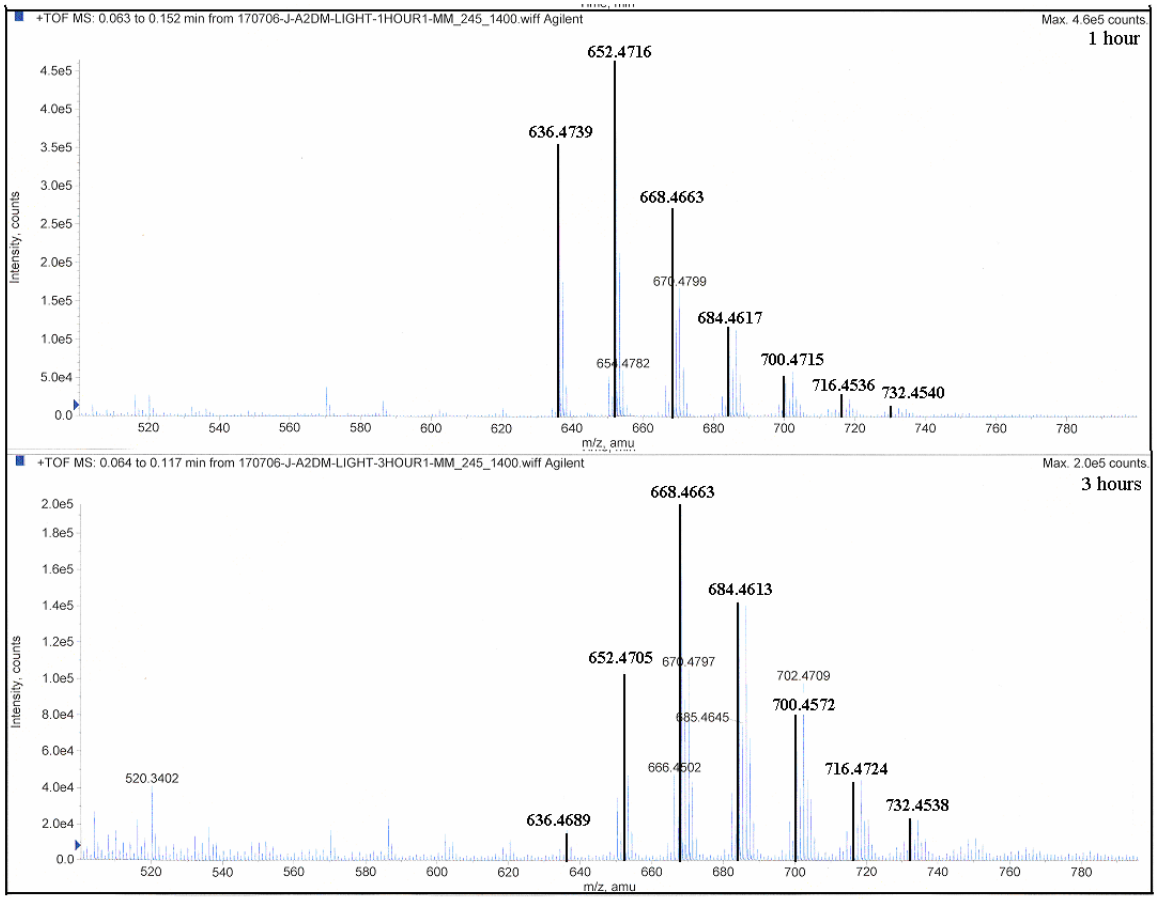


**Figure 3.9. ESI-MS of A2DM Blue-Light Irradiation**

HPLC analysis was performed as described in previous sections. A2DM was analyzed before blue-light irradiation and after one and two hours of irradiation. The corresponding HPLC chromatograms and UV-vis spectra are shown in Figure 3.10. The HPLC data at 0 hours show all-*trans* A2DM as the major peak (**B**), as confirmed by UV-vis, as well as 3 additional peaks. Peaks **A** and **C** appear to be *cis*-isomers of A2DM, and peak **D** is all-*trans*-retinal.

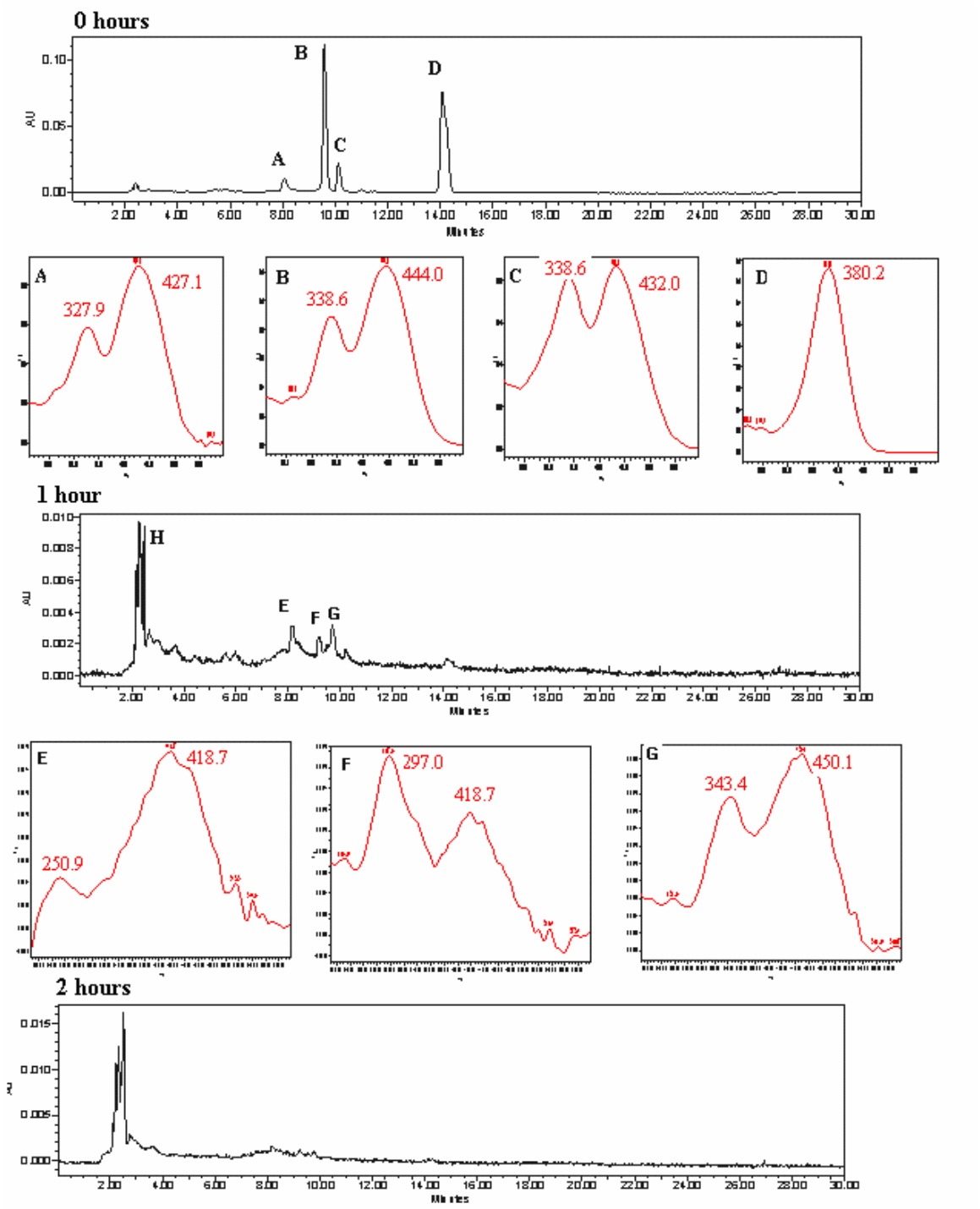


**Figure 3.10. HPLC Results of A2DM Blue-Light Irradiation**

After one hour, irradiation peaks E, F, G, and H appeared and no obvious A2DM peak was observed. MS data at one hour still shows the presence of A2DM, so it is likely

in quantities that are undetectable by HPLC. Based on the UV-vis data, peak E appears to be trioxidized A2DM, with more loss of conjugation on $\lambda_{max}$ S, than on $\lambda_{max}$ L (Figure 3.l). Peak F appears to be a bisoxidized compound, such as one of the compounds suggested in Figure 3.6. Peak G corresponds with an isomer of all-*trans* A2DM, and Peak H is solvent front or otherwise degraded A2DM.

After 2 hours, no A2DM peak was observed, which again likely has to do with the trace quantities that remain and are only detectable by MS. No A2DM or oxidation products were detected by HPLC after three hours. MS detected only small quantities of these compounds. A2DM appears to be more readily oxidized than A2P and A2EE, with even the trioxygenated compound observed by HPLC/UV-vis. Although A2DM can only form six oxidation products compared to the seven products observed for A2P, the oxidation of A2DM happens at a faster rate.

### 3.5. Summary and Conclusions

The blue-light irradiation of three novel pyridium bisretinoids has been studied using ESI-MS and HPLC chromatography. The results demonstrate that A2P, A2EE, and A2DM are photo-oxidized in the presence of blue-light. Analysis of the results by MS and HPLC revealed that epoxide, furanoxide, and peroxide oxidation products are forming—similar to the types of oxidation products formed by irradiation of A2E. A comparison of the UV-vis spectra suggest that the initial position of oxidation varies, as well as the rate of oxidation, and the number of total oxygen atoms added to each

molecule. The data still show that A2P and A2DM are far more efficiently oxidized under blue light than A2EE.

### 3.6. References


1. Dillon, J.; Wang, Z.; Avalle, L. B.; Gaillard, E. R. *Exp. Eye Res.* **2004**, *79*, 537-542.

2. Ben-Shabat, S.; Itagaki, Y.; Jockusch, S.; Sparrow, J.R.; Turro, N. J.; Nakanishi, K. *Angew. Chem. Int. Ed.* **2002**, *41*, 814–817.

3. Jang, Y. P.; Matsuda, H.; Itagaki, Y.; Nakanishi, K.; Sparrow, J. R. *J. Biol. Chem.* **2005**, *280*, 39732–39739.

## Chapter 4. Photoactivated Cytotoxicity of Pyridinium Bisretinoids

### 4.1. Introduction

The photoreactivity of A2E is illustrated in Chapter 1.[1-6] In addition to the cytotoxicity of photoirradiated A2E in RPE cells, results obtained in our laboratory indicate that A2E demonstrates photoinduced cytotoxicity in a selection of cancer cell lines.[7] Since A2P and A2EE (Chapter 2), which are structurally similar to A2E, were also photo-oxidized when irradiated with blue light (Chapter 3), we hypothesized that these compounds would undergo phototriggered cytotoxicity in HL-60 (human promyelocytic leukemia) cells.

To test this hypothesis, A2P and A2EE were incubated with HL-60 cells in 24-well plates for 24 hours and then irradiated using a 476 mW/cm$^2$ fiber optic source with a 442 nm (blue) filter (Figure 4.1). A range of drug concentrations and irradiation times were tested in order to find the optimal conditions, where the maximum number of irradiated cells[1] loaded with PBRs were killed compared to the controls. After irradiation and further incubation, we assayed the number of viable cells and compared these with control samples, which were not loaded with a PBR or not irradiated. In each experiment, either the trypan blue cell count (TBCC) procedure or the 3-(4,5-dimethyl-2-thiazolyl)-2-5-diphenyl-2H-tetrazolium bromide (MTT) assay was used to evaluate the response of the HL-60 cells to A2P and A2EE.

[1] *Cells* in this chapter refers to *HL-60 cells*, unless otherwise stated.

Trypan blue is the most common stain used to distinguish viable cells from nonviable cells. Only nonviable cells absorb the dye, appear blue, and may also be asymmetrical. The viable cells do not absorb the dye, appear refractile, and remain round.

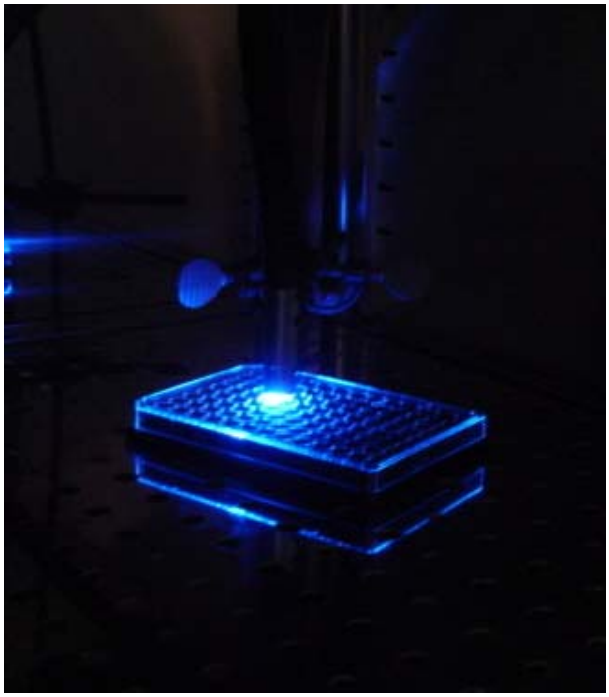

**Figure 4.1. Irradiation Setup**

The MTT assay is a standard colorimetric assay for measuring cellular proliferation. The yellow MTT is reduced to purple formazan in the mitochondria of living cells. This reduction only takes place when mitochondrial reductase enzymes are active, and therefore conversion can be directly related to the number of viable cells.

In column graphs showing the results of the cell assays, the heights of the columns are proportional to the cell viability. The red columns represent the cell viability

without any light exposure and the blue ones indicate the cell viability after blue light irradiation. The experiments were performed two or more times. Standard deviations were calculated and shown with error bars. All p-values in this chapter are calculated using the two tail type three t-test. If the reported p-values are below 0.05, then the two sets of experiments being compared are considered statistically significant.

## 4.2. Photoactivated Cytotoxicity of A2-Propanolamine in HL-60 Cells

***4.2.1. Optimization of A2P concentration.*** A2P (5 and 10 μM) was incubated with HL-60 cells for 24 hours and irradiated with blue light for 45 minutes. Media control experiments were performed with and without irradiation and with and without DMSO. Figure 4.2 illustrates the cell viability after incubation and irradiation as determined by the TBCC procedure.

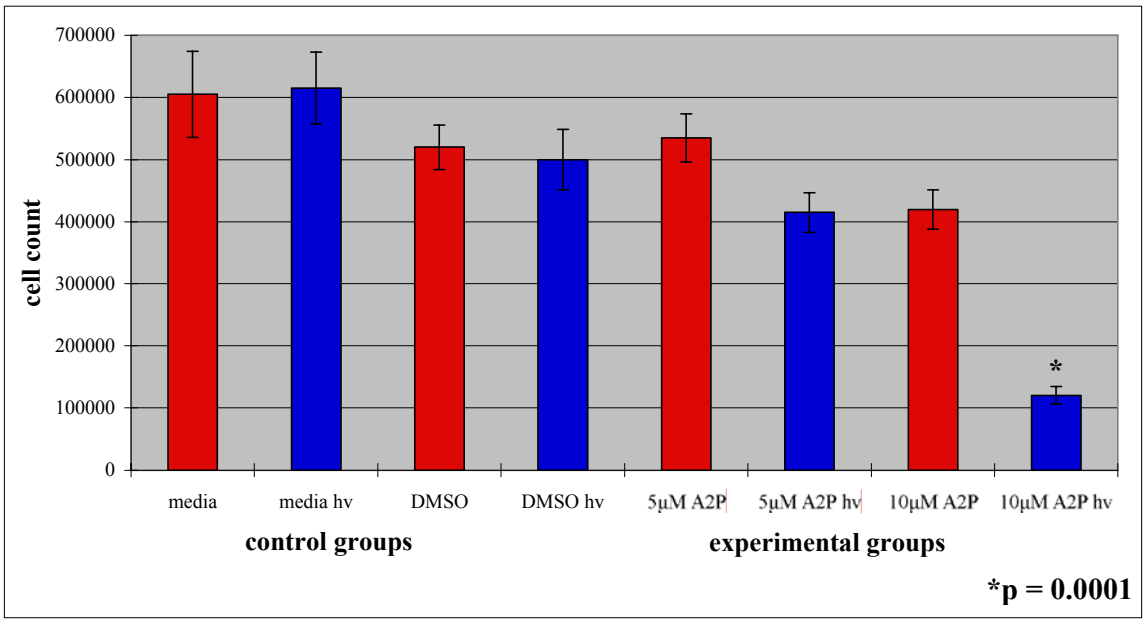


**Figure 4.2. A2P incubated in HL-60 cells with 45 minute blue-light irradiation.**

The control experiments performed with and without irradiation and with and without DMSO showed no statistically significant differences ($p > 0.5$), which means that light exposure and DMSO alone did not cause cell death. In addition, no statistically significant differences were observed when the media and DMSO controls were directly compared ($p > 0.1$) and when the 5 and 10 μM A2P experiments were compared to the media controls ($p > 0.1$ and 0.05, respectively). When 5 μM A2P was incubated with HL-60 cells with and without blue light irradiation no significant cell death was observed ($p > 0.5$). The irradiation of cells incubated with 10 μM A2P resulted in 80 % cell death compared to the nonirradiated samples of 10 μM A2P ($p = 0.0001$). The data show that 45-minute blue-light irradiation of 10 μM A2P effectively kills HL-60 cells.

***4.2.2. Optimization of A2P irradiation time.*** To determine the optimum blue-light irradiation time, we performed the celluar assays described above on 10 μM A2P and irradiated for 30 and 40 minutes. This time we used the MTT assay to determine cell viability. No statistically significant differences were observed when A2P was irradiated for 30 minutes ($p > 0.1$); therefore, only the data for the 40 minute irradiation is shown in Figure 4.3.

The analysis of the controls with and without irradiation, with and without DMSO, and directly comparing the media and DMSO controls showed no statistically significant differences ($p > 0.5$). Furthermore, no statistically significant differences were observed when 10 μM A2P experiments were compared to the media controls ($p > 0.05$). The irradiation of cells with 10 μM A2P resulted in >80 % cell death compared to the nonirradiated samples of 10 μM A2P ($p < 0.01$). The data show that 40-minute blue-light

irradiation of 10 μM A2P effectively kills HL-60 cells.

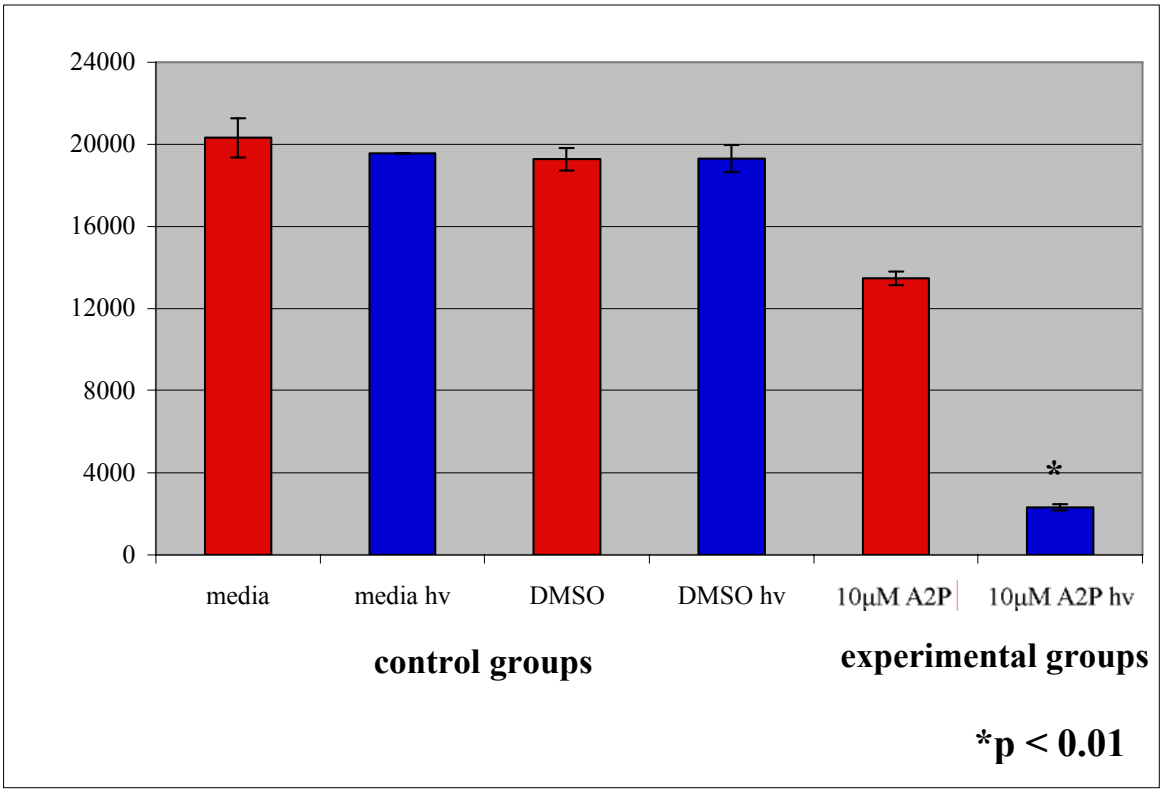


**Figure 4.3. A2P incubated in HL-60 cells with 40 minute blue-light irradiation.**

***4.2.3. Discussion.*** The results reported in the preceding sections reveal that blue-light irradiated A2P alone is responsible for the observed HL-60 cell death. Of the two A2P concentrations compared, only the higher 10 μM concentration caused significant cell death. The longer the 10 μM A2P was exposed to blue light, the more statistically significant the cell death observed; the optimal irradiation time was 45 minutes. Irradiation over 45 minutes began to damage the controls (data not shown). In the future, experiments will continue to be optimized by changing the light source,

intensity, and wavelength to determine whether lower concentrations of irradiated A2P can also cause significant cell death.

### 4.3. Photoactivated Cytotoxicity of A2-2(2-Aminoethoxy)ethanol in HL-60 Cells

The same cell culture care and assay procedures as described in the preceding sections were used when A2-2(2-aminoethoxy)ethanol was incubated in HL-60 cells with and without blue light. The MTT assay was performed to determine cell viability 24 hours after irradiation.

***4.3.1.Optimization of A2EE concentration.*** In order to determine the optimum concentration of A2EE for our cellular assays, we incubated 1–13 μM A2EE without blue-light irradiation in HL-60 cells. Results from the MTT assay showed that 5 and 7 μM A2EE were the best concentrations to run the blue-light irradiation assays. At higher and lower concentrations A2EE incubated in cells without irradiation begins to cause cell death. We are uncertain why lower concentrations cause cell death, but nevertheless moved forward with 5 and 7 μM A2EE.

A2EE (5 μM) was incubated with HL-60 cells for 24 hours and irradiated with blue light for 30 minutes. Media control experiments were performed with and without irradiation and with and without DMSO. No statistically significant differences were observed in any of the control experiments or when 5 μM A2EE was irradiated for 30 minutes ($p > 0.5$); therefore, only the experimental data for the irradiation of 7 μM A2EE is shown in Figure 4.4.

The analysis of the controls with and without irradiation, with and without DMSO, and directly comparing the media and DMSO controls showed no statistically significant differences ($p > 0.5$, 0.1, and 0.05, respectively). Furthermore, no statistically significant differences were observed when 7 μM A2EE experiments were compared to the media controls ($p > 0.1$). The irradiation of cells with 7 μM A2EE resulted in 20 % cell death compared to the nonirradiated samples of 7 μM A2EE ($p < 0.05$). The data show that 30-minute blue-light irradiation of 7 μM A2EE kills HL-60 cells.

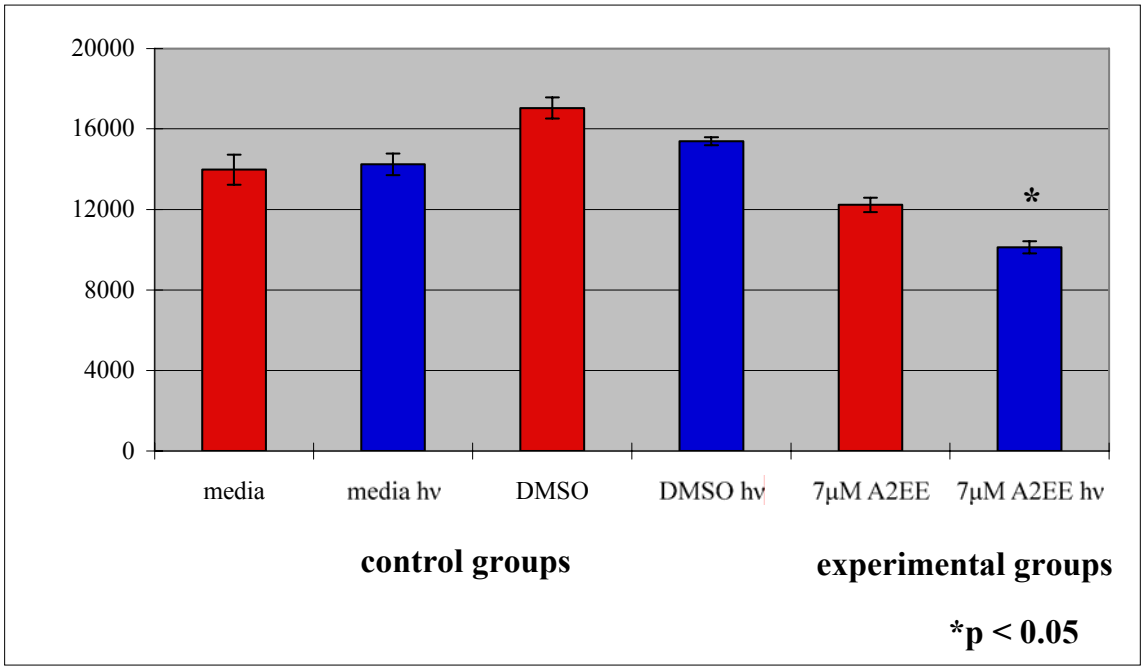


**Figure 4.4. A2EE incubated in HL-60 cells with 30 minute blue-light irradiation.**

***4.3.2. Optimization of A2EE irradiation time.*** To determine the optimum blue-light irradiation time, we performed the cellular assays described above on 7 μM A2EE and irradiated for 40, 45, and 50 minutes. Results from the MTT assay showed that no statistically significant differences were observed when A2EE was irradiated for

40 or 45 minutes ($p > 0.1$ and 0.5, respectively); therefore, only the data for the 50-minute irradiation is shown in Figure 4.5.

The control experiments performed with and without 50- minute irradiation and with and without DMSO showed no statistically significant differences ($p > 0.1$), which means that light exposure and DMSO alone did not cause cell death. In addition, no statistically significant differences were observed when the media and DMSO controls were directly compared ($p > 0.5$) and when the 7 μM A2EE experiments were compared to the media controls ($p > 0.1$). The irradiation of cells incubated with 7 μM A2EE resulted in 50 % cell death compared to the nonirradiated samples of 7 μM A2EE ($p < 0.05$). The data show that 50-minute blue-light irradiation of 7 μM A2EE effectively kills HL-60 cells.

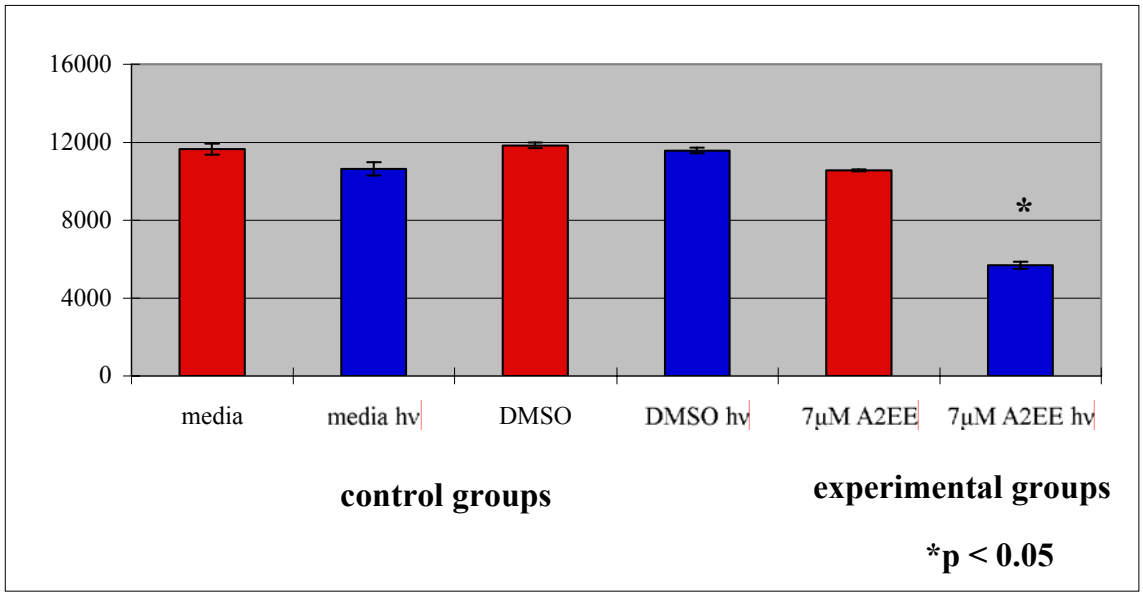


**Figure 4.5. A2EE incubated in HL-60 cells with 50 minute blue-light irradiation.**

***4.3.3. Discussion.*** The results reported in the preceding sections reveal that blue-light irradiated A2EE causes HL-60 cell death. Of the two A2EE concentrations compared, only the higher 7 μM concentration caused significant cell death. When 7 μM A2EE was irradiated for 30 and 50 minutes, statistically significant cell death was observed. Blue-light exposure over 50 minutes began to damage the controls (data not shown).

In these cellular assays anomalous behavior was observed in two areas. First, the control concentration experiments without irradiation revealed cell death at low concentrations of A2EE (1–3 μM), while higher concentrations did not result in cell death (5–9 μM). Second, irradiation for 40 and 45 minutes did not cause significant cell death, but 30 minute irradiation did result in cell death. These anomalous results suggest a need to run more experiments to confirm current A2EE irradiation results. After confirming these results, we will continue to optimize the experiments as described in section 4.2.3.

## 4.4. Summary and Conclusions

Two PBR compounds, A2P and A2EE were incubated and irradiated in HL-60 cells. Under the right conditions, both caused cell death after irradiation. The exact mechanism of HL-60 cell death has not yet been studied, but based on A2E photoirradiation studies in RPE cells,[1,2,4] the HL-60 cells may also be undergoing apoptosis.

A2P appears to be more readily photo-oxidized than A2EE. The photo-oxidation results in Chapter 3 support this claim, because A2EE takes longer to form oxidation products than does A2P; only 20 % of A2EE is oxidized in the first hour.

Although there is still room for optimization, the results from both the A2P and A2EE cellular assays are promising. These compounds exhibit phototriggered cytotoxicity. Future studies involve the attachment of folic acid to these compounds so that they can be specifically targeted to cancer cells. If successful, A2P, A2EE, and other pyridinium bisretinoid compounds may be developed into a targeted and triggered drug delivery system for cancer.

### 4.5. References


1. Sparrow, J. R.; Nakanishi, K.; Parish, C. A. *Invest. Ophthalmol. Vis. Sci.* **2000**, *41*, 1981–1989.

2. Sparrow, J. R.; Cai, B. *Invest. Ophthalmol. Vis. Sci.* **2001**, *42*, 1356–1362.

3. Sparrow, J. R.; Zhou, J.; Ben-Shabat, S.; Vollmer-Snarr, H. R.; Itagaki, Y.; Nakanishi, K. *Invest. Ophthalmol. Vis. Sci.* **2002**, *43*, 1222–1227.

4. Sparrow, J. R.; Vollmer-Snarr, H. R.; Zhou, J.; Jang, Y. P.; Jockusch, S.; Itagaki, Y.; Nakanishi, K. *J. Biol. Chem.* **2003**, *278*, 18207–18213.

5. Dillon, J.; Wang, Z.; Avalle, L. B.; Gaillard, E. R. *Exp. Eye Res.* **2004**, *79*, 537-542.

6. Jang, Y. P.; Matsuda, H.; Itagaki, Y.; Nakanishi, K.; Sparrow, J. R. *J. Biol. Chem.* **2005**, *280*, 39732–39739.

7. Vollmer-Snarr laboratory, unpublished results.

# Chapter 5. Experimental

## 5.1. General Experimental

All reactions and column purifications were conducted in the dark at room temperature. All solvents and reagents were obtained from Fluka or Aldrich, unless otherwise noted, and used as purchased. Silica gel powder (40-63 μm gel) for column chromatography was purchased from Sorbent Technologies. Reactions were monitored by TLC and/or ESI-MS prior to work-up. TLC was performed using aluminum backed 200 μm plates from Sorbent Technologies. TLC plates were visualized using $UV_{254}$ light. Solvents were removed *in vacuo* on a Büchi RE 47 rotary evaporator combined with a water condenser, using a Büchi 461 water bath combined with a water pump. HPLC and UV-vis spectra were obtained from a Waters 600 HPLC system equipped with a Waters 2998 photodiode array detector and with a Cosmosil packed column $5C_{18}$-P-MS 4.6 x 250 mm or a Phenomenex Synergi Max 250 x 4 mm column. HPLC grade $H_2O$ spiked with 0.1% trifluoracetic acid (TFA), acetonitrile (ACN), and methanol were used as eluants. MS data were obtained on an Agilent Technologies Multimode Electrospray APCI mass spectrometer running in $ES^+$ $APCI^+$ mode. All $^1$H-NMR spectra were obtained from a Varian Unity Inova 500 MHz spectrometer using tetramethylsilane (TMS) (0.00 ppm) and chloroform (7.26 ppm) as internal standards. Signals are reported as s (singlet), d (doublet), t (triplet), m (multiplet), dd (doublet of doublets), and bs (broad singlet). Coupling constants are reported in hertz (Hz). $^{13}$C-NMR spectra were obtained with a 125 MHz Varian NMR using TMS (0.00 ppm) and chloroform (7.26 ppm)

as internal standards. $^{1}$H-$^{1}$H COSY and $^{1}$H -$^{13}$C HETCOR correlations are reported as follows: w (weak), m (medium), s (strong).

An Edmund Optics' Mille Luce™ Fiber Optic Illuminator M1000 with a 442 nm (blue) filter is used to irradiate cells. The intensity of the light reaching the samples is ~ 476 mW/cm$^2$.

HL-60, human promyelocytic leukemia cells are obtained from Dr. Kim O′Neill, Department of Microbiology and Molecular Biology Brigham Young University. They are grown in RPMI supplemented with 10% fetal bovine serum. The cells are kept in a humidified 5% $CO_2$ incubator at 37° C and stock cultures are maintained in our laboratory. Growth curves for the HL-60 cells were completed using the trypan blue exclusion protocol described below. Trypan Blue solution was purchased from Sigma. Absorbance values in MTT cell proliferation assays were obtained from a VMax kinetic microplate reader.

## 5.2. Synthesis of Starting materials

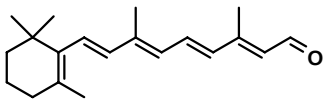


**All-*Trans*-Retinal (4)**

(2*E*,4*E*,6*E*,8*E*)-3,7-dimethyl-9-(2,6,6-trimethylcyclohex-1-enyl)nona-2,4,6,8-tetraenal

**All-*Trans*-Retinal (4):** According to the procedure by Sollaolie et al.,[2] $MnO_2$ (2.0 g, 23.2 mmol) was added to the solution of all-*trans*-retinol (3.3 g, 11.6 mmol). The

solution was stirred for 3 h, and the mixture was filtered and concentrated *in vacuo* to give crude all-*trans*-retinal. The crude material was purified by silica gel column chromatography (silica, eluted with 10:90 EtOAc:Hexane) to yield yellow crystals (2.6 g, 9.3 mmol, 80%) of all-*trans*-retinal. TLC and $^{1}$H-NMR were used to confirm the structure and compared to the literature values.

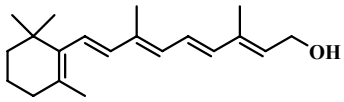


**All-*Trans*-Retinol (50)**

(2*E*,4*E*,6*E*,8*E*)-3,7-dimethyl-9-(2,6,6-trimethylcyclohex-1-enyl)nona-2,4,6,8-tetraen-1-ol

**All-*Trans*-Retinol (51):** According to the procedure by Duffy et al.,[1] vitamin A propionate (5.1 g, 15.5 mol) and $K_2CO_3$ (2.4 g, 17.1 mmol) were dissolved in THF (4.0 ml) and methanol (25.0 ml). The solution was stirred in the dark at room temperature for 2 h, and the reaction progress was monitored by TLC. Diethyl ether and hexane (2:1) were added, and the mixture was agitated, filtered, and concentrated *in vacuo* to give crude all-*trans*-retinol. The crude product was purified by silica gel column chromatography (silica, eluted with 5:95 EtOAc:Hexane) to give pure all-*trans*-retinol (3.8 g, 11.6 mmol, 85%) as a yellow oil. TLC and $^{1}$H-NMR were used to confirm the structure and compared to the literature values.

## 5.3 Synthesis of Bisretinoids

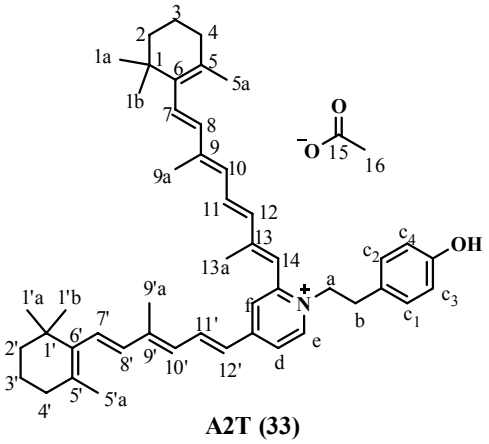

**A2T (33)**

2-((1*E*,3*E*,5*E*,7*E*)-2,6-dimethyl-8-(2,6,6-trimethylcyclohex-1-enyl)octa-1,3,5,7-tetraenyl)-1-(4-hydroxyphenethyl)-4-((1*E*,3*E*,5*E*)-4-methyl-6-(2,6,6-trimethylcyclohex-1-enyl)hexa-1,3,5-trienyl)pyridinium

**A2T (33)**: All-*trans*-retinal (200.0 mg, 0.7 mmol), tyramine (42.6 mg, 0.3 mmol), and acetic acid (18.4 µl, 0.3 mmol) were stirred in ethanol (25.0 ml) at room temperature in the dark for 48 h. The solvent was removed *in vacuo*, and the residue was purified 2–3 times by column chromatography (silica, eluted with $CH_2Cl_2$ first, then with 10:90:0.01 MeOH:$CH_2Cl_2$:$CH_3COOH$) to afford A2T (31.1 mg, 15 %) as a dark-red oil. **HRMS (ESI$^+$)** calcd 668.4826 for $[C_{48}H_{62}NO]^+$, found 668.4819; **UV-vis** $\lambda_{max}$ 339.8 nm, 442.08 nm; **$^1$H-NMR ($CDCl_3$, 500 MHz)** δ 8.80 (bs, 1H), 7.64-7.69 (m, 2H), 7.27 (d, *J* =2 Hz, 1H), 6.94 (t, *J* = 12.5 Hz, 1H), 6.79 (bs, 2H), 6.64 (d, *J* = 7, 2H), 6.52 (bs, 1H), 6.48 (bs, 1H), 6.44 (d, *J* = 15 Hz, 1H), 6.38 (bs, 1H), 6.34 (d, *J* = 8 Hz, 1H), 6.27 (dd, *J* = 16.5, 9 Hz, 1H), 6.20 (bs, 1H), 6.17 (d, *J* = 6 Hz, 1H), 6.07 (bs, 1H), 4.59 (bs, 2H), 2.96 (bs, 2H), 2.12 (bs, 3H), 2.02-2.04 (m, 7H), 1.97 (s, 3H), 1.74 (bs, 6H), 1.62-1.63 (m, 4H), 1.48-1.49 (m, 4H), 1.04-1.05(m, 6H); **$^{13}$C-NMR ($CDCl_3$, 125 MHz)** δ 178.18, 158.71, 152.42, 150.96, 146.97, 146.38, 140.71, 138.07, 137.85, 137.77, 137.39, 136.86, 133.67,

132.58, 131.99, 131.39, 130.60, 129.88, 129.40, 128.97, 125.21, 124.41, 120.86, 118.72, 116.84, 58.50, 39.84, 36.01, 34.54, 34.51, 33.52, 33.38, 29.95, 29.24, 25.09, 22.11, 22.06, 19.44, 19.63, 15.10, 13.61, 13.23; **DEPT ($CDCl_3$, 125 Hz)**: 9-$CH_3$, 8- $CH_2$, 18- CH, 13-C; **$^1$H-$^1$H COSY ($CDCl_3$, 500Hz)**: 8.80/7.66-7.69 (w, H-e/H-d), 7.66-7.69/7.64 (s, H-d-H-f), 6.79/6.64 (s, H-$c_1$,$c_2$/H- $d_1$,$d_2$), 4.59/2.96 (w, H-a/H-b), 2.04/1.62-1.63 (m, H-4,4'/H-3,3'), 1.62-1.63/1.48-1.49 (s, H-3,3'/ H-2,2'); **$^1$H -$^{13}$C HETCOR ($CDCl_3$)**: 8.80/146.38 (w, H-e/C-e), 7.64-7.69/138.07 (w, H-d, f/C-d, f), 6.64/131.39 (w, H-$c_3$, $c_4$/C-$c_3$, $c_4$), 4.59/58.51 (H-a/C-a), 2.96/36.01 (w, H-b/C-b), 1.95-1.97/33.38-33.52 (m, H-9a, 9'a/C-9a, 9'a), 1.04/29.24 (s, H-1a, 1b, 1'a,1'b/C-1a, 1b, 1'a,1'b), 1.74/22.07-22.11 (w, H-5a, 5'a/C5a, 5'a), 1.48/19.36-19.44 (H-2, 2'/C2, 2').

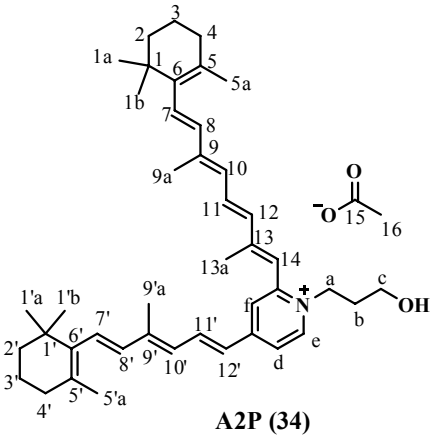


**A2P (34)**

2-((1*E*,3*E*,5*E*,7*E*)-2,6-dimethyl-8-(2,6,6-trimethylcyclohex-1-enyl)octa-1,3,5,7-tetraenyl)-1-(3-hydroxypropyl)-4-((1*E*,3*E*,5*E*)-4-methyl-6-(2,6,6-trimethylcyclohex-1-enyl)hexa-1,3,5-trienyl)pyridinium

**A2P (34)**: All-*trans*-retinal (100.0 mg, 0.4 mmol), 3-amino-1-propanol (11.7 mg, 0.2 mmol), and acetic acid (9.2 µl, 0.2 mmol) were stirred in ethanol (10.0 ml) at room temperature in the dark for 48 h. The solvent was removed *in vacuo* and the residue was

purified 2–3 times by column chromatography (silica, eluted with $CH_2Cl_2$ first, then with 15:85:0.01 MeOH:$CH_2Cl_2$:$CH_3COOH$) to afford A2P (12.2 mg, 13 %) as a dark-red oil. **HRMS ($ESI^+$)** calculated (calcd) for $[C_{43}H_{60}NO]^+$ 606.4669, found m/z 606.4664; **UV-vis** $\lambda_{max}$ 337.4 nm, 438.0 nm; **$^1$H-NMR ($CDCl_3$, 500 MHz)** δ 9.69 (bs, 1H), 7.92 (bs, 1H), 7.73 (m, 1H), 7.33 (bs, 1H), 7.00 (dd, *J* = 14.8, 12 Hz, 1H), 6.43-6.55 (m, 4H), 6.17-6.37(m, 5H), 4.75 (bs, 2H), 3.72 (bs, 2H), 2.15 (s, 3H), 2.09 (s, 3H), 2.04-2.06 (m, 9H), 1.75 (s, 3H), 1.74 (s, 3H), 1.63-1.64 (m, 4H), 1.48-1.51 (m, 4H), 1.06 (s, 6H), 1.05 (s, 6H); **$^{13}$C-NMR ($CDCl_3$, 125 MHz)** δ 177.21, 152.67, 150.60, 147.78, 147.29, 146.60, 141.05, 138.18, 137.79, 137.27, 136.76, 134.38, 133.67, 132.82, 132.05, 131.689, 130.71, 129.77, 129.19, 128.81, 125.49, 125.06, 120.88, 118.29, 57.49, 54.82, 39.84, 34.54, 33.52, 33.38, 32.92, 29.21, 26.203, 23.92, 22.06, 19.42, 19.36, 15.24, 13.59, 13.23; **$^1$H-$^1$H COSY ($CDCl_3$, 500Hz)**: 9.70/7.92 (m, H-e/H-d), 7.71-7.76/6.52 (s, H-f/H-12'), 7.71-7.76/6.33-6.37 (s, H-f/H-14), 6.52/7.00 (s, H-12'/H-10'), 7.00/6.20-6.22 (s, H-10'/H-11') 4.75/2.05 (s, H-a/H-b), 3.72/2.05 (H-c/H-b); **$^1$H -$^{13}$C HETCOR ($CDCl_3$)**: 9.70/147.78 (w, H-e/C-e), 7.71-7.76/138.18 (m, H-f/C-f), 6.33-6.37/136.76(s, H-14/C-14), 6.52/133.67 (m, H-12'/C-12'), 7.00/131.69 (m, H-10'/C10'), 6.20-6.22/129.19 (s, H-11'/C-11'), 4.75/54.82 (w, H-a/C-a), 3.72/57.49 (m, H-c/C-c), 2.10/33.52 (m, H-9'/C-9'), 2.04/33.38 (m, H-9/C-9), 2.06/32.92 (m, H-4, 4'/C-4, 4'), 2.05/23.92 (m, H-b/C-b), 1.74-1.75/22.06 (s, H-5, 5'/C5, 5'), 1.63-1.64/19.36-19.42 (s, H-3, 3'/C-3, 3'), 1.05/29.21 (s, H-1, 1'/C1, 1').

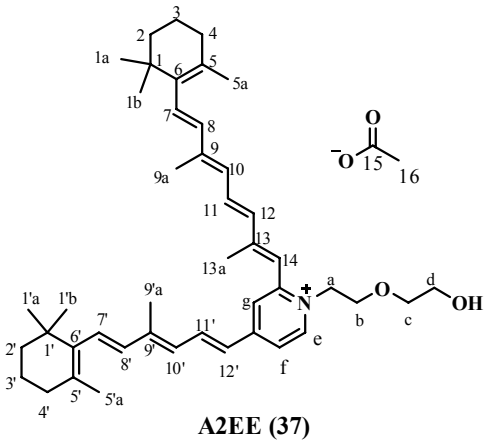

**A2EE (37)**

2-((1*E*,3*E*,5*E*,7*E*)-2,6-dimethyl-8-(2,6,6-trimethylcyclohex-1-enyl)octa-1,3,5,7-tetraenyl)-1-(2-(2-hydroxyethoxy)ethyl)-4-((1*E*,3*E*,5*E*)-4-methyl-6-(2,6,6-trimethylcyclohex-1-enyl)hexa-1,3,5-trienyl)pyridinium

**A2EE (37)**: All-*trans*-retinal (200.0 mg, 0.7 mmol), 2-(2-aminoethoxy) ethanol (32.5 mg, 0.3 mmol), and acetic acid (18.4 µl, 0.3 mmol) were stirred in ethanol (25.0 ml) at room temperature in the dark for 48 h. The solvent was removed *in vacuo* and the residue was purified 2–3 times by column chromatography (silica, eluted with $CH_2Cl_2$ first, then with 20:80:0.01 MeOH:$CH_2Cl_2$:$CH_3COOH$) to afford A2EE (32.2 mg, 16 %) as a dark-red oil. **HRMS (ESI$^+$)** calcd 636.4775 for $[C_{44}H_{62}NO_2]^+$, found 636.4823; **UV-vis** $\lambda_{max}$ 337.4 nm, 441.60 nm; **$^1$H-NMR ($CDCl_3$, 500 MHz)** δ 9.70 (bs, 1H), 7.91 (bs, 1H), 6.98 (dd, *J* = 14.75, 11 Hz, 1H), 7.31 (bs, 1H), 6.98 (dd, *J* = 15, 11 Hz, 1H), 6.54 (bs, 1H), 6.49 (d, *J* = 14.5 Hz, 1H), 6.44 (d, *J* = 5 Hz, 1H), 6.34-6.37 (m, 1H), 6.28-6.32 (m, 1H), 6.16-6.25 (m, 4H), 4.87 (bs, 2H), 3.94 (bs, 2H), 3.74 (d, *J* = 8 Hz, 4H), 2.14 (bs, 3H), 2.08 (bs, 3H), 2.03-2.06 (m, 7H), 1.74 (d, *J* = 6 Hz, 6H), 1.62-1.65 (m, 4H), 1.48-1.50 (m, 4H), 1.05 (d, *J* = 5.5 Hz, 6H); **$^{13}$C-NMR ($CDCl_3$, 125 MHz)** δ 177.282, 152.76, 150.76, 148.48, 147.03, 146.51, 140.93, 138.09, 137.85, 137.78, 137.27, 137.05,

136.76, 133.60, 132.78, 132.04, 131.51, 130.10, 129.69, 129.17, 128.81, 125.26, 125.14, 120.52, 118.59,73.44, 68.62, 61.60, 56.19, 39.84, 39.82, 34.55, 34.52, 33.52, 33.38, 29.94, 29.21,24.06, 22.07, 22.00, 19.42, 19.36, 15.17, 13.59, 13.23; **$^{1}$H-$^{1}$H COSY ($CDCl_3$, 500Hz)**: 9.70/7.91 (s, H-e/H-f), 6.98/6.54 (m, H-g/H-14), 6.98/6.34-6.37 (m, H-g/H-12'), 4.87/3.94 (s, H-a/H-b), 2.06/1.62-1.65 (s, H-4, 4'/H-3, 3'), 1.62-1.65/1.48-1.50 (s, H-3, 3'/H-2, 2'); **$^{1}$H -$^{13}$C HETCOR ($CDCl_3$)**: 9.70/148.48 (w, H-e/C-e), 7.91/120.52 (w, H-f/C-f), 6.98/137.27 (H-f/C-f), 6.34-6.37/129.17 (w, H-12'/C-12'), 4.87/56.19 (m, H-a/C-a), 3.94/68.62 (m, H-b/C-b), 3.75/61.60 (m, H-c/C-c), 3.73/73.45 (m, H-d/C-d), 2.14/, 2.08/13.17 (w, H-13a/C-13a), 2.08/15.17 (w, H-9'a/C-9a), 2.06/13.23 (w, H-4, 4'/C-4, 4'), 2.03/24.06 (w, H-9a/C-9a), 1.74/22.01-22.07 (m, H-5a, 5'a/C-5a, 5'a), 1.62-1.65/19.36-19.42 (m, H-3, 3'/C-3, 3'), 1.48-1.50/39.82-39.84 (s, H-2, 2'/C2, 2'), 1.05-1.06/29.21 (s, H-1a, 1b, 1'a, 1'b/C-1a, 1b, 1'a, 1'b).

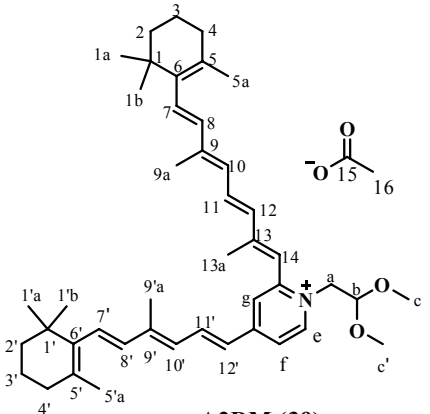

**A2DM (39)**

1-(2,2-dimethoxyethyl)-2-((1*E*,3*E*,5*E*,7*E*)-2,6-dimethyl-8-(2,6,6-trimethylcyclohex-1-enyl)octa-1,3,5,7-tetraenyl)-4-((1*E*,3*E*,5*E*)-4-methyl-6-(2,6,6-trimethylcyclohex-1-enyl)hexa-1,3,5-trienyl)pyridinium

**A2DM (39)**: All-*trans*-retinal (200.0 mg, 0.7 mmol), amino acetaldehyde dimethyl acetate (32.6 mg, 0.3 mmol), and acetic acid (18.6 µl, 0.3 mmol) were stirred in ethanol (25.0 ml) at room temperature in the dark for 48 h. The solvent was removed *in vacuo* and the residue was purified 2–3 times by column chromatography (silica, eluted with $CH_2Cl_2$ first, then with 10:90:0.01 MeOH:$CH_2Cl_2$:$CH_3COOH$) to afford A2DM (15.8 mg, 8 %) as a dark-red oil. **HRMS (ESI$^+$)** calcd 636.4775 for $[C_{44}H_{62}NO_2]^+$, found 636.4733; **UV-vis** $\lambda_{max}$ 338.6 nm, 444.0 nm; **$^1$H-NMR ($CDCl_3$, 500 MHz)** δ 9.44 (d, *J* = 6.5 Hz, 1H), 7.92 (dd, *J* = 7, 1 Hz, 1H), 7.75 (dd, *J* = 15.5, 11.5 Hz, 1H), 7.29 (d, *J* = 1 Hz, 1H), 6.96 (dd, *J* = 15, 11.5 Hz, 1H), 6.64 (bs, 1H), 6.46-6.54 (m, 3H), 6.16-6.34 (m, 6H), 4.85 (t, *J* = 5 Hz, 1H), 4.78 (d, *J* = 5 Hz, 2H), 3.47 (bs, 6H), 2.15 (bs, 1H), 2.02-2.06 (m, 10 H), 1.74 (d, *J* = 5.5 Hz, 6H), 1.63-1.65 (m, 4H), 1.48-1.51 (m, 4h), 1.06 (d, *J* = 5 Hz, 6H); **$^{13}$C-NMR ($CDCl_3$, 125 MHz)** δ 176.26, 152.70, 152.44, 147.63, 146.66, 146.47, 140.44, 138.21, 137.88, 137.82, 137.38, 136.80, 134.14, 132.70, 132.00, 131.00, 130.54, 129.37, 128.90, 125.27, 125.18, 120.44, 120.11, 103.56, 57.27, 56.70, 39.82, 34.54, 34.51, 33.51, 33.37, 29.21, 23.18, 22.08, 22.02, 19.44, 19.35, 15.10, 13.56, 13.20; **$^1$H-$^1$H COSY ($CDCl_3$, 500Hz)**: 9.44/7.92 (s, H-e/H-f), 7.75/6.64 (s, H-g/H-14), 7.75/6.28-6.34 (s, H-g/H-12'), 2.06/1.63-1.65 (m, H-4, 4'/H-3, 3'), 1.63-1.65/1.48-1.51 (m, H-3, 3'/H-2, 2'); **$^1$H -$^{13}$C HETCOR ($CDCl_3$)**: 9.44/147.63 (w, H-e/C-e), 7.92/120.11 (w, H-f/C-f), 7.75/137.38 (w, H-g/C-g), 6.64/125.13 (w, H-14/C-14), 6.28-6.34/128.90 (w, H-12'/C-12'), 4.78/57.25 (w, H-a/C-a), 3.47/56.70 (H-c/C-c), 2.15/13.20 or 13.56 (w, H-13a/C-13a), 2.06/15.10 (w, H-4, 4'/C-4, 4'), 2.05/23.18 (w, H-9'a/C-9'a), 2.02/33.37 (s,

H-9a/C-9a), 1.74/22.02-22.08 (s, H-5a, 5'a/C-5a, 5'a), 1.63-1.65/19.35-19.44 (s, H-3, 3'/C3, 3'), 1.50-1.51/39.82 (H-2, 2'/C2, C2'), 1.06/29.21 (s, H-1a, 1b, 1'a, 1'b/C-1a, 1b, 1'a, 1'b). '

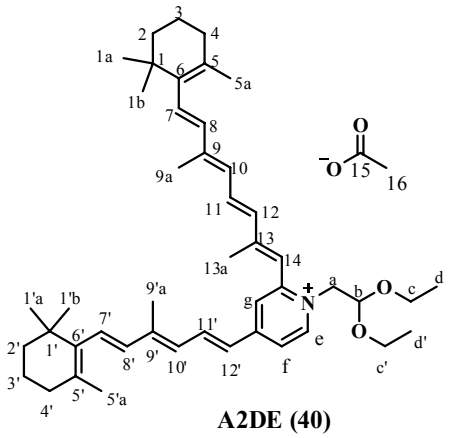

**A2DE (40)**

1-(2,2-diethoxyethyl)-2-((1*E*,3*E*,5*E*,7*E*)-2,6-dimethyl-8-(2,6,6-trimethylcyclohex-1-enyl)octa-1,3,5,7-tetraenyl)-4-((1*E*,3*E*,5*E*)-4-methyl-6-(2,6,6-trimethylcyclohex-1-enyl)hexa-1,3,5-trienyl)pyridinium

**A2DE (40)**: All-*trans*-retinal (200.0 mg, 0.7 mmol), amino acetaldehyde diethyl acetate (41.3 mg, 0.3 mmol), and acetic acid (18.6 µl, 0.3 mmol) were stirred in ethanol (25.0 ml) at room temperature in the dark for 48 h. The solvent was removed *in vacuo* and the residue was purified 2–3 times by column chromatography (silica, eluted with $CH_2Cl_2$ first, then with 10:90:0.01 MeOH:$CH_2Cl_2$:$CH_3COOH$) to afford A2DE (20.6 mg, 10 %) as a dark-red oil. **HRMS (ESI$^+$)** calcd 636.5088 for $[C_{46}H_{66}NO_2]^+$, found 664.5068; **UV-vis** $\lambda_{max}$ 337.5 nm, 442.3 nm; **$^1$H-NMR ($CDCl_3$, 500 MHz)** δ 9.35 (bs, 1H), 7.95 (bs, 1H), 7.76 (dd, *J* = 14.5, 11.5 Hz, 1H), 7.73, (bs, 1H), 6.95 (dd, *J* = 15, 11.5 Hz, 1H), 6.72 (bs, 1H), 6.44-6.52 (m, 2H), 6.16-6.33 (m, 6H), 4.99 (bs, 1H), 4.73 (bs, 2H), 3.73-3.78 (m, 2H), 3.59-3.65 (m, 2H), 2.15 (bs, 3H), 2.02-2.05 (m, 10 H), 1.74 (d, *J* = 3.5 Hz, 6H), 1.61-1.64 (m, 4H), 1.47-1.49 (m, 4H), 1.16 (t, *J* = 7 Hz, 6H), 1.05 (d, *J* =

3.5 Hz, 6H); **$^{13}$C-NMR ($CDCl_3$, 125 MHz)** δ 176.26, 168.59, 152.70, 152.44, 147.63, 147.53, 146.66, 146.47, 140.44, 138.21, 137.88, 137.78, 137.38, 137.13, 136.98, 134.14, 132.70, 132.00, 131.00, 130.75, 130.65, 130.54, 129.79, 129.37, 128.90, 127.18, 126.18, 125.27, 128.19, 120.64, 120.44, 120.11, 118.29, 103.56, 57.27, 56.70, 39.82, 34.54, 34.51, 33.51, 33.37, 33.73, 29.21, 23.18, 22.08, 22.02, 19.44, 19.35, 15.10, 13.56, 13.20. **$^{1}$H-$^{1}$H COSY ($CDCl_3$, 500Hz)**: 9.34/7.96 (m, H-e/H-f), 7.76/6.51-6.52 (w, H-g/H-14), 7.76/6.28-6.33 (w, H-g/H-12'), 2.05/1.61-1.64 (s, H-4, 4'/H3, 3'), 1.61-1.64/1.47-1.49 (s, H-3, 3'/H-2, 2'); **$^{1}$H -$^{13}$C HETCOR ($CDCl_3$)**: 9.34/152.70 (w, H-e/C-e), 7.96/120.11 (w, H-f/C-f), 7.76/138.21 (w, H-g/C-g), 6.51-6.52/125.27 (w, H-14/C-14), 6.28-6.33/128.90 (w, H-12'/C-12'), 4.73/57.27 (w, H-a/C-a), 2.15/13.56 (w, H-13a/C-13a), 2.05/15.10 (w, H-4, 4'/C-4, 4'), 2.02/13.20 (w, H-9'a/C-9'a), 2.02/23.18 (s, H-9a/C-9a), 1.74/22.02 or 22.08 (s, H-5a, 5'a/C-5a, 5'a), 1.61-1.64/19.35-19.44 (s, H-3, 3'/C3, 3'), 1.47-1.49/34.51-34.54 (H-2, 2'/C2, C2'), 1.16/15.10 (m, H-d, d'/C-d, d'), 1.05/29.21 (s, H-1a, 1b, 1'a, 1’b/C-1a, 1b, 1'a, 1'b).

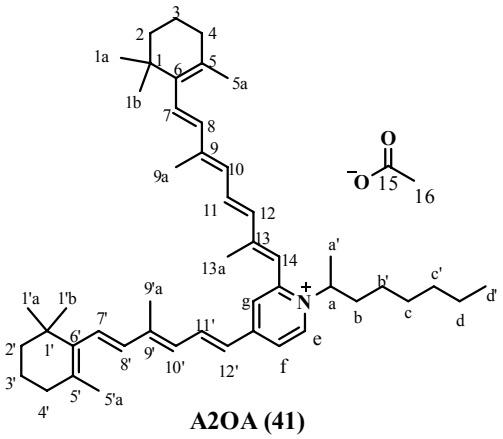

**A2OA (41)**

2-((1*E*,3*E*,5*E*,7*E*)-2,6-dimethyl-8-(2,6,6-trimethylcyclohex-1-enyl)octa-1,3,5,7-tetraenyl)-4-((1*E*,3*E*,5*E*)-4-methyl-6-(2,6,6-trimethylcyclohex-1-enyl)hexa-1,3,5-trienyl)-1-(octan-2-yl)pyridinium

**A2OA (41)**: All-*trans*-retinal (200.0 mg, 0.7 mmol), 2-octanamine (40.1 mg, 0.3 mmol), and acetic acid (18.6 µl, 0.3 mmol) were stirred in ethanol (25.0 ml) at room temperature in the dark for 48 h. The solvent was removed *in vacuo* and the residue was purified 2–3 times by column chromatography (silica, eluted with $CH_2Cl_2$ first, then with 5:95:0.01 MeOH:$CH_2Cl_2$:$CH_3COOH$) to afford A2OA (20.5mg, 10%) as a dark-red oil. **HRMS (ESI$^+$)** calcd 660.5503 for $[C_{48}H_{70}N]^+$, found 660.5495; **UV-vis** $\lambda_{max}$ 340.7 nm, 439.3 nm; **$^1$H-NMR (CDCl$_3$, 500 MHz)** δ 7.71 (d, *J* = 7.5 Hz, 1H ), 8.48 (*J* = 6.5 Hz, 1H), 7.90 (dd, *J* = 14.5, 11.5 Hz, 1H), 7.25 (bs, 1H), 6.97 (dd, *J* = 15, 11.5 Hz, 1H), 6.45-6.53 (m, 2H), 6.16-6.35 (m, 2H), 4.70-4.75 (m, 1H), 2.17 (bs, 3H), 2.02-2.04 (m, 10 H), 1.69-1.74 (m, 11H), 1.61-1.64 (m, 4H), 1.47-1.50 (m, 4H), 1.16-1.25 (m, 6H), 1.02-1.05 (m, 8H), 0.84 (t, *J* = 7 Hz, 3H); **$^{13}$C-NMR (CDCl$_3$, 125 MHz)** δ 152.41, 150.85, 148.13, 146.88, 16.15, 140.80, 137.86, 137.76, 137.61, 137.30, 136.78, 133.67, 132.63, 131.97, 131.37, 130.61, 129.60, 129.20, 128.79, 125.25, 125.12, 120.11, 118.79,

65.96, 62.88, 39.81, 34.54, 34.51, 33.49, 33.36, 29.93, 29.21, 22.06, 22.00, 21.01, 19.42, 19.35, 15.18, 13.54, 13.22.

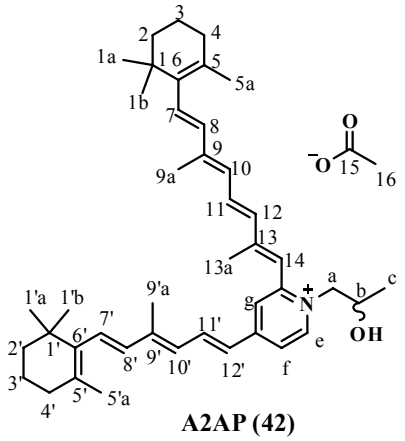

**A2AP (42)**

2-((1*E*,3*E*,5*E*,7*E*)-2,6-dimethyl-8-(2,6,6-trimethylcyclohex-1-enyl)octa-1,3,5,7-tetraenyl)-1-(2-hydroxypropyl)-4-((1*E*,3*E*,5*E*)-4-methyl-6-(2,6,6-trimethylcyclohex-1-enyl)hexa-1,3,5-trienyl)pyridinium

**A2AP (42)**: All-*trans*-retinal (200.0 mg, 0.7 mmol), 1-amino-2-propanol (23.3 mg, 0.3 mmol), and acetic acid (18.6 µl, 0.3 mmol) were stirred in ethanol (25.0 ml) at room temperature in the dark for 48 h. The solvent was removed *in vacuo* and the residue was purified 2–3 times by column chromatography (silica, eluted with $CH_2Cl_2$ first, then with 30:70:0.01 MeOH:$CH_2Cl_2$:$CH_3COOH$) to afford A2AP (16.2 mg, 8.6 %) as a dark-red oil. **HRMS (ESI$^+$)** calcd 606.4669 for $[C_{43}H_{60}NO]^+$, found 606.4675; **UV-vis** $\lambda_{max}$ 326.8 nm, 426 nm; **$^1$HNMR ($CDCl_3$, 500 MHz)** δ 9.50 (bs, 1H), 7.63-7.74 (m, 2H), 7.34 (bs, 1H), 6.97 (dd, *J* = 14.5, 11.5 Hz, 1H), 6.15-6.51 (m, 9H), 4.69 (bs, 1H), 6.45 (d, *J* = 11.5 Hz, 1H), 4.06 (bs, 1H), 2.12 (bs, 3H), 2.00-2.07 (m, 10 H), 1.73 (d, dd, *J* = 5.5 Hz, 6H), 1.61-1.62 (m, 4H), 1.47-1.49 (m, 4H), 1.32 (d, dd, *J* = 5.5 Hz, 3H), 1.01-1.05 (m, 6H); **$^{13}$C NMR ($CDCl_3$, 125 MHz)** δ 152.41, 150.85, 148.13, 146.88, 146.15, 140.80, 137.86, 137.76, 137.61, 136.78, 133.67, 132.63, 131.97, 131.37, 130.61, 129.61, 129.20,

128.80, 125.25, 125.12, 120.11, 118.79, 65.96, 62.88, 39.81, 34.54, 34.51, 33.49, 33.36, 29.93, 29.21, 22.06, 22.00, 21.01, 19.42, 19.35, 15.18, 13.36, 13.22.

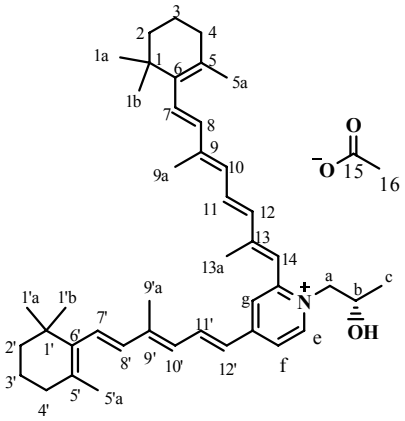

***S*-A2AP (42-*S*)**

2-((1*E*,3*E*,5*E*,7*E*)-2,6-dimethyl-8-(2,6,6-trimethylcyclohex-1-enyl)octa-1,3,5,7-tetraenyl)-1-((*S*)-2-hydro-xypropyl-4-((1*E*,3*E*,5*E*)-4-methyl-6-(2,6,6-trimethylcyclohex-1-enyl)hexa-1,3,5-trienyl)pyridinium

***S*-A2AP (42-*S*)**: All-*trans*-retinal (200.0 mg, 0.7 mmol), *S*-1-amino-2-propanol (23.3 mg, 0.3 mmol), and acetic acid (18.6 µl, 0.3 mmol) were stirred in ethanol (25.0 ml) at room temperature in the dark for 48 h. The solvent was removed *in vacuo* and the residue was purified 2–3 times by column chromatography (silica, eluted with $CH_2Cl_2$ first, then with 30:70:0.01 MeOH:$CH_2Cl_2$:$CH_3COOH$) to afford *S*-A2AP (15.1 mg, 8 %) as a dark-red oil. **HRMS (ESI$^+$)** calcd 606.4669 for $[C_{43}H_{60}NO]^+$, found 606.4675; **UV-vis** $\lambda_{max}$ 327.9 nm, 427.5 nm; **$^1$H-NMR ($CDCl_3$, 500 MHz)** δ 9.37 (d, *J* = 5 Hz, 1H ), 7.63-7.75 (m, 2H), 7.37 (d, *J* = 22.5 Hz, 1H), 6.95-7.05 (m, 1H), 6.45-6.52 (m, 2H), 6.03-6.40 (m, 6H), 4.62 (t, *J* = 9 Hz, 1H), 4.45 (d, *J* = 13 Hz, 1H), 4.05 (d, *J* = 2.5 Hz, 1H), 2.13 (bs, 3H), 1.97-2.11 (m, 10H), 1.73 (d, *J* = 5.5 Hz, 6H), 1.60-1.63 (m, 4H), 1.45-1.49 (m, 4H), 1.32 (d, *J* = 6 Hz, 3H), 1.00-1.05 (m, 6H); **$^{13}$C- NMR ($CDCl_3$, 125**

**MHz)** δ 178.00, 152.58, 151.00, 147.49, 147.04, 146.53, 146.35, 137.85, 137.75, 137.58, 137.30, 137.07, 136.78, 133.66, 133.49, 132.72, 132.03, 131.45, 130.83, 130.62, 130.02, 129.63, 139.29, 128.84, 126.63, 126.13, 126.21, 120.38, 120.17, 118.77, 116.98, 72.74, 66.00, 64.19, 62.94, 39.81, 34.52, 33.49, 33.35, 29.21, 22.06, 22.00, 19.41, 19.35.

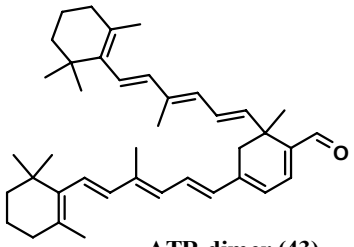

**ATR dimer (43)**

6-methyl-4,6-bis((1*E*,3*E*,5*E*)-4-methyl-6-(2,6,6-trimethylcyclohex-1-enyl)hexa-1,3,5-trienyl)cyclohexa-1,3-dienecarbaldehyde

**ATR dimer (43)**: All-*trans*-retinal (100.0 mg, 0.4 mmol), 3-amino-1-propanol (11.7 mg, 0.2 mmol), and acetic acid (9.2 µl, 0.2 mmol) were stirred in ethanol (10.0 ml) at room temperature in the dark for 48 h. The solvent was removed *in vacuo* and the residue was purified by column chromatography (silica, eluted with $CH_2Cl_2$) to afford the ATR dimer (2.9 mg, 3 %) as a yellow oil. **HRMS (ESI$^+$)** calcd 551.4247 for $[C_{40}H_{54}O]^+$, found 551.4225; **UV-vis** [3] $\lambda_{max}$ 290.3 nm, 432.5 nm; **$^1$H-NMR (CDCl$_3$, 500 MHz)** [3] δ 9.46 (s, 1H), 6.94-7.00 (q, *J* = 11.5 Hz, 1H), 6.82 (d, *J* = 6.4 Hz, 1H), 5.98-6.45 (m, 9H), 5.83-5.86 (d, *J* = 15.1 Hz, 1H), 2.66-2.71 (d, *J* = 16.6 Hz, 1H), 2.40-2.45 (d, *J* = 17.1 Hz, 1H), 2.02-2.06 (m, 5H), 1.99 (t, *J* = 6.4 Hz, 2H), 2.02-2.06 (m, 5H), 1.99 (t, *J* = 6.4 Hz, 2H), 1.85 (s, 3H), 1.73 (s, 3H), 1.67 (s, 3H), 1.56-1.65 (m, 4H), 1.48 (s, 3H), 1.43-1.48 (m, 4H), 1.04 (s, 6H), 0.98 (s, 6H); **$^{13}$C- NMR (CDCl$_3$, 125 MHz)** [3] δ 192.29, 144.45, 144.28, 141.75, 139.83, 138.51, 138.05, 137.53, 132.90, 130.46, 130.35, 129.94, 129.09,

128.96, 126.51, 123.99, 122.91, 39.87, 39.76, 38.80, 34.43, 33.41, 33.18, 29.22, 29.12, 24.64, 22.03, 21.89, 19.50, 19.45, 13.23, 12.91.

**5.4. Blue-Light Irradiation of Pyridinium Bisretinoids**

**5.4.1. *Blue-Light Irradiation of A2P.*** A2P (15.0 mg, 24.7 mmol) was dissolved in $H_2O$ (2.0 mL) and DMSO (18.0 mL). An aliquot (4.0 mL) of this solution was placed in a two sided, 10 mm, polystyrene vis-cuvette. The solution was irradiated with fiber optic illuminator equipped with a blue light (442 nm) interference filter. Samples (100 μL) were taken for ESI-MS and HPLC analysis every hour for five hours. An HPLC solvent gradient (20 % $H_2O$ with 0.1% TFA to 100 % ACN) was used to elute A2P.

**5.4.2. *Blue-Light Irradiation of A2EE.*** A2EE (17.0 mg, 26.7 mmol) was dissolved in $H_2O$ (2.0 mL) and DMSO (18.0 mL). An aliquot (4.0 mL) of this solution was placed in a two sided, 10 mm, polystyrene vis-cuvette. The solution was irradiated with fiber optic illuminator equipped with a blue light (442 nm) interference filter. Samples (100 μL) were taken for ESI-MS and HPLC analysis every hour for five hours. An HPLC solvent gradient (93.0 % $H_2O$ with 0.1% TFA to 100 % ACN) was used to elute A2EE.

**5.4.3. *Blue-Light Irradiation of A2DM.*** A2DM (16.0 mg, 25.1 mmol) was dissolved $H_2O$ (2.0 mL) and DMSO (18.0 mL). An aliquot (4.0 mL) of this solution was placed in a two sided, 10 mm, polystyrene vis-cuvette. The solution was irradiated with a fiber optic illuminator equipped with a blue light (442 nm) interference filter. Samples (100 μL) were taken for ESI-MS and HPLC analysis every hour for three hours. An

HPLC solvent gradient (20 % $H_2O$ with 0.1 % TFA to 100 % ACN) was used to elute A2DM.

**5.5. Cytotoxicity Assays of A2P and A2EE**

Sterile, filtered DMSO solutions (20.0 mM) of A2P and A2EE were prepared. Cell viabilities of the controls were maintained as close to or greater than 95%. The HL-60 cells were grown to selected concentrations (~ 4 X $10^5$ cells/ml) and plated onto two 24-well plates. The cells are incubated with specified concentrations (Chapter 4) of A2P and A2EE for 24 hours, along with media and DMSO controls. One 24-well plate was irradiated inside the incubator for the specified times with a fiber optic illuminator equipped with a blue light (442 nm) interference filter, then allowed to incubate for another 24 hours. The other plate was incubated for another 24 hours without irradiation. After incubation, the cell viabilities were monitored using the TBCC or MTT assays.

**5.5.1.** ***Trypan Blue Cell Count.*** Cell suspension (10 μL) was mixed into 0.4% trypan blue (10 μL). A cover glass was centered over the hemacytometer and the cell/TB mixture (10 μL) was then added to one chamber. The number of cells per mL and percent viability were then calculated after viewing under the microscope.

**5.5.2.** ***Cell Proliferation Assay.***

***5.5.2.1. Preparation of MTT solution:*** To a centrifuge tube (15.0 mL) was added 3-(4,5-dimethylthiazol-2-yl)-2,5-diphenyltetrazolium bromide (MTT) (50 mg) dissolved in 0.1 M phosphate buffer saline (PBS) solution (10.0 mL). The solution was incubated in a 37℃ water bath for 5 h.

***5.5.2.2. Colorimetric quantitative analysis:*** Cell solutions (1200 μL/well) were incubated as described above in 24-well plates, and then half of the solution (600 μL/well) was removed from the top of each well. MTT solution (90 μL) was added to each well and incubated for 1-4 hours to allow the cells to convert the substrate into the purple-colored formazan product. Sterile, filtered DMSO (1.2 mL) was added into each well to stop the reaction. Aliquots (200 μL) were removed from each well and transfered into a 96-well plate. This plate was read using a VMax kinetic microplate reader and the absorbance was determined at 490 nm.

### 5.5.3. *Some Cell Assay Data.*

**A2P *vs* HL-60 30 min Irradiation with 10 μM A2P**

| Item | media | media hv | 10 μM A2P | 10 μM A2P hv | DMSO | DMSO hv |
|---|---|---|---|---|---|---|
| Data 1 | 1.144 | 1.228 | 0.724 | 0.505 | 1.023 | 1.077 |
| Data 2 | 1.376 | 1.162 | 0.634 | 0.519 | 1.153 | 0.919 |
| Average* 20000 | 25200 | 23900 | 13580 | 10240 | 21760 | 19960 |
| Standard Deviation* 10000 | 1640.488 | 466.690 | 636.396 | 98.995 | 919.239 | 1117.229 |

**A2EE *vs* HL-60 30 min Irradiation with 5 μM A2EE**

| Item | media | media hv | 5 μM A2EE | 5μM A2EE hv | DMSO | DMSO hv |
|---|---|---|---|---|---|---|
| Data 1 | 0.611 | 0.636 | 0.675 | 0.619 | 0.858 | 0.806 |
| Data 2 | 0.655 | 0.649 | 0.609 | 0.602 | 0.57 | 0.749 |
| Average* 20000 | 12660 | 12850 | 12840 | 12210 | 14280 | 15550 |
| Standard Deviation* 10000 | 311.127 | 91.924 | 466.690 | 120.208 | 2036.470 | 403.050 |

**A2EE vs HL-60 40 min Irradiation with 7 µM A2EE**

| Item | media | media hν | 7µM A2EE | 7µM A2EE hν | DMSO | DMSO hν |
|---|---|---|---|---|---|---|
| Data 1 | 0.778 | 0.815 | 0.687 | 0.432 | 0.815 | 0.920 |
| Data 2 | 0.783 | 0.792 | 0.699 | 0.593 | 0.890 | 0.766 |
| Average*20000 | 15610 | 16070 | 13860 | 10250 | 17050 | 16860 |
| Standard Deviation*10000 | 35.360 | 162.634 | 84.852 | 1138.441 | 530.330 | 1088.944 |

## 5.6. References


1. Duffy, J. A.; Teal, J. J.; Garrison, M. S.; Serban, G. P. *PCT Int. Appl.* 9516659, **1995**.

2. Sollaolie, G.; Girradin, A.; Lang, G. *J. Org. Chem.* **1989**, *54*, 2620-2628.

3. Alvarez, M. A. L. Pyridinium *Bis*-Retinoids: Extraction, Synthesis, and Folate Coupling. M.S. Thesis, Brigham Young University, April 2007.